Power Management and Control Strategies in Hybrid AC/DC Microgrids

A thesis submitted for the degree of

Doctor of Philosophy

University of Technology Sydney (UTS)

Faculty of Engineering and Information Technology

Mohammad M. Abuhilaleh

(2020)

Title of the thesis:
Power Management and Control Strategies in Hybrid AC/DC Microgrids

PhD student:
Mohammad M. Abuhilaleh
E-mail: [redacted]@student.uts.edu.au

Supervisor:
A/Prof. Li Li
E-mail: Li.Li@uts.edu.au

Co-Supervisor:
Prof. Jianguo Zhu
E-mail: jianguo.zhu@sydney.edu.au

Co-Supervisor:
A/Prof. Jahangir Hossain
E-mail: Jahangir.Hossain@uts.edu.au

Address:
School of Electrical and Data Engineering
Faculty of Engineering and IT
University of Technology Sydney
15 Broadway
Ultimo, NSW 2007
Australia

Certificate of Original Authorship

I, Mohammad Abuhilaleh declare that this thesis, is submitted in fulfilment of the requirements for the award of Doctor of Philosophy (PhD), in the Electrical and Data Engineering School / Faculty of Engineering and Information Technology (FEIT) at the University of Technology Sydney.

This thesis is wholly my own work unless otherwise reference or acknowledged. In addition, I certify that all information sources and literature used are indicated in the thesis.

This document has not been submitted for qualifications at any other academic institution.

This research is supported by the Australian Government Research Training Program.

Signature: Production Note:
Signature removed prior to publication.

Date: 21 March, 2020

Acknowledgments

First and foremost, my sincere thanks go to Allah, who has endowed me to complete this PhD degree. The research has been mainly financed by AL-Hussein bin Talal University, Ma'an, Jordan. Thanks must be made to them for their financial support of this project. This thesis would not have been possible without the inspiration and support of a number of wonderful individuals, my thanks and appreciation to all of them for being part of this journey and making this thesis possible. I owe my deepest gratitude to my principal supervisor A/Prof Li Li, Co-supervisors Prof. Jianguo Zhu and A/Prof. Jahangir Hossain.

Most importantly, my wife and Parents, who are always by my side and help me through thick and thin; I could not have done this without you. Last but not least, my UTS colleagues' knowledge, advice, and experience have encouraged me to do better and better, through this journey. Hasan Miqdadi, Mohammad Shalby, Omar Elshaweesh, Amin R Ahmad Salah and many others were along the way.

Abstract

The future trend of the power system is to ensure reliable, flexible, affordable and efficient power supply for customers with lower emissions. Conventional AC or DC microgrid suffers from increased losses and lower efficiency due to several AC-DC and DC-AC conversions. Therefore, hybrid microgrid (HMG) is getting popular to meet the growing penetration of modern DC loads and renewable energy sources with DC outputs into the existing AC power systems. The main objective of this dissertation is to develop and implement improved power management and control strategy to improve the performance of the hybrid microgrid.

The first study proposes an improved power management and control coordination strategy for an autonomous HMG. The HMG considered in this part consists of multiple AC and DC sub-microgrids (SMGs) with different voltage levels. The hierarchical coordination of power management and control strategy for the autonomous HMG is introduced and analyzed. The designed system incorporates both the primary and secondary control levels to ensure a seamless and accurate transfer of power among the SMGs. A new technique for transferring power with a focus on the secondary control level is presented.

The second study proposed in this thesis is a novel approach of distributed coordination control for multiple SMGs within the HMG. The traditional control method for power flow management among AC and DC SMGs is based on the proportional power-sharing principle. The proposed method suggests a distributed control system that ensures total controllability for the parallel interlinking converters (ILCs). It overcomes the total dependency on a specific variable for power exchange. The proposed method not only enables control of the power

flow between SMGs but also ensures the continuity of power transfer in the event of a single SMG failure.

The third study in this work focuses on coordinating the control and power management strategy for the multiple parallel ILCs that link the AC and DC SMGs together. The proposed new approach aims to manage the power flow across the HMG while regulating the voltage and frequency for the SMGs as part of the process. The main objective of the proposed method is to keep the HMG in autonomous operation with active power proportionally shared among its ILCs and distributed sources. The presented outer control loop is a modified arrangement that could not only ensure accurate power-sharing but also suppresses the circulating current at the DC side.

Keywords: Autonomous hybrid microgrids; Power management; Control coordination strategy; Multiple bidirectional power converters; Power-sharing.

Table of Contents

List of Publications

The following publications are part of the thesis.

Peer-reviewed international journal publications

[1] Abuhilaleh M, Li L, Hossain J. Power management and control coordination strategy for autonomous hybrid microgrids. IET Generation, Transmission & Distribution. 2019 Nov 11 (**Published**).

[2] Abuhilaleh M, Li L, Hossain J, Zhu J. Power Management and Control Strategy for Multiple Bidirectional Power Converters in an Autonomous Hybrid Microgrid. Journal of Modern Power Systems and Clean Energy (under review).

Peer-reviewed international scientific conference publications

[3] Abuhilaleh M, Li L, Begum M, Zhu J. Power management and control strategy for hybrid AC/DC microgrids in autonomous operation mode. In 2017 20th International Conference on Electrical Machines and Systems (ICEMS) 2017 Aug 11 (pp. 1-6). IEEE.

[4] Beiranvand A, Abuhilaleh M, Li L. A novel method for optimizing distributed generation in distribution networks using the game theory. In 2017 20th International Conference on Electrical Machines and Systems (ICEMS) 2017 Aug 11 (pp. 1-5). IEEE.

[5] Begum M, Abuhilaleh M, Li L, Zhu J. Distributed secondary voltage regulation for autonomous microgrid. In 2017 20th International Conference on Electrical Machines and Systems (ICEMS) 2017 Aug 11 (pp. 1-6). IEEE.

[6] Abuhilaleh M, Li L, Zhu J, Hossain MJ. Distributed Control and Power Management Strategy for an Autonomous Hybrid Microgrid with Multiple Sub-Microgrids. In 2018 Australasian Universities Power Engineering Conference (AUPEC) 2018 Nov 27 (pp. 1-6). IEEE.

[7] Abuhilaleh M, Li L Hossain MJ, Zhu J. Distributed Control and Power Management Strategy for Parallel Bidirectional Power Converters in Hybrid Microgrids. In 2019 45th Annual Conference of the IEEE Industrial Electronics Society (IES) (IECON) 2019.

List of Figures

List of Tables

Nomenclature

Global abbreviations used in this thesis

AC	=	Alternative Current
HMGs	=	Hybrid Microgrids
CAES	=	Compressed Air Energy Storage
CHP	=	Combined Heat And Power
MG	=	Microgrid
ILC	=	Interlinking Converter
SEE	=	Storage Element
SMG	=	Sub-Microgrid
DG	=	Distributed Generation
DC	=	Direct Current
HVDC	=	High Voltage DC
RES	=	Renewable Energy Sources
SE	=	Storage Elements
GHG	=	Greenhouse Gas
EES	=	Electrical Energy Storage
PV	=	Photovoltaics
FC	=	Fuel Cells
FES	=	Flywheel Energy Storage
HPES	=	Hydraulic Pumped Energy Storage
MPPT	=	Maximum Power Point Tracking

P	=	Active Power
Q	=	Reactive Power
VSI	=	Voltage Source Inverter
SMES	=	Superconducting Magnetic Energy Storage
SCI	=	Current Source Inverter
Z_D	=	Virtual Output Impedance
PI	=	Proportional-Integral
PR	=	Proportional Resonance
PLL		Phase Lock Loop
THD		Total Harmonic Distortion
D		Distorted Power
CCP		Common Coupling Point
MGCC		Microgrid Central Controller
SCADA		Supervisory Control and Data Acquisition

Chapter 1

Introduction

Hybrid microgrid (HMG) concept has been the focus of research in recent decades due to the rapid and diverse changes in renewable energy technologies and the complexity of their integration. HMGs are formed by linking DC and AC microgrids together using ILCs. This combination is considered to be the future trend of integrated power systems. Power management and control aspects are the main concerns in the HMG. Although many techniques and strategies have been proposed in the literature to manage the power flow and control the voltage and frequency in such an arrangement, there are still many challenges and drawbacks in them. One of the challenges in HMG is the control strategies used to manage the power flow between AC and DC SMGs. Droop control method is one of the most common techniques suggested in the literature that relies on the surplus power of each SMG. This control method is mainly used when microgrid only works at the primary control level. However, to improve power quality and achieve a higher level of stability in HMG structures, it is highly recommended to perform the analysis according to the sequential hierarchy of control.

Although linking of AC and DC SMGs by ILCs would constitute the HMG structure, different topologies for such arrangement can be made by linking multiple SMGs together. This complexity of the HMG structure became necessary and practical due to the urgent need to meet the increased penetration of modern DC and AC loads. Consequently, considering this

structure requires more focus on controlling and managing power flow between connected SMGs. The ILC control scheme should also ensure a viable power exchange strategy in HMG by overcoming the continuous operation of the ILC in all conditions that would lead to a significant power loss on the ILC which adversely affects the operational feasibility of HMGs. With the above concerns in mind, the challenge is then to perform multiple parallel ILCs that are used due to the converters' current limitations and planned maintenances or unplanned faults during the converter operation. One of the key gains of this structure is the mitigation of the circulating current that results from the parallel operation of the ILCs. Coordination between these ILCs is crucial since these ILCs have to carry out the responsibility to manage the power flow between the AC and DC SMGs and simultaneously support the voltage and frequency regulation at the AC bus and support the voltage regulation at the DC bus.

This thesis contributes to a vast knowledge to the engineering community by studying and investigating the power flow management, voltage and frequency regulation in the healthy and defective conditions all within the HMG. The most significant and novel feature of this research is the introduction of power management approaches and control strategies that are able to solve many of the above challenges and issues. Many other findings and original research contributions are detailed in the summary for each chapter.

1.1 Research Statement and Objectives

This work contributes to the improvements and verifications of the computational efficiency of the simulation models that are used to improve the performance of the power management and control strategies in the HMG under different operating and loading conditions. The most significant and novel aspects of this research are:

1) Discussions on key HMG concepts, components, structure, power management and control strategies used in different operating modes.
2) Discussion and investigation on the hierarchical control scheme of the individual and HMG systems. This includes studying energy management and control techniques for each microgrid system structure, focusing on the power flow between AC and DC buses all within a hybrid network.
3) Development of a new topology for the HMG network based on bus connectivity to the AC SMG network with multiple DC SMG at different voltage levels. The improved power management and control coordination strategy used in this structure aims to reduce the continuous operation of ILCs under all load conditions and thereby avoids the significant power loss on the ILC that adversely affects the operational feasibility of the HMGs.
4) Ensure a seamless and accurate power-sharing among the SMGs by implementing a new distributed control approach that guarantees total controllability for the ILCs. Unlike the conventional method, the proposed scheme overcomes the total dependency on a specific variable for power exchange.
5) Management and regulation of the power, voltage and frequency parameters of the HMG during the parallel operation of the ILCs. Furthermore, one of the main objectives of this work is eliminating the circulation current that would result from the parallel operation of distributed generations.

1.2 Structure of the Thesis

In this thesis, detailed analysis and discussion methods are presented to help build a sound understanding of the overall control and power management strategies presented in the

following chapters. This thesis is divided into six chapters, and each chapter is subdivided into sections to maintain the flow of the chapters. The thesis is organized as follows:

Chapter 1 provides an introduction at the beginning of this thesis stating the main research problem, thesis argument, research objectives, novelties, and significance.

Chapter 2 presents a detailed introduction to the microgrid's concepts, components, structure, types, power management, and control techniques that have been used in the literature. Although this chapter represents a review of the main literature of this project, a brief explanation and exploration are also adopted at the beginning of each chapter to address the significant relevance of the proposed research work to the existing literature.

Chapter 3 examines the power management and control strategies of HMG. The analysis develops an expression that takes into account a new structure of the HMG by linking multiple SMGs with different voltage levels and frequencies. This chapter also examines the use of a hierarchical level of control to achieve complete control over the HMG and ensure a high level of stability and reliability for each part of the system.

Chapter 4 proposes a relatively simple but robust control method that can accurately share power flow among SMGs proportionally based on a distributed coordination control of SMGs within the HMG. The HMG structure mentioned in this chapter is similar to the structure proposed in Chapter 2. A comparison between the traditional and proposed method is conducted by discussing their theoretical background, improvements, implementation, and results.

Chapter 5 studies and investigates the multiple parallel operations of ILCs between AC and DC SMGs within the HMG. The proposed approach discusses ILC control systems that include power flow management between SMGs, voltage regulation in the DC SMG, voltage

amplitude and frequency regulation in the AC SMG. One of the key gains of this structure is the mitigation of the circulating current that results from the parallel operation of the ILCs. In the HMG studied in this chapter, three interlinking converters are connected in parallel between the AC and DC SMGs operating under different control strategies. These ILCs have to carry out the responsibility to manage the power flow between the AC and DC SMGs and simultaneously support the voltage and frequency regulation at the AC bus and support the voltage regulation at the DC bus.

Chapter 6 summarizes and reviews the main contribution, research results, and relevant and new findings of the previous chapters. This chapter also discusses future work that can be employed in the proposed research. Recommendation and proposal to improve the proposed technique are also considered.

1.3 Novelties of the Project

This research focuses on developing techniques to manage the power flow between AC and DC SMGs and regulate the corresponding microgrid parameters all within the HMG. In summary, the developments and novelties of this project include the following:

1) Modify a new topology of hybrid AC/DC microgrid structure by linking the AC SMG with multiple DC SMGs at different voltage levels.
2) Develop a new power management and control coordination strategy for autonomous HMGs consisting of multiple AC and DC SMGs at different voltage levels. The designed system includes hierarchical control with a focus on the primary and secondary control levels to ensure a seamless and accurate transfer of power among the SMGs. The new strategy aims to reduce the continuous operation of ILCs under all load conditions.

3) A new technique is introduced to ensure a continuous power flow among the SMGs while minimising the continuous operation of the ILCs in the islanded mode with a focus on the secondary control level.
4) Develop a novel approach of distributed coordination control for multiple SMGs within a hybrid AC/DC microgrid. Unlike the conventional methods, the proposed technique overcomes the total dependency on a specific variable for power exchange between AC and DC systems.
5) Develop a coordinated control and power management strategy for multiple parallel ILCs that link the AC and DC SMGs in an autonomous HMG. In the conventional method, the multiple ILCs utilized have the same control strategy while the proposed approach assumes that each converter operates under a different control scheme.
6) Propose a modified outer control loop that ensures accurate power-sharing while also suppressing the circulating current at the DC side. The proposed scheme has to carry out the responsibility for managing the power flow between the AC and DC SMGs while supporting voltage and frequency regulation at the AC bus and supporting the voltage regulation at the DC bus.

Chapter 2

Background and Literature Review of Microgrids

Microgrids are the main focus of this thesis, and this chapter provides a brief introduction of contents, control schemes, power management and some examples of microgrids. Discussing and analysing the concept of the operation of microgrids are also considered in this to help understand the proposed novel studies.

2.1 Introduction

Nowadays, almost every home, farm, industry, and business is connected to the electric grid. Such a revolution in the technology field was not an overnight decision. A variety of discoveries and developments across all over the world led to a full-scale battle between alternating current (AC) and direct current (DC) distribution.

The story began by the end of the 18th century when Nicolas Tesla and Thomas Edison were involved in the battle that is known as the currents war. DC current was established by Thomas Edison, and the current moves from one point to another continuously and in one direction. This kind of currents was the main source of electric power in many countries during the early years, such as the U.S. However, converting the voltage to higher levels was the main challenge in the use of DC current. The AC current was raised as a logical solution to this problem with the current alternating the direction a certain number of times per second. Tesla believed that the AC currents have the ability to replace DC currents and AC voltage can be converted to higher and lower levels using a special technique known as transformers.

Finally, the AC form won the currents war, and since then, the AC power system is the base for power transmission across the world. However, the interest in DC systems has increased dramatically, mainly due to the advantage of storing electricity generated for later use when needed [1, 2].

Today, AC and DC systems operate simultaneously to provide consumers with reliable and stable electrical services. Figure 2.1 illustrates the stages in which electricity moves from generation to consumption in households. In more detail and above all, electricity is produced by giant generators at the power plant using a different type of resource that varies between AC systems such as coal, natural gas and DC systems such as wind and solar. The currents in DC form are converted to AC form using power electronic converters. Thereafter, the produced currents are transmitted through step-up transformers to increase the voltage level and then are transmitted over long-distance overhead wires. Once the current reaches the local substation, the voltage is converted to a low-voltage level using step-down transformers, which in turn travels across distribution lines to local consumer areas. Other step-down transformers are used to convert voltage within a safe and usable level in our homes. Finally, the power goes to the service panel where the meter measures the energy usage of homes [3, 4].

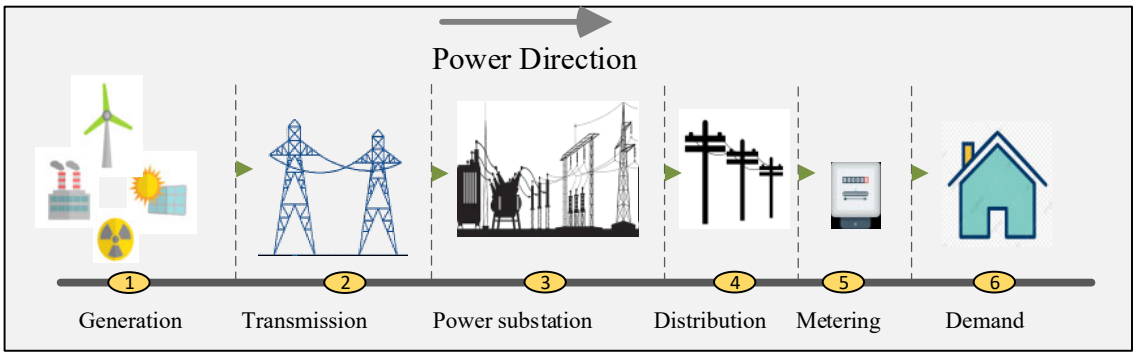

Figure 2.1 The structure of electric power systems from production to consumption.

Recently, DC applications have become the current and future trend of modern loads in industrial systems, residential and commercial buildings. The increased attention is due to the urgent need to meet the increasing penetration of modern DC loads that require a high level of stability. DC is commonly used in most devices that have a circuit board because of the fact that the chips in these devices require a unidirectional constant flow of electrons to operate and store data. Most home electronic devices such as computers, mobile phones, laptops and televisions have an inverter to convert the AC current to the DC one compatible with the hardware components in these devices [3].

Moreover, DC systems are also recognized with the growth of advanced power electronics systems. High voltage DC (HVDC) transmission based on power electronics is an application of integration of AC and DC systems. Switching from AC to DC systems simplifies load control efficiently and allows the integrating of distributed energy storage with renewable energy sources (RESs). These arrangements are the future direction of integrated energy systems [5].

2.2 Basic Principles of Microgrids

The microgrid is defined as a centralized cluster of power sources and loads that are typically connected to a traditional home network with the ability to operate independently under specific physical and/or economic conditions. The microgrid is also defined as a small power grid that involves distributed generations (DGs), storage elements (SE) and different types of loads. Cooperation of these elements under appropriate supervision of control systems can ensure a seamless and secure system operation [6].

Microgrid is gaining momentum in power system research in the last decade because of its economic, environmental and sustainable incentives. Moreover, it is the solution to the complexity of integrating different renewable energy technologies. Microgrid also has the ability to integrate RESs with non-renewable energy sources, all within the main grid [7-9].

The main purpose of building a microgrid network is to ensure reliable and affordable local energy security for urban and rural communities which are sometimes far from the main grid. Moreover, it also provides solutions for consumers in the commercial, industrial and federal government. Benefits beyond public utilities and society as a whole include reducing greenhouse gas (GHG) emissions and reducing pressure on the transmission and distribution system. Also, it can make a profit for those who have their own microgrid network and support home network with electric power [5, 10].

2.3 Review of Microgrids

The microgrid is very similar to the traditional power system from the physical point of view. It contains a power source, power storage elements, distribution network, loads and many other components. The following sections address these components in detail.

2.3.1 Distributed Generation (DG)

Distributed generation is a technology that relies on small-scale generation systems to produce electricity near energy consumers. DGs extend to include all energy sources that can be possible in the microgrid range and structure. In the literature, a considerable variation in definitions was used to explain DG concepts. These definitions take into account location, purpose, environmental impact, classifications and many other issues related to ownership and regulatory policies. DGs have different names depending on their country. For example, in North America, distributed generation is called "dispersed generation" while "embedded generation" and "decentralized generation" are called in some European and Asian countries. DGs can be divided into renewable and non-renewable sources of energy [11-13].

A). DG based on renewable energy sources

Due to the environmental impacts of fossil fuels, the use of sustainable energy has become a global trend in the last two decades. DGs based on the RESs have become an increasingly important choice in current and future generation technologies [8, 9]. One or more RESs can be widely used according to the local conditions of environmental situations and energy potential. It is the best solution for generating electricity in rural areas far from the national grid. Moreover, renewable DGs not only produce clean and economical energy but also require fewer constructions and infrastructures. Photovoltaic, wind and waves are some examples of this power source [14, 15].

B). DG based on non-renewable energy sources

Non-renewable sources are of limited supply that cannot be replaced over time. Natural gas, crude oil/petroleum and coal-powered systems are examples of the most common sources of

non-renewable sources used in distributed generators. Reciprocating engines and microturbines are some of the example technologies used in non-renewable sources.

The DGs based on non-renewable energy sources are very popular and efficient in generating electricity in microgrids. These DGs are mainly used to supply critical loads and increase the reliability and efficiency of power systems within microgrids. The capacity of the DGs is primarily dependent on the capacity of the local distribution system, which in turn depends on the voltage level of the utility network. The technical challenges associated with distribution systems vary widely with the rating of DG. Below are some classifications of DGs as proposed in the literature [11, 16, 17].

A. Micro DG: ~1 Watt < 5 kW;
B. Small DG: 5 kW < 5 MW;
C. Medium DG: 5 MW < 50 MW;
D. Large DG: 50 MW < 300 MW.

Normally, the distribution system is utilized by integrating a particular generation technology category through installing a number of small DG modules such as solar thermal systems, diesel engines, battery storages and fuel cells. Units assembled in factories are designed to be installed in a short time and can be easily transported according to the necessity of the distribution system. Each DG can operate independently of other modules; therefore, the effect of adding or disconnecting a module is too small for the entire distribution system [16, 18].

Moreover, the co-generation of heat and power (CHP) can be an innovative achievement. This can be achieved by using a thermal engine to generate electricity and heat at the same time. Internal combustion engines, combustion turbines, biomass gasification, geothermal

and fuel cell are some examples of heat and power production combination technologies. Such a CHP arrangement can be installed as an autonomous system in houses or small businesses to produce electricity and heat the water or space at the same time.

2.3.2 Electrical Energy Storage (EES)

Electric energy storage is defined as the method of storing electrical energy generated from a DG in a form that can be converted again and used when needed. This technique allows the production of electricity at the time of low generation cost or low demand and the use of electricity at the time of high generation cost or high demand.

This process is more common for RES applications where energy is produced at a specific time, according to weather and environmental conditions [10]. EES technology is applied to many applications including fixed energy resources such as distribution network, transmission, distributed power resources, power generation and local commercial and industrial customers. Transport vehicles and mobile devices are also other applications of EES [19, 20].

In a conventional electric power system, the electrical power produced flows in one direction from the power plant (generation) to the consumer side (demand). This means that the energy generated must be used precisely when produced, and must always be equal to or higher than the energy demand at any time. Since peak demand lasts only a few hours during the day, and demand varies significantly throughout the day and seasons, designing a power plant under these conditions will result in an inefficient, overly designed and costly plants.

Therefore, the use of EESs for conventional and especially industrial systems is highly recommended. Instead of building a peak demand based power plant, EES enables the system

designer to build sufficient generating capacity to cover the average demand for electric power. Figure 2.2 shows significant benefits that can be achieved when there is a large storage capacity over a period of time. ESSs can operate in a peak shaving state where the stored energy is discharged to cover the peak demand or operate in the case of load adjustment balancing the energy stored according to the load profile. A nuclear power plant is an example of large power generation systems, which typically operates within the maximum capacity for economic reasons. In this case, the ESS provides significant benefits from peak capacity and load monitoring [21, 22].

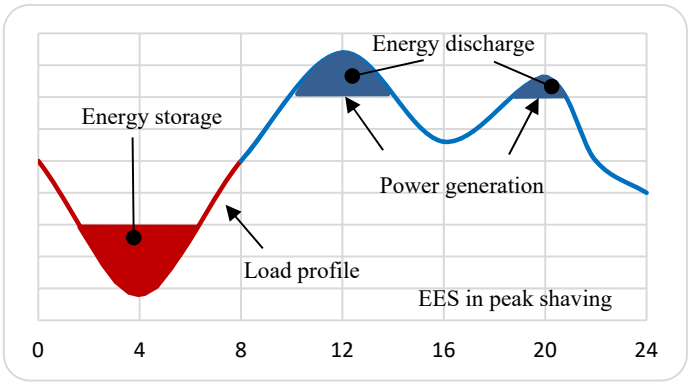

(a)

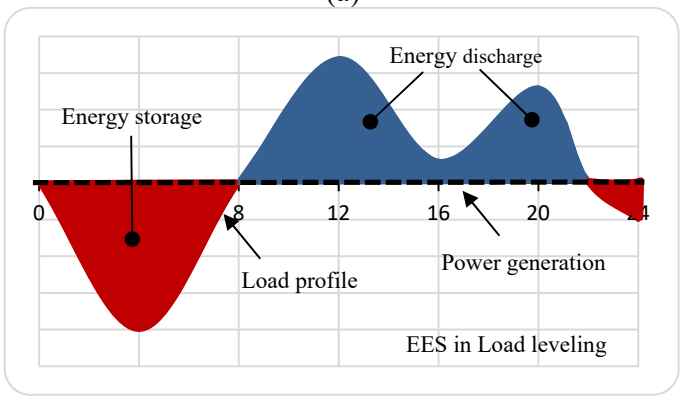

(b)

Figure 2.2 Large scale of electricity storage system under load profile (a) EES in peak shaving; (b) EES in load levelling.

There are many criteria for classifying storage models. Here the storage methodologies are classified in terms of their function and the state in which energy is stored. This gives four main sectors: mechanical, electrical, chemical and thermal [23]. However, in this work and its context, a detailed economic and technical review will particularly focus on the mechanical and electrical sectors of storage technologies, as illustrated in Figure 2.3 below.

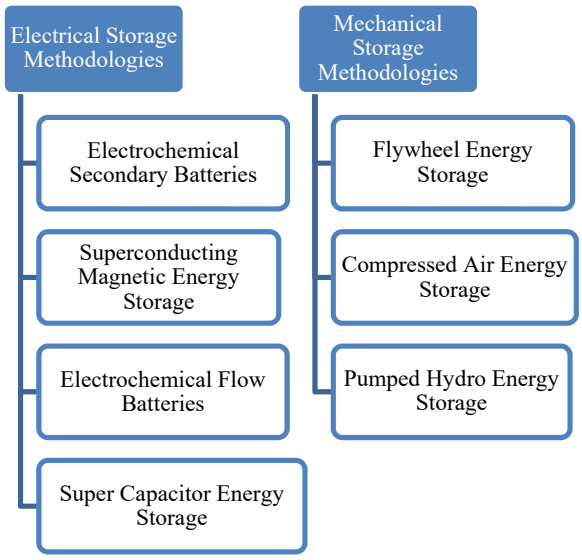

Figure 2.3 Electrical & mechanical storage methodologies.

A). Electrochemical secondary batteries

Secondary batteries are identified as the most widespread electrical storage form in the electrical storage industry. In its simplest definition, the secondary battery is a rechargeable electrochemical device that utilizes chemical reactions between two electrodes submerged in an electrolyte to transform the chemical energy in the electrolyte into electrical energy in a bi-directional manner. The two electrodes together with their electrolyte are called a cell. Each battery is a series or parallel combination of several cells. The number and configuration of these connected cells are determined based on the required capacity and voltage [24].

B). Electrochemical flow batteries

It is like the previously mentioned methodologies in terms of being a rechargeable electrochemical form of electrical energy storage that is considered most promising for increasing the reliability of renewable systems. Nevertheless, the conceptual differences from conventional batteries grant it the upper hand. In flow batteries, unlike the previous technologies, the liquid electro-active substances are externally stored in separate tanks of electrolysis. These electroactive substances (electrolytes) are pumped through the reactor (cell stack) which contains two electrolyte compartments separated by ion-selective membranes. The pumping triggers a bidirectional chemical reaction through which electricity is produced or stored. Based on the concentration of the electroactive component and type in the electrolyte, such technology can be segmented into two different categories that are hybrid flow and redox flow batteries [24, 25].

C). Superconducting magnetic energy storage (SMES)

This technology is considered unique as a method that stores electricity without transforming it into any other form. The typical configuration of such technology involves a power conditioning unit, a refrigeration and vacuum subsystem and a superconducting coil unit. Its concept exploits the magnetic field generated in a superconducting coil to store energy. More specifically, it takes advantage of the superconductivity phenomenon. This phenomenon occurs when the electricity flows through the superconducting coil which results in an infinite attenuation time for the flowing current due to the absence of electric resistance (no attenuation). Throughout this, if the superconducting coil ends are shorted, and the coil is cryogenically cooled to below its superconducting critical temperature, the current will keep flowing in the circuit without attenuation while generating a magnetic field, thus storing

electric energy with no losses. Each superconducting material has its superconducting critical temperature. For instance, Niobium-Titanium has a critical superconducting temperature of 9.2 K [25, 26].

D). Supercapacitor energy storage

Named the ultracapacitor or an electric double-layer capacitor, this method of energy storage follows the same concept as a typical capacitor in which energy is stored in the electric field between two metal plates (electrodes) separated by an insulator (dielectric). However, its use of an electrolyte and a porous membrane separator enables a unique structure that allows it to combine the characteristics of both rechargeable batteries and typical capacitors. Its strength lies in its extraordinary long lifespan and relatively high cycle efficiency (up to 97 %). Moreover, its robustness to varying operating temperatures and impressive energy density make it popular for boosting the stability of an electric system. Nevertheless, the high self-discharge rates (up to 40%) together with its high associated costs that exceed 6000$/kWh limits its attractiveness. [20, 27, 28].

E). Flywheel energy storage (FES)

Also known as the mechanical battery, the flywheel is considered as the oldest form of energy storage. It stores the energy in the kinetic form utilising a high-speed rotating disk (flywheel); the disk is coupled to the shaft of an electrical machine that provides (as a generator) and stores (as a motor) the energy when required. In more detail, in the charging phase, the flywheel speeds up its rotating disk through the reversible coupled motor with the amount of energy to be stored, thus gaining higher kinetic energy, and then preserves it in the standby mode by the continuous and steady rotation of the disc. When the stored energy is needed,

the flywheel uses the same reversible coupled electrical motor as a generator to reconvert the kinetic energy into its electrical form [29, 30].

F). Hydraulic pumped energy storage (HPES)

This technology constitutes over 99% of the existing installed bulk energy storage capacity on a global level with over 125 GW. The typical pumped hydro storage system stores the electrical energy as gravitational potential energy. The charging phase takes place at off-peak demand periods where the electricity being generated exceeds the demand. During this phase, the system pumps water from the lower reservoir to a higher one utilising pumps that convert the electricity into mechanical energy (flowing water) and then to its gravitational potential form (once it gets to the higher reservoir). When the demand hits the peak levels, and excess electricity is needed, the discharging state takes place. The system releases the stored water from the elevated reservoir to the previously mentioned lower reservoir while energising a turbine that generates electricity on its way, thus reconverting the stored gravitational potential energy back to mechanical energy (water flow) that ends up as generated electricity (turbine output) [25, 31].

G). Compressed air energy storage

This technology is considered the second-largest installed bulk energy storage capacity on a global level following the pumped hydro energy storage with an installed capacity of 440 MW [31]. The concept of this technology is highly similar to the technology deployed in typical gas turbines. The energy is stored in the form of potential energy by the mean of highly compressed air in the confined storage tank [32].

2.4 Microgrid System Definitions

Microgrids can function either in islanded or grid-connected mode. In the islanded mode, the system is disengaged from the main grid, and this has been noted for avionics, automotive, and marine-related systems. On the other hand, while operating in the grid-connected mode, the power is exchanged through a common coupling point, a static switch or a typical circuit breaker [33-36].

There are many criteria for microgrid classification. Here the structures are classified in terms of the form of electric power and the manners of power delivery from DGs to loads. These structures are also classified based on how DGs of DC and AC microgrids are connected to the loads. Thus, the three main structures of microgrids discussed in this work are AC, DC, and hybrid AC/DC microgrid [37-39].

2.4.1 DC Microgrid Structure

Interest in DC microgrids is growing rapidly due to the nature of the presence of DC power sources in microgrids such as photovoltaics (PV), fuel cells (FC), energy storage units and modern DC loads. In such a system, DGs and EES are connected to the common DC bus directly or indirectly through electronic power devices. Note that such a structure is used when DC power sources are the main power generating units. Although each unit in the DC microgrid is connected to a DC bus, the AC bus is connected to the DC bus through a bidirectional converter. These arrangements enable AC loads to be connected directly to the AC bus and improve system stability when the AC bus is connected to the utility network.

Figure 2.4 shows a typical example of a small DC network connected to the main utility network by a static switch [37].

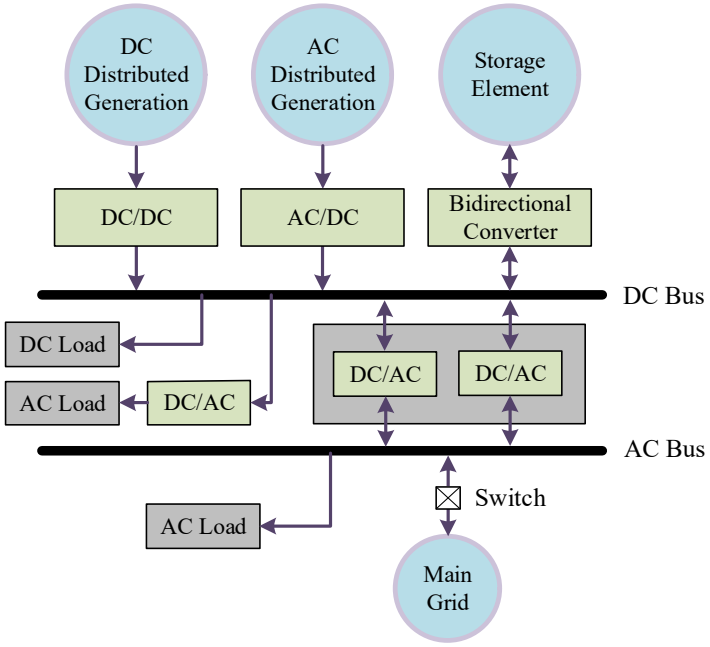

Figure 2.4 DC microgrid structure.

Here are some example projects using the DC microgrid structure.

1) CESI RICERCA DER test microgrid: This low-voltage microgrid (400V) is connected to the 23 kV medium-voltage network implemented in Italy. The microgrid can deliver power to the main grid with a maximum capacity of 350 kW. PV, diesel generator, CHP system and various types of batteries are the main components of this microgrid. The project is part of a larger project aimed at assessing and improving the economy, security and quality of the Italian electrical system. The microgrid adopts a centralized control system to regulate the voltage and manage the energy flow all within the microgrid.

2) Kahua Ranch Hawaii Hydrogen Power Park: This microgrid was implemented in the US with a wind turbine, PV, battery, and FC.

2.4.2 AC Microgrid Structure

The AC microgrid structures are commonly used when AC power sources are the main power generation units and produce power according to the grid voltage level. Figure 2.5 shows a typical example of AC microgrid connected to the main utility grid by a static switch. DGs and EES are connected to the common AC bus through power electronics devices. Note that, the EES need AC/DC bidirectional converter to be able to charge and discharge power when needed.

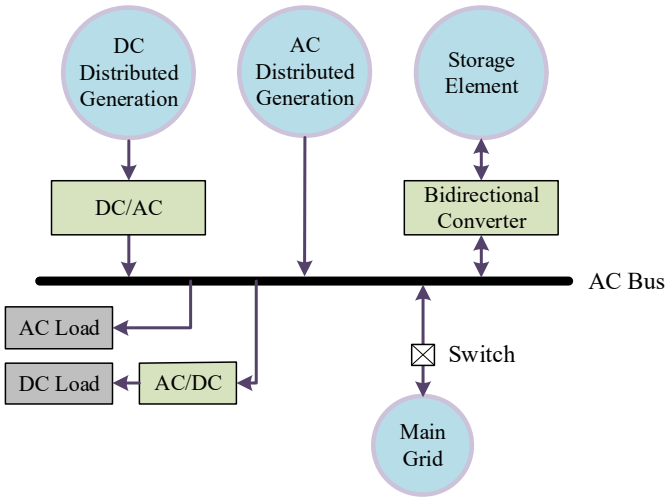

Figure 2.5 AC microgrid structure.

AC microgrid is a very common structure because of its simple structure and simple power management and control. Many AC microgrids have been implemented around the world. Here are some examples of these microgrids [40]:

1) Bronsbergen Holiday Park microgrid in Netherland [35]: This project is supported by the European Union and has 208-holiday homes installed in the park. The system consists primarily PVs as the main source of power generation and two battery banks connected at the common connection point. Peak generation capacity for the microgrid is 315 kW [41].
2) Aichi microgrid in central Japan airport city [41]: The microgrid was built as part of a demonstration project commissioned by the New Industrial Energy and Technology Development Organization (NEDO). The system consists of FCs, PV, and battery with a total capacity of 600 kW [42].

2.4.3 Hybrid AC/DC Microgrid Structure

The combination of the previous two structures forms the third type, HMG. In this arrangement, both the DC and AC buses exist in the microgrid. The AC bus and DC bus are linked together using an ILC to facilitate the power transfer between AC and DC SMGs when needed. Research interests are increasing rapidly in this configuration because the characteristics of modern and emerging load profiles involve both DC and AC loads/sources [35, 43-45].

Most of the previous literature suggests an HMG that links a single AC and DC SMG using an ILC that functions as a bi-directional converter. However, the interest in designing a multiple-SMG cluster is gaining momentum due to the growing number of DC and AC sources/loads with different voltage and frequency levels within the same system. In this sense, each SMG behaves as a voltage source inverter with high inertia. This type of microgrid is usually used if the main power sources include both AC and DC power [46].

Figure 2.6 shows a typical example of a hybrid AC/DC microgrid. In general, the AC bus acts as a common bus connecting other SMGs and mediating any power exchange that takes place. AC and DC SMGs should have the ability to manage the power flow in accordance with their own respective loads. Excess power will be transferred to other SMGs to compensate for any power shortage.

In this work, six IGBT-diode switches are used for the ILC that acts as a bidirectional power converter and operates in two modes depending on the direction of the power flow. In the first mode, when it acts as a rectifier, the DC side is seen as a load on the AC side, and the power flows from the AC side to the DC side. On the other hand, in the second mode, when the ILC acts as an inverter, the AC side is considered a load from the DC side point of view, and the power flows in the opposite direction. The amount of power transferred from one SMG to another depends mainly on supply (DGs output) and demand (load) in each SMG [8].

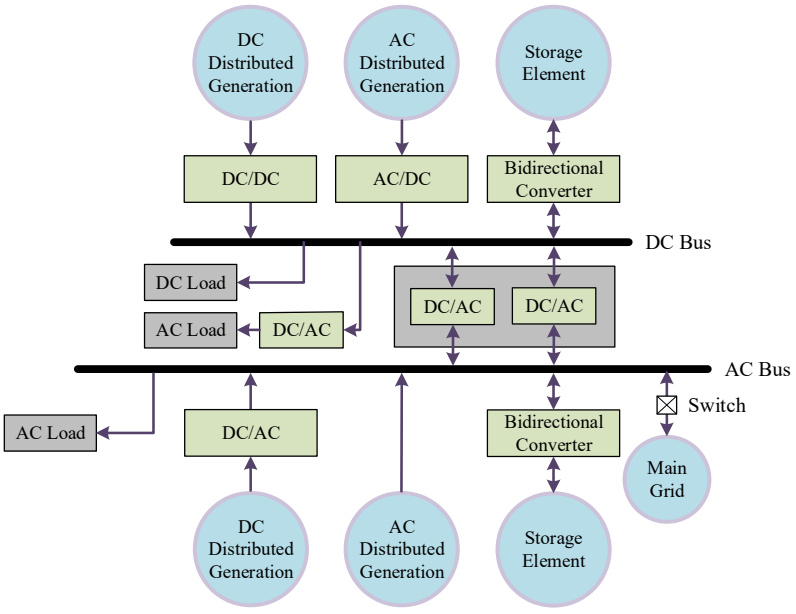

Figure 2.6 Hybrid AC/DC microgrid structure.

Microgrid usually works in the grid-connected mode to maintain voltage and frequency within high levels of stability. By that, it overcomes any contingencies that may occur due to power shortages. The intelligent transfer switch or circuit breaker connecting the microgrid to the main network remains closed in the normal state. In emergencies such as regular maintenance or malfunction, the switch is opened, and the microgrid operates in the autonomous stand-alone mode. This situation usually lasts for short periods [9]. There are many advantages to adopting such a hybrid structure (multi-SMG). It can reduce the total cost by reducing the required switching devices, thus improving the overall system efficiency and reducing the overall conversion losses due to the elimination of excess stages of power conversion. Connecting more SMGs to the HMG will increase the total power capacity and improve system reliability.

Water and Energy Research Lab (WERL) is a real example for HMG that is implemented with support from Schneider Electric Singapore and Nanyang Technological University (NTU), Singapore. On the DC side, the SMG consists of a solar emulator of 1.45 kW, a resistive load of 3.3 kW, an electrical load of 14.5 kW, battery storage of 28.8 kW, and a DC programmable source of 20 kW; all these components running at 380 V. On the AC side, the main components are an 18 kW programmable source and a 7.5 kW emulator that operate at 400 V. The AC and DC sides are connected by two bidirectional converters. HMG structure can be formed to work in radial and ring configuration. Table 2-1 summarizes some examples of the microgrid structures listed above.

Table 2-1 Examples of different microgrid structures.

Microgrid type	Name	Location	Sources	Capacity
DC Microgrid	Cesi Ricerca Der	Italy	PV, batteries, a diesel engine, solar thermal plant	350 kW
	Kahua Ranch Hawaii Hydrogen Power Park	US	PV, wind turbine, battery, and FC	107.5 kW
AC Microgrid	Hachinohe	Japan	a gas engine, PV systems, a small wind farm and battery	714 kW
	Bronsbergen Holiday Park	Netherland	PV units, two battery banks	315 kW
	Kythnos CSIRO	Greece	PV units, battery bank, diesel generator	75 kW
	Newcastle	Australia	PV	110 kW
AC/DC Microgrid	Griffith University	Australia	PV panels, lithium-ion polymer battery	76 kW

2.5 Why Hybrid AC/DC Microgrids?

The significance of this project lies in the necessity of connecting the AC systems to the DC systems due to the following aspects.

- On the generation side, most of the DESs that have emerged in the past decade generate power in the form of DC. PV systems are an example of the primary sources of electricity that are growing rapidly these days.
- Many modern electrical loads, in addition to energy storage systems, either have a fully internal DC voltage or work well with DC power. These components are ultimately connected to the AC systems through converters.

- The use of HMG with the application of DC voltage would allow the cancellation of several DC/AC and AC/DC conversion stages, resulting in a significant reduction in component costs, power loss and increased system stability and reliability.
- Also, there are many power quality issues, such as harmonics, unbalances, and circulating current in parallel AC sources that can be avoided in HMG systems.

2.6 Power Management and Control Scheme of Microgrid

It is necessary to design a reliable and flexible microgrid with the ability to operate in either the islanded or grid-connected mode. This design can be achieved by integrating various aspects of power electronic interface, protection, security, and communication technologies. The main challenge of the microgrid process is to bring them all into a well-established power management and control strategy. This section studies and analyses the hierarchical control levels for each microgrid individually.

As an individual microgrid, various aspects of combining RESs have been discussed in terms of scheme design, control strategy and power management [9, 47-49]. This integration needs more focus on the conversion interface and thus control coordination for ensuring stable and reliable operations.

Power management and control strategy are considered to be the main challenge, especially for those operating in the islanded mode. This is mainly due to the fact that the microgrid must regulate voltage and frequency in addition to the flow of power. Several methods have been proposed in the literature to analyse the power-sharing strategies for AC and DC microgrids.

To improve the power quality and achieve a higher level of stability in all microgrid structures, it is strongly recommended to perform the analysis according to a control hierarchy. The hierarchical control scheme is an effective way to control the power fluctuations of DGs under unbalanced voltage [50].

This hierarchical structure consists of primary, secondary and tertiary control levels as shown in Figure 2.7. At the primary control level, voltage and frequency in the AC systems and the voltage in the DC ones are regulated. The secondary control level compensates for the deviations that are resulted at the primary level.

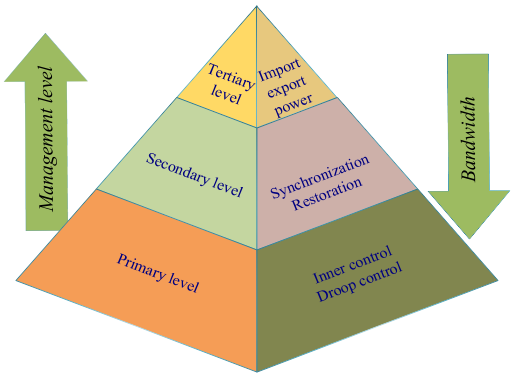

Figure 2.7. Hierarchical control levels in microgrids [7].

At the tertiary control level, the power flow between the microgrid and the whole system is defined and organised. Each of these levels will be discussed in detail in the next sections. In the literature, the power management of HMG after engaging these three control levels has not been considered yet. It is necessary to mention here that as the level of management increases, the frequency bandwidth decreases [5, 48, 51].

2.7 Hierarchical Control in the Islanded AC Microgrid

The main focus of power management and control strategies of AC microgrid is to regulate voltage and frequency and to balance power between DGs and loads and among DGs themselves. These strategies are different depending on whether the microgrid is operating in the grid-connected or stand-alone mode. When a microgrid operates in the grid-connected mode, the power exchange between the microgrid and the main grid can be classified into a dispatched or un-dispatched output power. Dispatched output power is usually regulated by a higher level of control known as optimization [7, 52]. During this mode, voltage and frequency references are determined by the main grid, and the microgrid acts as a controllable source or load from the main grid view. Furthermore, DGs and EES operate in the power control mode to track the output power signals that are controlled by regulating the DG output voltage. Unlike the dispatched mode, all the DGs operate on the maximum power point (MPP) when the microgrid works on the undispatched mode in which, all the generated power is transferred to the main grid [53].

On the other hand, the independent situation (stand-alone) mode is the focus of our research. In this operating mode, DGs and EESs are responsible for regulating voltage and frequency and managing the flow of power simultaneously within the entire microgrid. In the literature, many techniques have been proposed to realize this aspect.

This section studies and analyses the hierarchical control levels for each individual AC microgrid. Firstly, the primary control level emulates physical behaviours. Secondly, the secondary level ensures that the voltage and/or frequency be within the required range and

operator specifications. Finally, at the tertiary level, the power exchange between the microgrid and the main grid is defined [7, 54, 55].

2.7.1 Primary Control Level

Primary control level emulates the physical behaviours that make the system stable and more damped. The most common technique utilized in this level is the droop control method that is also named by autonomous, wireless, and independent control. One of the main features of the droop control method is the ability to avoid critical communication links.

The concept of this method mimics the behaviour of synchronous generators where active and reactive power varies with frequency and voltage magnitude, respectively. As active power increases, the frequency decreases. This loop also determines the exact amount of output power for each DG proportionally to its capacity.

The primary control inputs are the internal active power (P) and reactive power (Q) derived from the local measurements of voltage and current. These values are utilized in the droop control loop to adjust the frequency and amplitude of the voltage reference provided to the inner control loop [56].

The internal control loop involves primarily voltage and current control loops selected according to the classification of inverters connecting the power source to the microgrid. These inverters are categorized into voltage source inverter (VSI), consisting of outer voltage and inner current loops, and current source inverter (CSI), consisting of the phase-locked loop and inner current loop. These inverters are highly stimulating to the microgrid and have the ability to change their behaviour from the current source to the voltage source according to the purpose of these inverters [4, 57].

VSI typically operates in the islanded mode to maintain and control voltage stability, while CSI operates in the grid-connected mode to regulate the injection current to the grid. However, to achieve a stable and reliable microgrid, VSI and CSI must work together within a single system. Figure 2.8 shows an equivalent scheme of two parallel VSIs supplying a common load Z_L connected to the AC bus through the line impedances $Z_1\angle\theta_1$ and $Z_2\angle\theta_2$.

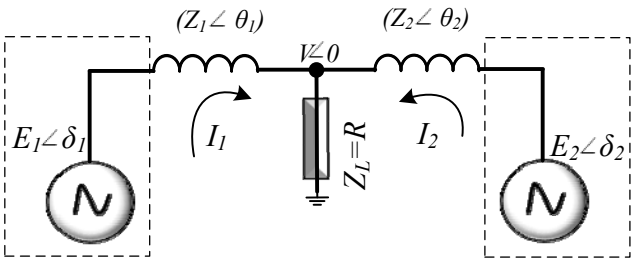

Figure 2.8 Equivalent scheme of two parallel VSIs.

The complex power transferred from each DG to the common load can be given by:

$$S = P + jQ \tag{2-1}$$

where P and Q are the active and reactive power generated from each DG, and they can be expressed as [58]:

$$\begin{aligned} P &= \frac{EV}{Z}\cos(\theta - \delta) - \frac{V^2}{Z}\cos\theta \\ Q &= \frac{EV}{Z}\sin(\theta - \delta) - \frac{V^2}{Z}\sin\theta \end{aligned} \tag{2-2}$$

E and V are the magnitude of inverter voltage and common bus voltage respectively. The equivalent of output line impedance ($Z_1\angle\theta_1$ and $Z_2\angle\theta_2$) are usually inductive (θ=90º) and

this is due to the use of a sizeable inductive filter. Accordingly, the following expressions simplify the active and reactive power obtained given that there is a slight phase difference δ between the voltage of the AC common bus V and the output voltage of the inverter E where $\sin\delta \approx \delta$ and $\cos\delta \approx 1$ [58, 59].

$$P = \frac{EV}{X}\sin\delta \approx \frac{EV}{X}\delta$$
$$Q = \frac{EV\cos\delta - V^2}{X} \approx \frac{V}{X}(E - V) \tag{2-3}$$

where X is the inverter output reactance. The above equations clearly show that the active power P is mainly influenced by the power angle δ (for example, a slight increase in δ leads to an increase in P), while Q is primarily dependent on the amplitude difference (E-V). Thus, P-ω and Q-V are an artificial droop scheme that is often adopted in the output voltage reference including frequency and magnitude. The mathematical form that expresses the droop control law can be given as follows:

$$\omega = \omega^* - \alpha(P - P^*)$$
$$E = E^* - \beta(Q - Q^*) \tag{2-4}$$

where ω is the angular frequency of the output voltage, $\omega^*$and E^* the references of ω and E. P^* and Q^* are the references of active and reactive power. These values are usually designed to be the maximum values that can be obtained at the no-load condition. α and β are the droop control coefficients that indicate the allowable frequency and amplitude variance of the output voltage references.

It is important to note here that each inverter cannot know the initial value of the phase angle (δ) of the other inverters while, in the absence of load, it is easy to adjust the initial frequency ω^*. As a result, although (2-3) shows the relationship between the effective power P and δ, ω is used instead of δ in (2-4). P^* and Q^* are usually set to zero ($P^*=0$ and $Q^*=0$) when parallel inverters are operating in the islanded mode. Notice that the angular frequency ω in (2-4) can always be replaced by frequency (f). Finally, the amplitude (E) and frequency (f) of the output voltage for the i^{th} DG (DG_i) are given as follows [51, 60]:

$$\begin{aligned} f &= f^* - \alpha .P \\ E &= E^* - \beta .Q \end{aligned} \tag{2-5}$$

Coefficient α and β should be tuned appropriately since a steeper slope will lead to better power-sharing but with wider variations in voltage and frequency. Such variations might not be acceptable in accordance with the international specific standards as in ISA-95 and electrical dispatching standards. Most literature specifies that frequency and amplitude deviations are predominantly within 2% and 5%, respectively [58]. Thus, α and β can be designed depending on the following equations [56, 61]:

$$\alpha = \frac{\Delta f}{P_{\max}} = \frac{f_{\max} - f_{\min}}{P_{\max}} \tag{2-6}$$

$$\beta = \frac{\Delta E}{Q_{\max}} = \frac{E_{\max} - E_{\min}}{Q_{\max}} \tag{2-7}$$

where E_{max} & E_{min} and f_{max} & f_{min} are the maximum and minimum allowable voltages and frequency respectively. P_{max} and Q_{max} are the maximum output of active and reactive power for each DG. If multiple inverters of different rating are used in parallel connection, the coefficient of droop control (α and β) must be adjusted so that the output power is proportional to its maximum capacity. This can be achieved by adopting the following equations [59]:

$$\alpha_1 P_1 = \alpha_2 P_2 = \alpha_3 P_3 = \cdots = \alpha_i P_i \tag{2-8}$$

$$\beta_1 Q_1 = \beta_2 Q_2 = \beta_3 Q_3 = \cdots = \beta_i Q_i \tag{2-9}$$

where P_i and Q_i are the active and reactive output power of the i^{th} DG (DG_i).

Despite the fact that inverter output impedances resulting from a large inductance filter are likely to be inductive, this is not always true for low-voltage systems that usually have a resistive impedances. The output impedance loop also affects the accuracy of power-sharing since the closed-loop output impedance depends on the control strategy used. Consequently, Eq. (2-2) can be rewritten according to the default output impedance of each inverter $Z\angle\theta$ as follows [3, 56]:

$$\begin{aligned} P &= \left(\frac{EV}{Z}\cos\delta - \frac{V^2}{Z}\right)\cos\theta + \frac{EV}{Z}\sin\delta\sin\theta \\ Q &= \left(\frac{EV}{Z}\cos\delta - \frac{V^2}{Z}\right)\sin\theta - \frac{EV}{Z}\sin\delta\cos\theta \end{aligned} \tag{2-10}$$

Thus, we can redefine the droop equation (2-4) in the standard form as [56]:

$$f = f^* - \alpha (P \sin\theta - Q \cos\theta)$$
$$E = E^* - \beta (P \cos\theta - Q \sin\theta) \quad (2\text{-}11)$$

According to (2-11), the output impedance angle θ determines the droop control law. Table 2-2 illustrates the droop control law classified according to the type of output impedance. Note that the droop coefficients are designed by recognizing the maximum (nominal) values of both P and Q as well as the maximum permissible variation in frequency and amplitude of the output voltage reference.

Table 2-2 Variation of droop control function depending on the output impedance.

Output impedance	Z=jX (inductive: θ=90º)	$Z=R$ (resistive: θ=0º)
Active power (P)	$P = \frac{EV}{X}\sin\delta \approx \frac{EV}{X}\delta$	$P = \frac{EV\cos\delta - V^2}{R} \cong \frac{V}{R}(E-V)$
Reactive power (Q)	$Q = \frac{EV\cos\delta - V^2}{X} \approx \frac{V}{X}(E-V)$	$Q = -\frac{EV}{R}\sin\delta \cong -\frac{EV}{R}\delta$
Frequency droop (f)	$f = f^* - \alpha \cdot P$	$f = f^* + \alpha \cdot Q$
Amplitude droop (E)	$E = E^* - \beta \cdot Q$	$E = E^* - \beta \cdot P$
α	$\alpha = \frac{\Delta f}{P_{\max}} = \frac{f_{\max} - f_{\min}}{P_{\max}}$	$\alpha = \frac{\Delta f}{Q_{\max}} = \frac{f_{\max} - f_{\min}}{Q_{\max}}$
β	$\beta = \frac{\Delta E}{Q_{\max}} = \frac{E_{\max} - E_{\min}}{Q_{\max}}$	$\beta = \frac{\Delta E}{P_{\max}} = \frac{E_{\max} - E_{\min}}{P_{\max}}$

From the table above, it can be seen that the control function varies depending on the output impedance. This means that when the impedance is inductive (angle θ=90º), the droop approach of *P/f* and *Q/E* should be used in the control diagram, while *P/E* and *Q/f* droop are more appropriate in the case of resistive impedance (angle θ=0º). Thus, it is important to design an appropriate output impedance not only to ensure accurate power-sharing between inverters but also to promote the complete separation (decoupling) of active and reactive power. The *P-Q* curves shown in Figure 2.9 define the droop characteristic of the amplitude (*E*) and frequency (*f*) of the output voltage for the i^{th} DG (DG_i) for inductive and resistive impedances.

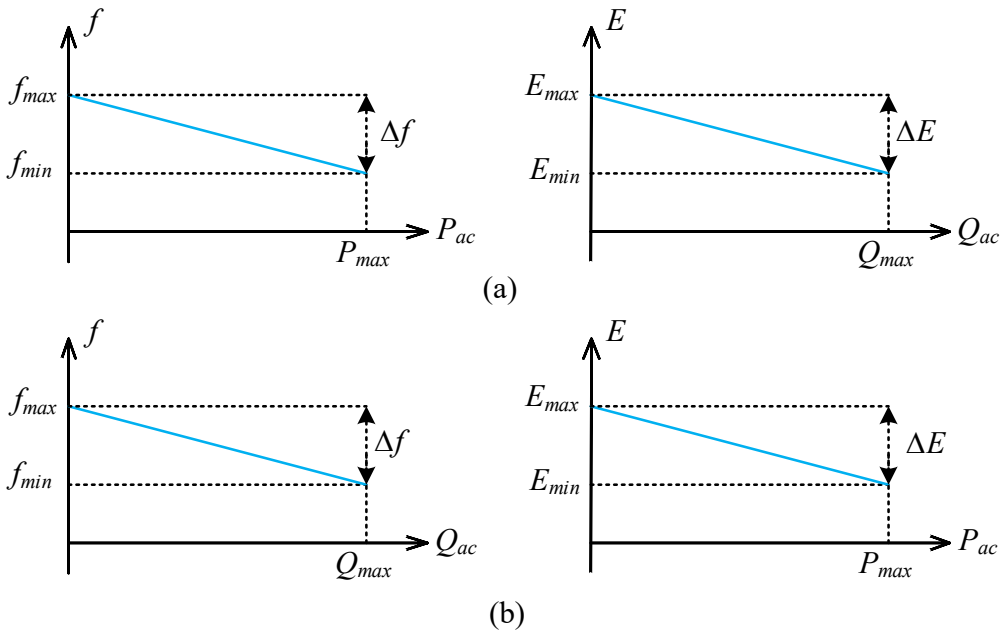

Figure 2.9 Active and reactive power droop characteristics of AC microgrid (a) inductive impedance and (b) resistive impedance.

The control diagram shown in Figure 2.10 illustrates the basic process of controlling the P&Q using the droop technique in (2-5). Active and reactive power is calculated by continuous

measurement of the inverter output voltage and current before averaging these values using a low-pass filter. The resulting filter values are then fed to the droop control method taking into account f^* and E^* references. Finally, a three-phase voltage reference is generated as an input to the voltage control loop.

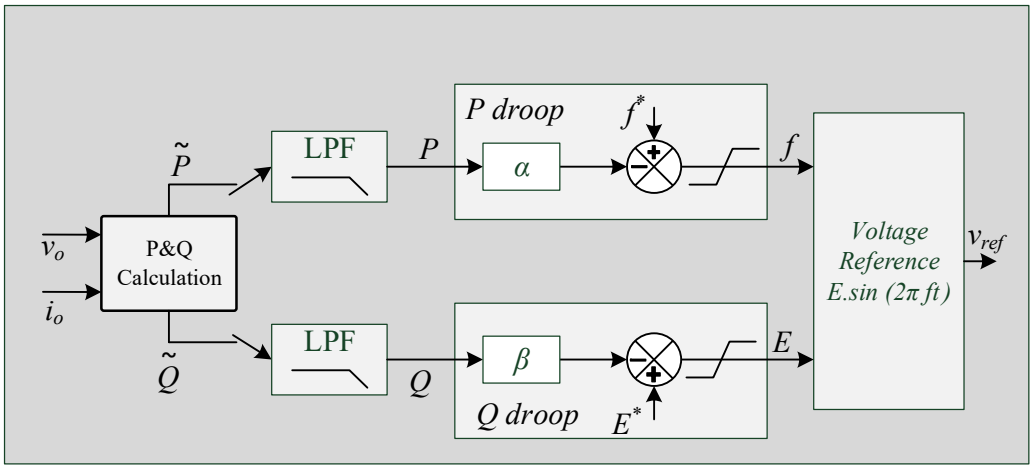

Figure 2.10 Control block diagram for the droop control scheme.

In the inverter control scheme, there are two main loops within the control loop, the outer voltage loop and the inner current loop. Unlike the current loop, which is relatively fast and controls the inverter output current, the voltage loop is slow and responsible for regulating the DC voltage link. The control strategies used in the control loops are also categorized according to the reference frame applied in the control diagram. These reference frames are natural (*abc*), synchronous (*dq*) and stationary ($\alpha\beta$) frame [62]*:*

A). Synchronous reference frame control

This reference frame is also called *dq* control frame and can be achieved by converting the current and voltage waveforms from the three-phase reference frame (*abc*) to a *dq* reference

frame that rotates synchronously with the network voltage. This makes the control and filtering process easier because the reference becomes a constant value [63]. The simplified transformation can be written using Clark's conversion equation as follows:

$$\begin{bmatrix} x_d \\ x_q \\ x_0 \end{bmatrix} = \frac{2}{3} \begin{bmatrix} \cos\theta & \cos\left(\theta - \frac{2\pi}{3}\right) & \cos\left(\theta + \frac{2\pi}{3}\right) \\ -\sin\theta & -\sin\left(\theta - \frac{2\pi}{3}\right) & -\sin\left(\theta - \frac{2\pi}{3}\right) \\ \frac{1}{2} & \frac{1}{2} & \frac{1}{2} \end{bmatrix} \times \begin{bmatrix} x_a \\ x_b \\ x_c \end{bmatrix} \quad (2\text{-}12)$$

The illustration of the *dq* control appears in Figure 2.11. The input of this diagram is the result of the droop control method. In this structure, the voltage amplitude *E* resulting from the droop control is used as an active voltage reference (v^*_{od}) to the voltage control loop. Its output (i^*_{ld}) is the reference for the active current controller, while the reactive voltage reference (v^*_{oq}) is usually set to zero if reactive power control is not allowed. On the other hand, the frequency (*f*) of the droop control is used to create the angle (δ) so that the *dq* reference frame rotates simultaneously with the voltage line frequency [62].

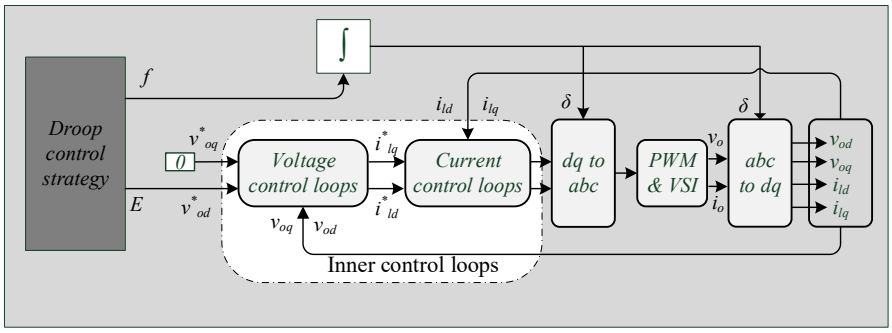

Figure 2.11 Control scheme for synchronous rotating frame strategy.

Synchronous reference frame control normally employ the proportional-integral (PI) controllers since they have satisfactory behaviour when regulating the DC variables. The mathematical equation of the matrix transfer function that expresses the PI controller in *dq* frame is given by:

$$G_{PI}^{dq}(s) = \begin{bmatrix} K_p + \frac{K_i}{s} & 0 \\ 0 & K_p + \frac{K_i}{s} \end{bmatrix} \quad (2\text{-}13)$$

where K_p and K_i are the proportional and integral gains of the controller.

B). Stationary reference frame control

The stationary reference frame is also called the *αβ* control frame. Figure 2.12 shows the schematic diagram of the implementation of this structure usually associated with the *abc* to *αβ* transformation. In this case, voltage and current waveforms are converted to *αβ* values that have a sinusoidal signal. Unlike the synchronous reference frame control, the PI control fails to remove the static state error when dealing with the sinusoidal signal [64]. Thus, the proportional resonance (PR) control unit is more common in the *αβ* reference frame. The simplified transformation can be written using Clark's conversion equation as follows:

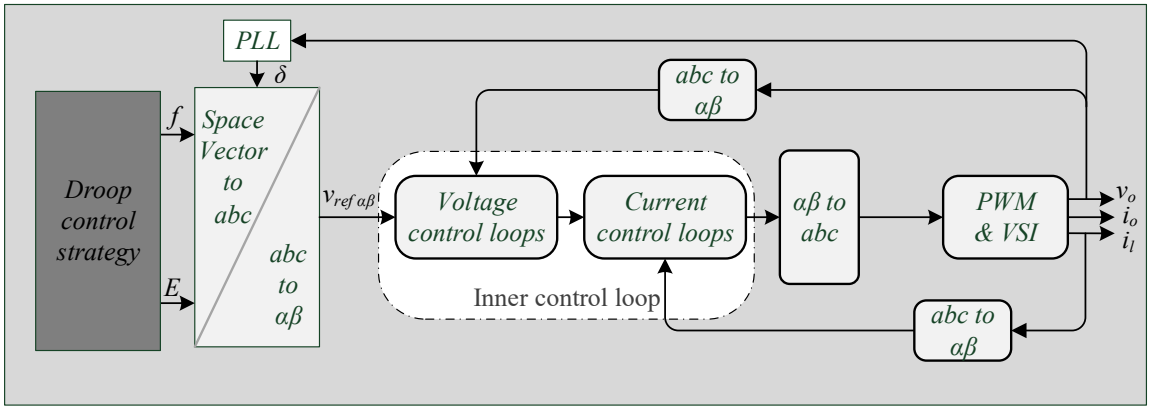

Figure 2.12 Control scheme for stationary reference frame strategy.

$$i_{\alpha\beta}(t) = \frac{2}{3}\begin{bmatrix} 1 & -\frac{1}{2} & -\frac{1}{2} \\ 0 & \frac{\sqrt{3}}{2} & -\frac{\sqrt{3}}{2} \end{bmatrix}\begin{bmatrix} i_a(t) \\ i_b(t) \\ i_c(t) \end{bmatrix} \tag{2-14}$$

The mathematical equation of the matrix transfer function that expresses the PR controller in $\alpha\beta$ frame is given by:

$$G_{PI}^{dq}(s) = \begin{bmatrix} K_p + \frac{K_i}{s^2 + \omega^2} & 0 \\ 0 & K_p + \frac{K_i}{s^2 + \omega^2} \end{bmatrix} \tag{2-15}$$

where K_p and K_i are the proportional and integral gains of the controller, ω is the resonance frequency of the controller. The performance of the dynamic characteristics of the PR controller is relatively high due to the ability to achieve high gains around the resonant frequency. Moreover, the PR control unit has the ability to eliminate the steady-state error

between the controlled signal and its references. Note that K_i determines the frequency bandwidth around the resonance point [65, 66].

C). Natural frame control (abc)

In this reference frame, each current phase is controlled separately. In this case, the control scheme should take into account differences in the connection of three-phase waveforms, i.e. star, delta with or without an isolated neutral when designing the controller. Such a structure is usually desirable when dealing with non-linear controllers such as dead beat or hysteresis due to its high dynamic performance [62].

Figure 2.13 shows a possible control block diagram where the inverter output voltage is used to detect the phase angle using a phase lock loop (PLL). The phase angle co-operates with the frequency and voltage amplitude from the droop control method to generate a three-phase reference signal. Each phase signal is compared with the corresponding measured signal, and the resulting error is fed to the controller. Both PI and PR controllers can be used in this reference frame, and each phase needs its own individual controller [67].

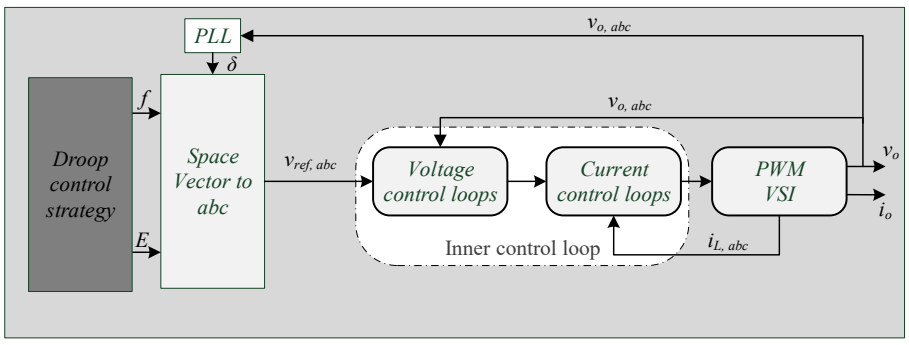

Figure 2.13 Control scheme for natural frame (*abc*) strategy.

2.7.2 Review of Improved Variants of Droop Control

Although the droop control method described above is a very attractive feature due to its ability to operate without communication among DGs, the traditional droop method still suffers from some disadvantages. These shortcomings and their corresponding solutions are summarized as follows:

A). Virtual output impedance: the multi-loop approach

Power-sharing accuracy is considerably affected by the line impedance, as discussed in previous sections. To mitigate this effect and avoid using a communication link, the virtual output impedance (Z_D) is used as a fast control loop to fix the output impedance [68]. Figure 2.14 shows the control diagram of the virtual impedance loop with respect to the inner and droop control loop. Typically, Z_D should be designed to be greater than the line impedance so that inductive behaviour can be ensured at line frequency [7].

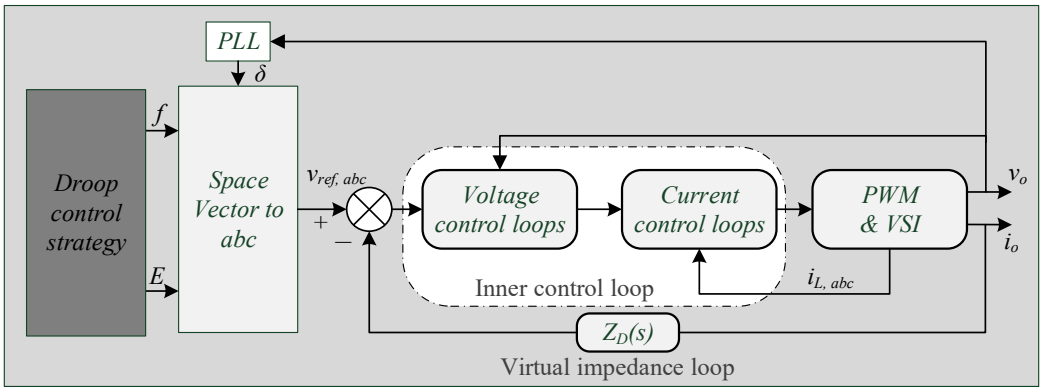

Figure 2.14 Block diagram of the closed-loop VSI with the virtual impedance loop.

Notice that the virtual impedance loop is engaged with the primary control loop in which the output voltage reference can be given as:

$$v_o^* = v_{ref,abc} - Z_D(s) \cdot i_o \quad (2\text{-}16)$$

where $v_{ref, abc}$ is the three-phase voltage reference produced from the droop control method, and $Z_D(s)$ is the transfer function of the virtual output impedance. It is important to note here that the output impedance value can be designed in the same way as the $\alpha\beta$ droop factors, according to the apparent power (S_i) of each DG and can be written as follows [58, 69] *:*

$$Z_{D1}S_1 = Z_{D2}S_2 = Z_{D3}S_3 = \cdots = Z_{Dn}S_n \quad (2\text{-}17)$$

B). Harmonic current sharing

The conventional droop control works correctly only when the load sharing is linear. However, the amount of distorted energy required by nonlinear loads is not considered in the standard approach. In fact, in nonlinear loads, the current total harmonic distortion (THD) can be up to 1.5 times the fundamental harmonic component. This means that these harmonics must be shared proportionately among parallel DGs to avoid the collapse of the entire system. To resolve this problem, the output voltage bandwidth is adjusted according to the amount of harmonic power supplied by adding an additional control loop to share nonlinear loads. This can be obtained by determining the distorted power (D) calculated from the apparent power *S*, the active power *P*, and the reactive power *Q* according to the following equation [70, 71].

$$D = \sqrt{S^2 - P^2 - Q^2} \quad (2\text{-}18)$$

Figure 2.15 shows the control block diagram of the additional loop of distorted power in which the VSI voltage and current are used as input into the distorted loop.

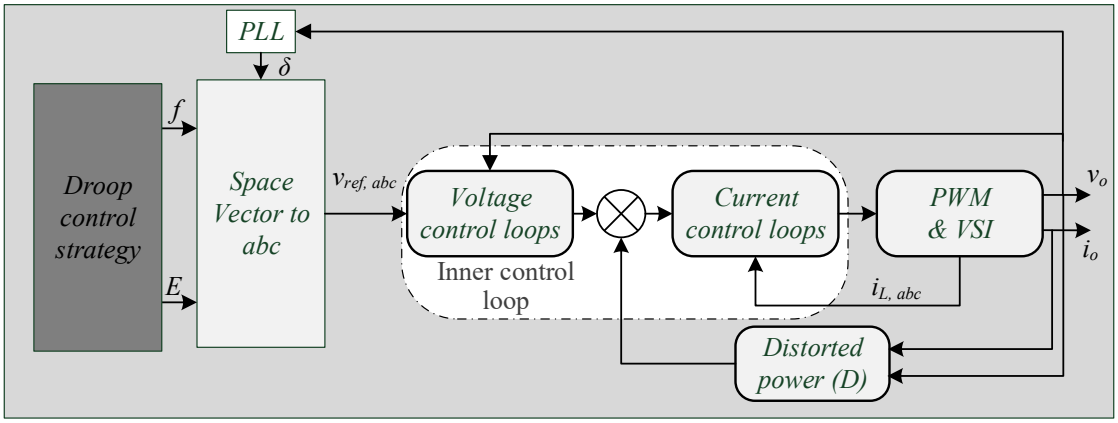

Figure 2.15 Block diagram of the closed-loop VSI with the distorted power-sharing loop.

C). Communication links

Although the lack of communication is the main feature of the droop control method, in some cases, this is considered as a drawback due to the need for sharing data and information among parallel DGs. Here are some of these cases:

- The distributed system is online to the utility network: in this case, the phase VSI parameters must be synchronized with the main grid. The communication between the DGs and the common coupling point (CCP) not only reduces the need for an additional control loop using PLL but also avoids the large circulating current among inverters which may result from minor errors in the phase measurement. Furthermore, communication is necessary to determine if there are any units separate from the system due to planned or unplanned conditions [58].
- Resynchronizing the distributed system to the main grid: when a microgrid is disconnected from the main grid due to malfunctions or for any other reasons, the DGs are able to balance the flow of power within the entire systems. However, the microgrid must be re-synchronized with the utility network after the defects are cleared. The

traditional method of synchronization proposed by some authors is to match the grid voltage phase or overload the DG units so that they are close to the main grid switch. Both solutions are unreliable and risky. It is therefore strongly recommended that DGs communicate with the main network to ensure smooth synchronization during connectivity [58, 71].

- Microgrid with multiple DGs over a large area: in applications such as microgrid, the use of many DGs distributed over a large area can lead to a parameter measurement error. This is due to the high imbalance of the power lines, which in turn contribute to a high circulating current [58].

2.7.3 Secondary Control Level

The secondary control loop is the highest level in the hierarchical structure of an islanded AC microgrid. At this level, the main objective is to compensate for the voltage and frequency deviations that are resulted at the primary level. This approach has been used to control frequency in large electrical grid systems for decades. It also contributes to global controllability of AC microgrid through the inter-communication among DGs. Different approaches have been proposed in the control architecture aspect of the secondary control level. The aforementioned control objective (eliminating the voltage and frequency deviation resulting from the primary control) is the same regardless of the strategy type used. The secondary control strategy is mainly classified into centralized and non-centralised approach [72, 73].

A). Centralized control strategy

The microgrid control is accomplished by a central controller normally called as microgrid central controller (MGCC), which is located at the global control level, as shown in Figure 2.16. MGCC collects all the microgrid parameters such as voltage, frequency, active and reactive power from its corresponding DGs, ESS and loads using a communication network connecting all hierarchical control levels [73]. MGCC then generates a reference for each element in microgrids according to the control and energy management strategy defined in the MGCC design. References are created based on the values set at the tertiary level when the microgrid is run in the grid-connected mode or are produced internally when islanding mode occurs [74]. This type of control is highly recommended only on a small scale. However, systems with a large number of devices deployed at different locations make MGCC extremely difficult especially when DGs and EESs do not have an interest in data sharing. Another drawback is that any failure of the communication links or controller may result in stopping the secondary control attainment [74].

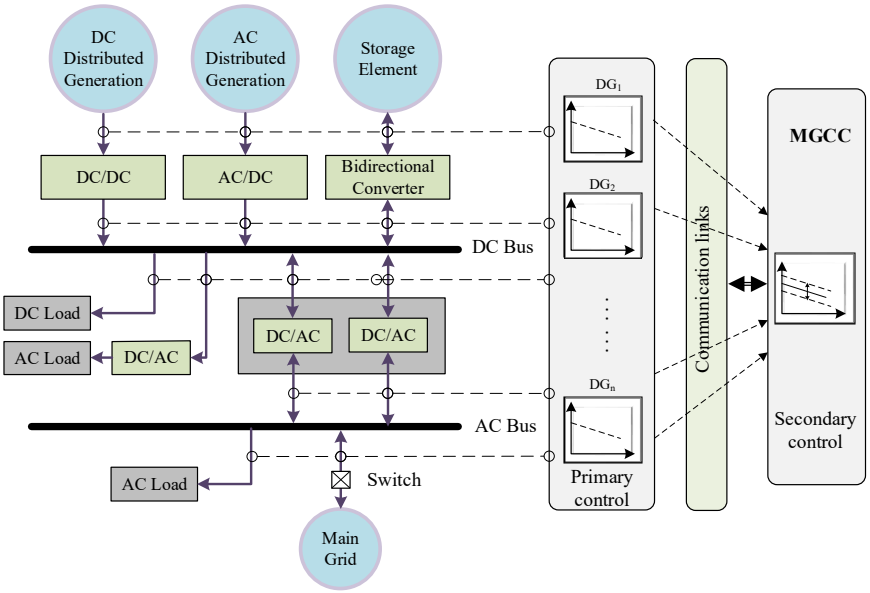

Figure 2.16 Centralized secondary control scheme in the AC microgrid.

B). Non-centralized control strategy

The idea of a non-centralized strategy is to avoid total reliance on communication between levels of control. Thus, instead of using MGCC, the control policy is implemented by integrating the primary and secondary control level into the local controller of each device. Such arrangement allows the control to overcome system breakdown when a single device failure occurs as well as improving the plug-and-play performance. The non-centralized control strategy can also be classified into distributed and decentralized secondary control [75].

- Distributed secondary control: Consensus and agent-based technologies are a typical example of this high-performance control strategy compared to other control methods. The control strategy based on this technique suggests that the control decision for each parameter depends on the local controller of each device acting as an individual agent. In this sense, relatively simple communication channels are used between adjacent units [76]. Figure 2.17 illustrates the concepts of using communication in decentralized secondary control level.

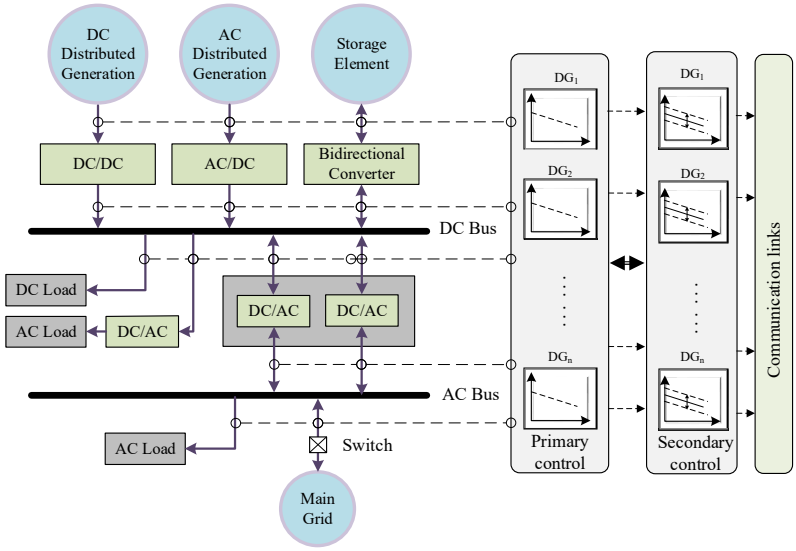

Figure 2.17 Distributed secondary control scheme in AC microgrid.

- Decentralized secondary control: Unlike the distributed controller, this control policy does not require any communication between the control level and adjacent units to regulate unit parameters. The concept of decentralization is illustrated in Figure 2.18 based on the measured local parameter to restore voltage and frequency deviations. This technology is more suitable for plug-and-play applications and power-sharing accuracy. Several techniques varying from the use of fussy inference to virtual impedance-based techniques have been proposed in the literature for decentralized secondary control [77, 78].

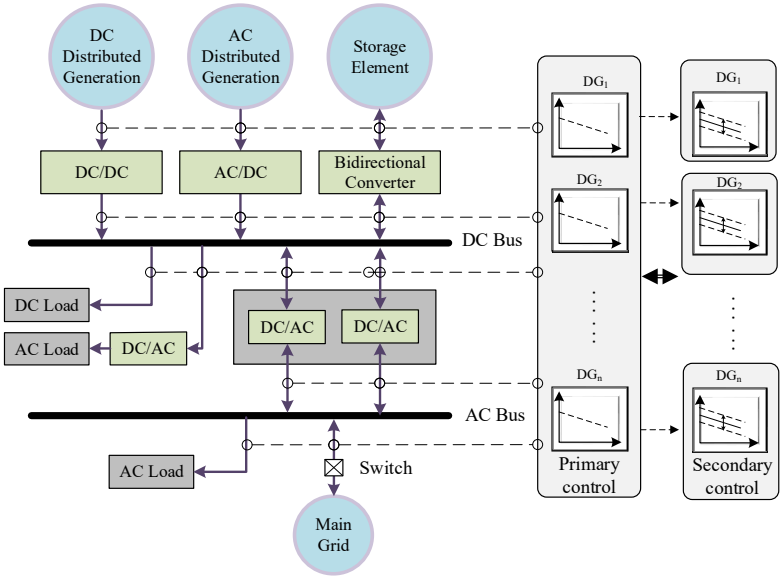

Figure 2.18 Decentralized secondary control scheme in AC microgrid.

Although the techniques used in the secondary control level differ, the main concepts of this level are to restore voltage and frequency deviation to zero after each generation or load change within the entire system. At this level, the microgrid output parameters f_{MG} and E_{MG} are compared to the microgrid references f^*_{MG} and E^*_{MG}. The resulting deviations are then accounted within the rest of the system control through a slow proportional-integral (PI) controller. This controller regulates the frequency and voltage within a specific range. The voltage and frequency restoration compensators can be derived as follows [7, 79].

$$\delta f = k_{Pf}(f^*_{MG} - f_{MG}) + k_{If}\int(f^*_{MG} - f_{MG}) \tag{2-19}$$

$$\delta E = k_{PE}(E^*_{MG} - E_{MG}) + k_{IE}\int(E^*_{MG} - E_{MG}) \tag{2-20}$$

where k_{PE} & k_{IE} *and* k_{Pf} & k_{If} are the secondary control parameters for voltage and frequency respectively. Figure 2.19 shows the block diagram of the primary and secondary control loops

for voltage and frequency in the AC microgrid. The secondary control is conventionally known as the external centralized controller that uses a microgrid reference to restore the deviation. It is worth mentioning that the ratio of the reactive power and active power-sharing is not affected by implementing the secondary control loop. The primary level can also include a virtual impedance loop that not only ensures an inductive output impedance of the converter but also eliminates the circulating current resulting from the parallel connection [9, 80].

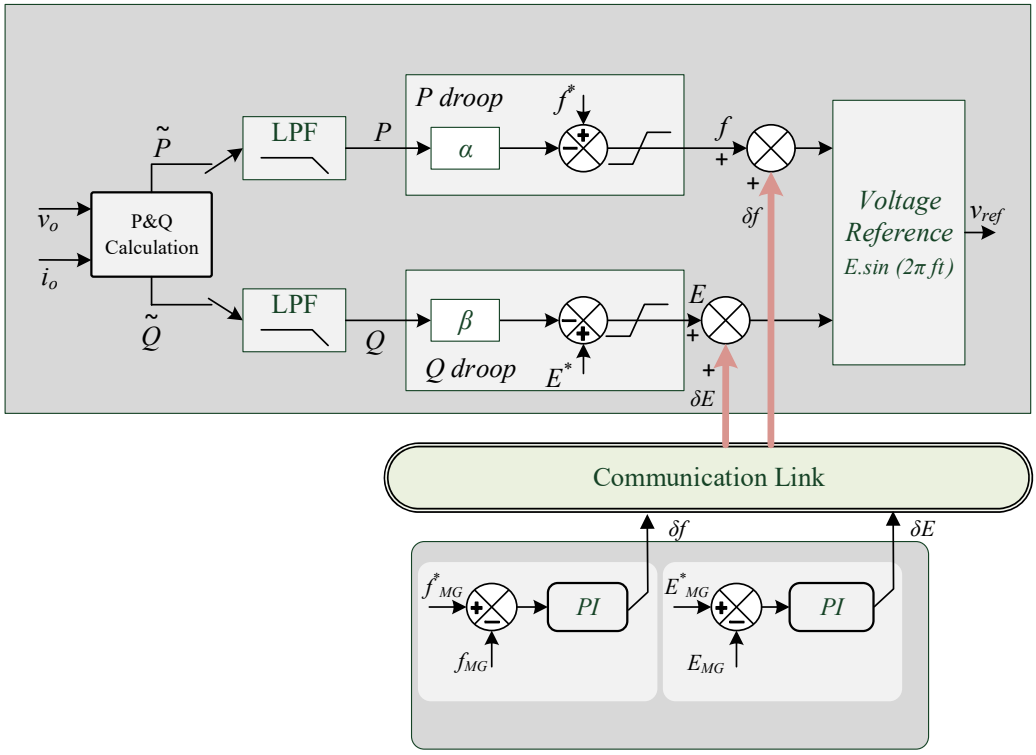

Figure 2.19 Primary and secondary control level for AC microgrid.

2.7.4 Tertiary Control

Although islanded microgrid is fully controlled by the primary and secondary control levels, in grid-connected mode, the tertiary or global control level is necessary to manage the power

flow between the microgrid and the main network. This power exchange can be regulated by controlling the voltage amplitude and frequency inside the microgrid so that the transferred power is optimal.

The tertiary level can be performed in two main categories similar to the secondary level as follows: distributed strategy where the high control algorithm is located directly in the local control unit of the microgrid, and centralized technique where the entire control is located in MGCC.

- Distributed tertiary management: communication networks in this strategy are typically used to connect devices using different facilities such as the Internet or supervisory control and data acquisition (SCADA) systems. In [81], a gossip-based tertiary control strategy was proposed to manage the flow of power between the main grid and the microgrid where the tertiary control unit is within the boundaries of the microgrid. Ref. [82] is another study which suggests a similar approach using a consensus-based technique as a tertiary control level where the three control levels (primary, secondary, and tertiary) are integrated into the local controller. The proposed approach uses one communication link between consensus-based controls and other control levels.
- Central tripartite management: In this strategy, MGCC collects the power measurement from the common coupling point and compares these values with the required references. These references are assigned according to microgrid energy status, demand, market status, optimization strategy, network generation, and forecasting issues. In [7], the authors suggest an example of central hierarchical control consisting of three levels. The measured active and reactive power are

compared with the desired parameters and the resulting references are fed to the secondary control level, which in turn is provided to the rest of the control system.

2.8 Hierarchical Control in the Islanded DC microgrid

It can be noted that there are several problems related to AC microgrids, such as reactive power flow, synchronization, inrush current in transformers, harmonic current, and three-phase unbalance. None of these problems exists in the DC microgrid, making it much easier and less complicated from the view of power management and control. Similar to AC systems, three hierarchical control levels are also adopted in DC systems to provide complete control and power management for the entire system. This section discusses and investigates the hierarchical control in DC microgrids.

2.8.1 Primary Control Level

The power management and control systems in the DC microgrid are less complicated than the AC one. It only involves the active power that varies with the DC voltage magnitude. According to the (*P/V*) droop technique, the output reference voltage V_{dc}^{ref} of the i^{th} DG can be written as:

$$V_{dc}^{ref} = V_{dc}^{*} - \lambda . P_{dc} \tag{2-21}$$

where V^{*}_{dc} is set as the maximum allowable output voltage resulting at the no-load condition, λ indicates the rate of change of the output voltage (V_{dc}) with regard to the output power (P_{dc}). In the DC microgrid, the output voltage of different DGs is slightly different, due to the limitation of droop control implementation and the voltage drop across distributed loads that

may result from the impedance of the interconnecting cable. This problem can be solved by adjusting the DC droop control by taking the cable impedance into account when designing the control system. The modified droop equation can be given as follows [18, 83]:

$$V_{dc,i}^{ref} = V_{dc}^{*} - \lambda.P_{dc,i} + i_{dc,i}.R_{dc,i} \tag{2-22}$$

where $i_{dc,i}$ is the i^{th} DG output current, while $R_{dc,i}$ is the cable resistance respectively. Coefficient λ should be appropriately adjusted as a sharp slope will result in a better power-sharing but wider voltage variations. λ can be given as:

$$\lambda_i = \frac{V_{dc,i}^{\max} - V_{dc,i}^{\min}}{P_{dc,i}^{\max}} \tag{2-23}$$

$V_{dc,i}^{max}$ and $V_{dc,i}^{min}$ are the maximum and minimum allowable value of $V_{dc,i}$ that usually lies within -6% and +10% of the nominal values [84, 85].

Figure 2.20 illustrates the effect of the DC droop coefficient on the power-sharing and voltage regulation of two parallel DGs connected to the system. It can be seen that when the droop gain is relatively small (blue line), the slight voltage deviation due to the aforementioned reasons will result in a large deviation of sources power (ΔP_2). However, similar gain will have less effect on the variance of the restricted voltage for the system to operate within a specified standard where high deviation is not acceptable. On the other hand, a steep gradient (large droop gain - black line) will result in significant variation in voltage but better performance in load sharing [86].

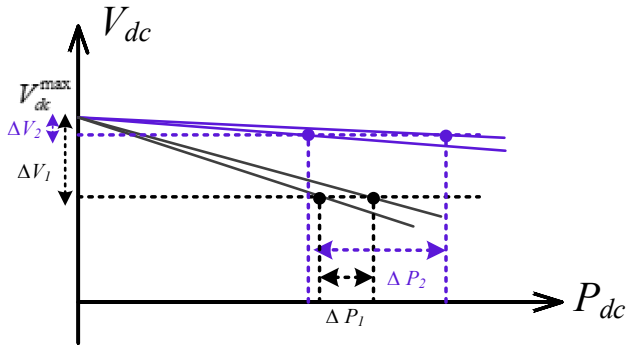

Figure 2.20 Impact of droop coefficient on power-sharing and voltage regulation.

Each DG$_i$ unit must share the total demand in the microgrid with an amount of power $P_{dc,i}$ that is proportional to its maximum power rating $P_{dc,i}^{\max}$. This can be formulated as:

$$\frac{P_{dc,1}}{P_{dc,1}^{\max}} = \frac{P_{dc,2}}{P_{dc,2}^{\max}} = ... = \frac{P_{dc,n}}{P_{dc,n}^{\max}} \tag{2-24}$$

where n represents the number of the participating DGs. The control scheme shown in Figure 2.21 illustrates the main process of adjusting the output voltage reference V_{dc}^{ref} based on the active output power (P_{dc}) of each DG using the P/V droop technique. The active power is calculated by measuring the actual DG output voltage ($V_{dc,i}$) and current ($i_{dc,i}$). The average active power is then passed through a low-pass filter before being fed to the droop control loop which takes into account the maximum allowable output voltage (V_{dc}^{*}). The output voltage reference (V_{dc}^{ref}) is then accounted within the rest of the system control where the impedance loop is triggered simultaneously to avoid voltage error in line impedance. This control system not only ensures the precise power-sharing of parallel inverters but also

improves the dynamic performance of the output voltage. Finally, the reference signal is provided to the inner voltage and current closed-loop control.

2.8.2 Secondary Control Level

Similar to the hierarchical control of the AC microgrid, at the secondary control level, the slow PI controller in the DC microgrid continuously corrects the voltage deviation resulting from the *P/V* droop control.

The microgrid voltage level is compared with the desired reference, and the error (deviation) value is fed to the slow PI controller mentioned above. The resulting signal is processed through communication links to the primary level in all parallel DGs. The following formula can express the voltage restoration parameter δV:

$$\delta V = k_{PV}(V^*_{MG} - V_{MG}) + k_{IV}\int (V^*_{MG} - V_{MG}) \qquad (2\text{-}25)$$

where k_{PV} and k_{IV} represent the PI parameters of the secondary-control compensator. Notice that δV must be limited not to exceed the maximum allowable voltage deviation. Figure 2.21 shows the block diagram of the primary and secondary control loops for voltage in the DC microgrid. The variation of secondary control schemes discussed in AC systems can also be adopted in the DC microgrid, bearing in mind that communication links mediate DC voltage deviations only.

However, the use of communication at the secondary control level is not always the case. Several studies in the literature suggest a different technique to avoid the use of communication channels [87]. The master/slave and concentrated/central control method are proposed as communication-based control techniques [88, 89]. On the other hand,

conventional and sophisticated line impedance droop methods are introduced as droop based techniques [90]. In [91, 92], a decentralized control strategy is introduced based on the *V/I* droop control technique with the absence of any communication among DGs.

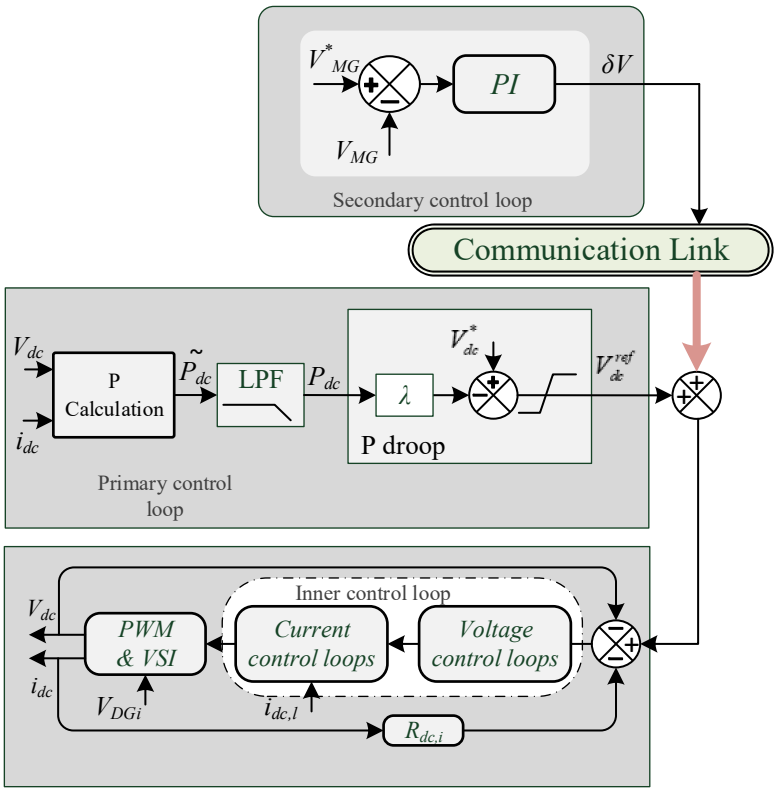

Figure 2.21 Primary and secondary control level for DC microgrids.

2.8.3 Tertiary Control Level

When the tertiary level is activated, and the microgrid is connected to the main grid, the inverter connecting the DC bus and the AC bus acts as a bidirectional converter. The amount of power transferred is determined by the highest level of control according to the demand and power generation in both the microgrid and the main grid. In this work, the focus of control and power management is limited to the islanded operating mode, so no in-depth discussion of this level is required in this section.

The combination of AC and DC microgrids would result in a HMG that is more economical and reliable than individual systems. The main issue of such system is the coordination and control of the power-sharing that takes place through the ILCs. The converter manages the active power transfer in a way that ensures the highest stability for the whole system. The operation of ILCs is a significant issue that must be addressed in detail through the emphasis on finding control technology so that it can work optimally.

2.9 Summary

In this chapter, a review of microgrid topologies, components, power managements and control structure has been presented. Based on the literature review, previous studies have focused on optimising the power flow in the microgrid without considering the detailed hierarchical control of hybrid structure. The review of the main control systems and the strategy used in both AC and DC microgrid is essential to build a sound understanding of the comprehensive HMG control and energy management strategies which is presented in the following chapter.

Chapter 3

Power Management and Hierarchical Control Coordination Strategy for Autonomous Hybrid Microgrids with Multiple Sub-Microgrid

Power management and hierarchical control coordination strategy of autonomous HMGs consisting of multiple AC and DC SMGs with different voltage levels are the focus of this chapter. Aiming to limit the continuous operation of ILC in all load conditions, an improved power management strategy has been proposed. Thereby, it avoids the significant power loss on the ILCs that adversely affects the operational feasibility of the HMG. The hierarchical coordination of power management and control strategy for autonomous HMG is introduced and analysed. The designed system includes both the primary and secondary control levels to ensure a seamless and accurate transfer of power among the SMGs. A new technique to ensure the continuous power flow among the SMGs while minimising the continuous operation of the ILCs in the islanded mode is presented with a focus on the secondary control level.

3.1 Background and Literature Review of Control Strategies in HMGs

Although many research in the literature studied power management and control strategies in the microgrid, only a few of these studies focus on the HMG structure. This section discusses the most important strategies in this area. HMG control strategies must fulfil a microgrid

characteristic such as protection, stability, reliability, power balance, synchronization and optimization. Therefore, these strategies are the major challenges in HMGs. As in an individual microgrid, a hierarchical level control strategy is also adopted for the HMG. Many of the studies introduced here has been originally mentioned on an individual microgrid network, but have also found feasible for the hybrid structure.

In the aspect of HMG, the importance of regulating the voltage and/or frequency at each side of the HMG is stressed. This motivates a proportional sharing of active power among DGs and among AC and DC SMGs. Several control and normalization techniques are developed for controlling and managing the bidirectional power flow. Extensive research has been devoted to new techniques of modifying droop control methods to compare the voltage at the DC bus and the frequency at the AC bus [35, 93-96]. The common concept of such methods is that the transferred active power from one SMG to another is based on the surplus power of each SMG. The result of this comparison determines the direction and amount of power delivered or absorbed. However, such methods are still dependent on the droop control method through which the surplus power is determined. In other words, this method is mainly used when the MG operates at the primary control level only where the voltage and/or frequency slightly vary with the active power at each side.

To improve the power quality and achieve a higher level of stability in all microgrid structures, it is strongly recommended to implement analysis in accordance with a sequential hierarchy of control. The hierarchical control scheme is an efficient method to control the power oscillations of DGs under unbalanced voltage [50]. This hierarchical structure consists of primary, secondary and tertiary control levels as discussed in Chapter 2. At the primary control level, the voltage and frequency in the AC systems and the voltage in the DC ones are

regulated. The secondary control level compensates for the deviations that are resulted at the primary level. At the tertiary control level, the power flow between the microgrid and the whole system is defined and organized. In the literature, the power management of HMG with engaging these three control levels has not been considered yet. It is necessary to mention here that as the management level increases, the frequency bandwidth decreases [5, 48, 51]. These control levels collaborate to regulate the frequency and voltage amplitude of the AC bus and the voltage of the DC bus, and thus manage the power flow between the AC and DC buses.

Previous studies have focused on optimising the power flow in the HMG without considering the detailed hierarchical control. The operational viability for the ILCs in the islanded microgrid under different loading conditions is not yet explored in detail. Furthermore, the HMG structures proposed in most of the literature are limited to linking a single AC and DC SMG. This chapter focuses on developing an improved power management scheme for HMGs that essentially manages the power exchange between SMGs when the system operates under the primary and secondary control levels. The challenge in this arrangement is the coordination of various control strategies and the bi-directional ILC with multiple AC and DC SMGs. The main purpose of the converter's controller is to coordinate the operation of SMGs in the system. It can regulate the exact amount of power that will be delivered or absorbed in accordance with the power-load balance across the SMGs. The major contributions proposed in this chapter are listed as follows.

1) A modified and progressive power flow tuning strategy for power management and control of the HMG at the primary control level is developed. Based on this strategy, the priority of each SMG is to manage the power flow within its local boundary avoiding any

unnecessary operation of the ILC, thus reducing the significant power loss on the ILC that adversely affects the operational feasibility of the HMG.

2) A new control technique is proposed to ensure the continuous power flow among the SMGs when the HMG operates at the secondary control levels. Therefore, a hierarchical control coordination for the HMG in the islanded mode is employed as an essential stage in the proposed method.
3) A new technique is proposed to define the parameters (voltage and frequency) that represent the exact active power transfer at the secondary control level. These parameters are used as a reference to the ILC initiating the required power transfer across the SMGs.

The primary level control in HMGs is mostly classified into two types depending on their function, namely grid-forming and grid-following/feeding strategies as presented in [97, 98]. In this sense, the control strategy not only focuses on controlling the AC and DC sides of the microgrid but also the ILCs [39].

3.1.1 Grid-Following/Feeding Control Strategies

In this strategy, the microgrid operates in the grid-connected mode, so the voltage and frequency references are set by the main grid. In this case, the responsibilities of local controllers are to extract as much power as possible from power sources– e.g. maximum power point tracking in PV or wind systems [97]. Although this type of control is more common in such a strategy, voltage and frequency references are not always determined by the main grid. In some cases, these values are established by higher levels of control such as optimization that improves the power-sharing within the entire system [99].

3.1.2 Grid-Forming Control Strategy

Under this strategy, when the HMG operates in the islanded mode, the voltage and frequency are determined by DGs and ESS units. One or more ILCs can be used to connect the AC and DC buses together and the AC bus with the main grid. Several studies in the literature distinguish whether or not of employing the communication between ILCs within an individual system [100, 101]. Master/slave, concentrated control, central, and instantaneous current sharing are some of the techniques that use communication, which in turn usually rely on the regulation of active load sharing [102]. On the other hand, droop-based control is one of the most common strategy proposed in the literature where no communication is used in all of the microgrid structures at the primary control level.

A lot of research efforts have been focused on this topic, not only due to the advantages it has over other control alternatives in individual microgrids, but also because of its ability to engage in hybrid AC/DC systems [7]. Normalization process of AC frequency and DC voltage are used in some studies to manage the power flow through the ILC [35, 61, 93]. Another study that relies on a decentralized method of power-sharing through the use of a droop control method to regulate the ILCs in the island mode is presented in [103]. Apart from droop-based control, some other studies [104, 105] suggest a power management strategy based on the theory of instantaneous power where no communication is required.

3.2 Hybrid AC/DC Microgrid Structure

Figure 3.1 illustrates the proposed hybrid AC/DC microgrid structure. The microgrid is composed of an AC SMG and two DC SMGs with different voltage levels. The AC bus works

as a common bus that links other SMGs and mediates any power exchange that takes place. This configuration of HMG will be used throughout this chapter. Each SMG should have the ability to manage the power flow in accordance with its own respective load. The surplus power will be transferred to other MGs to compensate for any power shortage. Six IGBT-Diode switches are used for the ILC which acts as a bi-directional converter and operates in two modes depending on the direction of the power flow. In mode one, when it acts as a rectifier, the DC side is viewed as a load from the AC side, and the power flows from the AC side to DC side. On the other hand, in mode two, when the ILC works as an inverter, the AC side is regarded as a load from the DC side point of view, and the power flows in the opposite direction. The amount of transferred power from one SMG to another depends mainly on the supply (DGs' output) and the demand (load) in each SMG [43] .

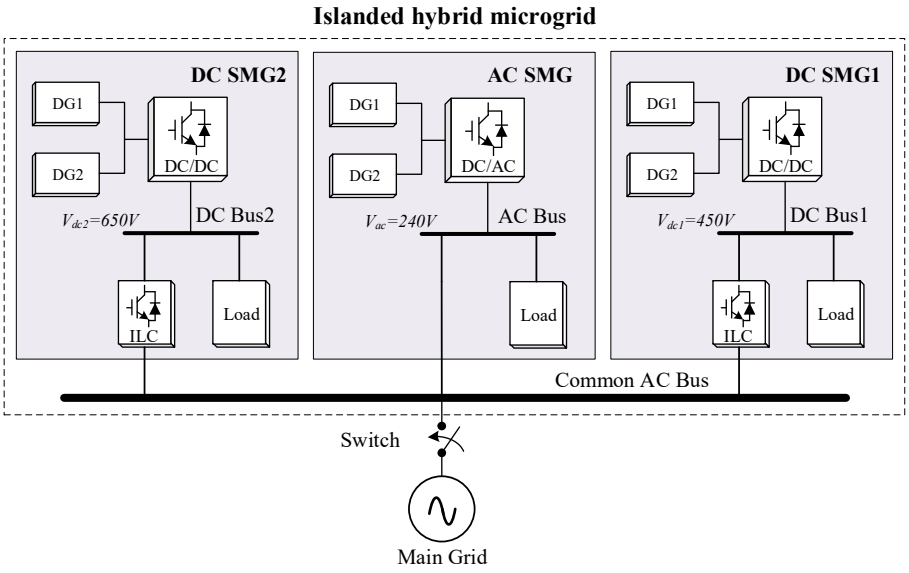

Figure 3.1 HMG structure with multiple SMGs.

There are many advantages of adopting such a hybrid structure (multi–SMG). It can reduce the total cost by reducing the required conversion devices, thus reducing the total conversion losses due to the elimination of redundant stages of power conversion and further improving the overall system efficiency. Connecting more SMGs to the HMG will increase the total power capacity and lead to the improved system reliability.

3.3 Power Management Coordination in Hybrid AC/DC MG

The HMG should be able to operate in both the islanded and grid-connected mode. However, this chapter focuses on the islanded mode which is more challenging. It represents a more realistic situation for a rural or urban area where renewable energy could be the main source. The power management of HMG is analysed at the primary and secondary control levels. The main aim is to manage a specific amount of active power from one SMG to another in response to any contingencies in any part of the system.

The principle of the droop control method is implemented to control the ILCs that link the AC and DC buses in an autonomous operation mode. The general idea of the proposed power-sharing strategy is that each SMG manages its own power flow and the surplus power is delivered to other SMGs based on the conditions of interfaced SMGs. When the power flows from the AC to DC side, the ILC works as a parallel DC source that feeds the load of DC SMGs. The same also applies in the opposite direction when the power flows from the DC to AC side. The continuous operation of ILC under all conditions could result in a significant power loss on the ILC that adversely affects the operational feasibility of HMGs. Based on the power-sharing method described above, the following points highlight the main keys of a more feasible power exchange strategy in the HMG.

1. Power exchange should only happen when at least one of the SMGs is over-loaded, and incapable of supplying the shortage autonomously.
2. The transferred power should be proportional to the excess power of supplying SMGs.
3. Power exchange will be limited when all the SMGs have excess power, or all have a shortage in supply.

The key determinants of power exchange strategy in the HMG are the frequency (f) at the AC bus and the voltage (V_{dc}) at the DC bus. These indices give a clear vision of the power situation in the AC and DC SMGs following the droop control method discussed in Chapter 2. The next sub-section discusses the process of employing these parameters in the power transfer at the primary and secondary control levels. The idea of this method was initially proposed for the primary level in [35].

3.3.1 Power Management and Control Coordination at the Primary Level

The main aim of this level is to define the amount of surplus power in each SMG and then define the exact amount and direction of the delivered power. This can be done by utilizing the frequency and voltage variations at the AC and DC sides respectively while satisfying the power exchange conditions as discussed earlier. The following steps list the sequential process of the power transfer:

(i). The individual droop curves of all DGs in an SMG are combined into one equivalent curve that represents each individual SMG. The resulting curve represents the total capacity of active power in each SMG as shown in Figure 3.2(a). For the resulting curve, the output frequency f at the AC SMG and the voltage V at the DC SMG can be given as:

$$f = f^* - \alpha_t P_{ac,t}, \quad \alpha_t = \frac{1}{\sum_{i=1}^{n} \frac{1}{a_i}}$$
$$V = V^* - \lambda_t P_{dc,t}, \quad \lambda_t = \frac{1}{\sum_{i=1}^{n} \frac{1}{\lambda_i}} \tag{3-1}$$

where α_t and λ_t represent the equivalent droop coefficients for the total output active power ($P_{ac,t}$ and $P_{dc,t}$) of all the DGs within the corresponding SMG. λi and αi are the active power droop coefficients of ith DG in the DC and AC SMG respectively.

(ii). The normalization process technique is used to bring these indicators (V, f) to a standardised scale and a common per unit (p.u.) range. The resulting values could then be compared together as a standardised indicator of the power condition. The mathematical expression of the normalization technique for frequency f' and voltage V' can be given as:

$$f' = (f - f_{\min}) / (f_{\max} - f_{\min})$$
$$V' = (V - V_{\min}) / (V_{\max} - V_{\min}) \tag{3-2}$$

where f and V are the SMG frequency and voltage respectively resulting from the previous step. $f_{\max}$ & $f_{\min}$ and $V_{\max}$ & $V_{\min}$ are the maximum and minimum allowable frequency at the AC SMG and voltages at the DC SMG respectively. These variables are discussed in Chapter 2 in detail (Section 2.7)

(iii). The normalised individual variation scales of the output voltage at the DC side and frequency at the AC side should be identical, that is, between 0 and 1 as illustrated in Figure 3.2(b). At the no-load condition, the frequency in the AC grid will reach its maximum rate $f_{\max}$ and at the normalized value $f'_{\max}$=1. The same applies for the $V_{\max}$ for

the DC SMG. The calculated parameters f' and V' in (3-3) represent the normalised excess power relative to the generation capacity for both the AC and DC SMGs (see later discussion on Eqs. (3-3) & (3-4), that is, the power that could be transferred among the SMGs after covering their own local demand.

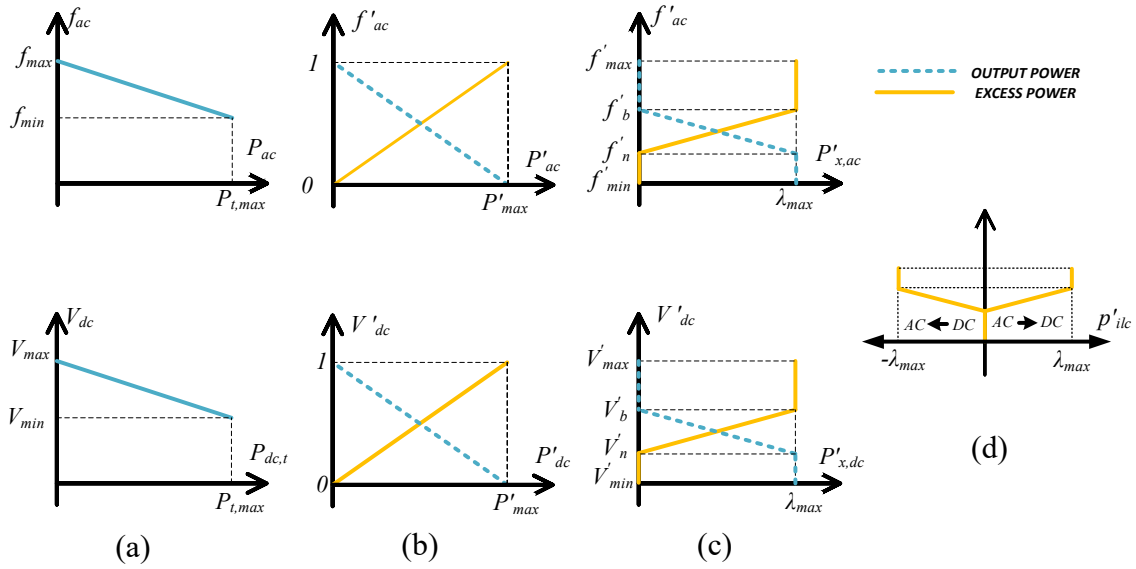

Figure 3.2 Normalized AC and DC droop characteristics for HMG (a) SMG total power, (b) normalization process, (c) multiple regions of control, (d) per unit transferred power.

(iv). As in Figure 3.2(c), an approach that separates the operational band into multiple regions of control is used for this part of the proposed scheme. The normalized values are divided into three regions: under-loaded region, loaded region and over-loaded region. This helps avoid any unnecessary operation of the ILC and increase its lifespan. These regions are defined in accordance with the power exchange conditions mentioned earlier. To express these determinants of separation in a mathematical form, Eqs (3-3) & (3-4) represent the normalised excess power transferable by the AC SMG ($P'_{x,ac}$) and DC SMG ($P'_{x,dc}$).

$$P'_{x,ac} = \begin{cases} \lambda_{\max}, \text{ when } & f'_b \le f' < f'_{\max} \\ (f' - f'_n), \text{when } & f'_n < f' < f'_b \\ 0, \text{ when } & f'_{\min} < f' \le f'_n \end{cases} \quad (3\text{-}3)$$

$$P'_{x,dc} = \begin{cases} \lambda_{\max}, \text{ when } & V'_b \le V' < V'_{\max} \\ (V' - V'_n), \text{ when } & V'_n < V' < V'_b \\ 0, \text{ when } & V'_{\min} < V' \le V'_n \end{cases} \quad (3\text{-}4)$$

where $\lambda_{\max}$ is the maximum p.u. transferred power. It is set as 0.8 to ensure the system stability in cases of unplanned additional load for the supplying SMG. f'_b and V'_b are the threshold points in the AC and DC SMGs at which the SMG's ability to supply excess power decays as the load increases. f'_n and V'_n are the threshold points at which the SMG is fully loaded and incapable of supplying any excess power. They are set to be 0.2 p.u. (20% of the supply capacity is kept as a reserve for unplanned loads). The transferred power through the ILC (P'_{ilc}) is the difference between the excess power in the AC and DC SMGs ($P'_{x,ac}$ and $P'_{x,dc}$). For example, when both interfaced AC and DC SMGs operate in the under-loaded region, $f'_b \le f' < f'_{\max}$ for the AC SMG and $V'_b \le V' < V'_{\max}$ for the DC SMG, both SMGs could supply the maximum excess power $\lambda_{\max}$. However, the actual transferred power will be zero since each SMG can supply its own load according to (3-3) & (3-4). Once the load at the DC SMG increases, the generation power will supply the new load and V' will naturally decrease. When V' drops beyond the V'_b point (loaded region) while the AC SMG is in the under-loaded region, the power management strategy will trigger a power transfer from the AC SMG to the DC one. This strategy not only avoids the over-load risk of DC SMG, but also maintains an

elevated system stability. The amount of transferred power P'_{ilc} in such a case can be given in accordance with the following equation:

$$P'_{ilc} = P'_{x,ac} - P'_{x,dc} \tag{3-5}$$

Table 3-1 concludes the previous description of normalized values for the interfaced SMGs and the p.u. amount of transferred power for each scenario. It is important to mention that in the case of multiple SMG clusters, the AC bus will act as the common bus, functioning as the AC SMG above.

Table 3-1 Summary of power transfer among multi-region bands.

	$f'_b < f' < f'_{max}$	$f'_n < f' < f'_b$	$f'_{min} < f' < f'_n$
$V'_b < V' < V'_{max}$	0	$(f' - f'_n) - \lambda_{max}$	$-(\lambda_{max})$
$V'_n < V' < V'_b$	$\lambda_{max} - (V' - V'_n)$	$(f' - f'_n) - (V' - V'_n)$	$-(V' - V'_n)$
$V'_{min} < V' < V'_n$	λ_{max}	$(f' - f'_n)$	0

Moreover, all the DC SMGs would be linked directly through the ILCs to the AC common bus. The power sharing among SMGs through individual ILCs still follows (3-5), coordinated by the common frequency at the AC common bus. According to (3-3) and (3-4), P'_{ilc} will be zero when both SMGs operate in the under-loaded region or in the over-loaded region. The maximum power exchange occurs when one SMG is over-loaded and the other SMG is under-loaded, and the transferred power will be 0.8 of the maximum generation of the under-loaded SMG (see Figure 3.2(d)). This value is chosen carefully to allow the under-loaded SMG to

respond to any sudden or unplanned load changes. The last step in this scheme is to convert the p.u. value to the actual value (P^*_{ilc}) using the following equation.

$$P^*_{ilc} = \begin{cases} P'_{ilc} \times P^{\max}_{dc} & \text{when, } P'_{ilc} < 0 \\ P'_{ilc} \times P^{\max}_{ac} & \text{when, } P'_{ilc} > 0 \end{cases} \tag{3-6}$$

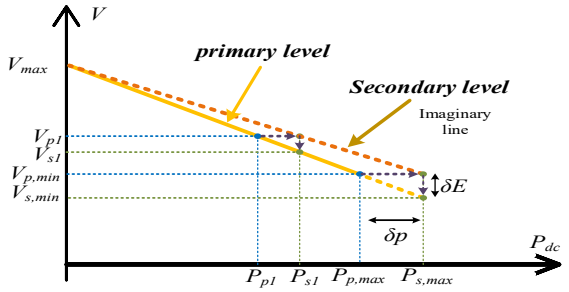

(a)

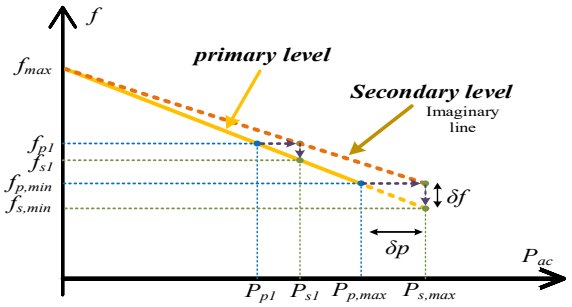

(b)

Figure 3.3 The proposed method of ILC reference during secondary control (a) Voltage reference (b) frequency reference.

3.3.2 Power Management and Control Coordination at the Secondary Level

A). Problem formulation:

During the islanded operation mode, the secondary control level is considered to be the highest level in the hierarchical control. After engaging the secondary control level for the

AC and DC side, the frequency and voltage will be restored towards an external or standard reference in response to respective changes in the load and generation. Accordingly, the standardized values of frequency (f') and voltage (V') parameters found through the primary level no longer reflect the amount of active power at each SMG. This would limit any power transfer among the SMGs. As a solution, a new technique is proposed. This remedy re-defines the parameters to reflect the amount of actual power at the secondary control level and use these values as a power references to the ILCs. It's implicitly understood throughout this chapter that once the secondary control level is engaged, the primary control level has already been engaged. Accordingly, in this section, the term secondary control level refers to primary and secondary control levels together.

B). Proposed method:

The frequency and voltage are the major keys of the transferred power at the secondary level as well as the primary level. The idea of the proposed method is to build an imaginary droop line, as the red line shown in Figure 3.3(a) and (b), to represent the exact active power during the secondary control level. This addition will help identify the voltage and frequency values that reflect the actual amount of power and act as a reference to the ILC, thus initiating the required power transfer from one SMG to another. The next two subsections detail the proposed method.

1) The DC voltage reference for ILC at the secondary control level.

When activating the secondary control at the DC side, a small increase in the active power (δP) is noted. Such an increase is triggered by the rectification of the voltage deviation that takes place at the secondary level (Figure 3.3). The term P_p represents the amount of output

power during the primary control only, while P_s represents the amount of output power after the secondary control is engaged. Thus, the *supposed* voltage reference at the DC side that reflects the amount of power at the secondary level will be V_s. This value serves as an indicator of the DC SMG output power. The term "*supposed*" is used here to represent the values of f_s and V_s needed in order to generate the delivered power references for the ILCs. It must be noted that these values might not reflect the "actual" values of V and f. The actual values (V, f) are eventually regulated by the secondary control discussed earlier. The formula that signifies the *supposed* voltage reference can be given as:

$$V_s = V_{\max} - \lambda_t . P_{dc,s} \tag{3-7}$$

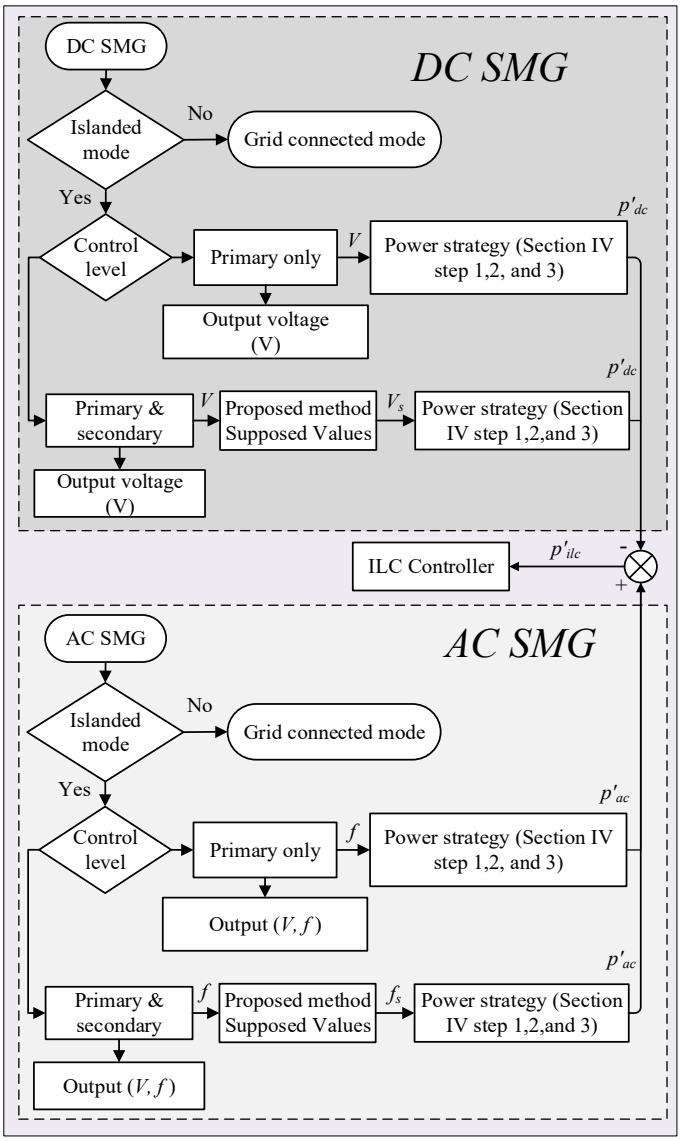

Figure 3.4 Proposed control process and power management flow chart

It is important to mention that the power difference between the primary and the secondary level relies heavily on the droop control coefficient of the total capacity of the SMG (α_t and λ_t) given in (3-1).

2) Frequency reference of the ILC at the secondary control level.

Frequency is the second reference needed in order to define the power reference of the ILC. Figure 3.3(b) illustrates the proposed method to determine the *supposed* frequency reference f_s. It is similar to the procedure used in the previous section but to produce the reference frequency f_s as follows.

$$f_s = f_{\max} - \alpha_t . P_{ac,s} \tag{3-8}$$

where $P_{ac,s}$ is the output active power resulted in the AC SMG through the secondary control level. Once the *supposed* voltage and frequency values are defined at each side of the HMG, the same steps used in the sequential process of power transfer at the primary level are implemented with f_s and V_s replacing V and f in (3-1).

Figure 3.4 summarizes the sequences of proposed control process and power management strategy presented in this chapter. Again, the references V_s and f_s found through the secondary control level of both the AC and DC SMGs, are used only for power transfer proposes. The actual values of voltage and frequency at the AC and DC buses are set according to the secondary references *(V, f)* found in Section 3.3.1 and not the supposed ones that are only for power transfer purposes.

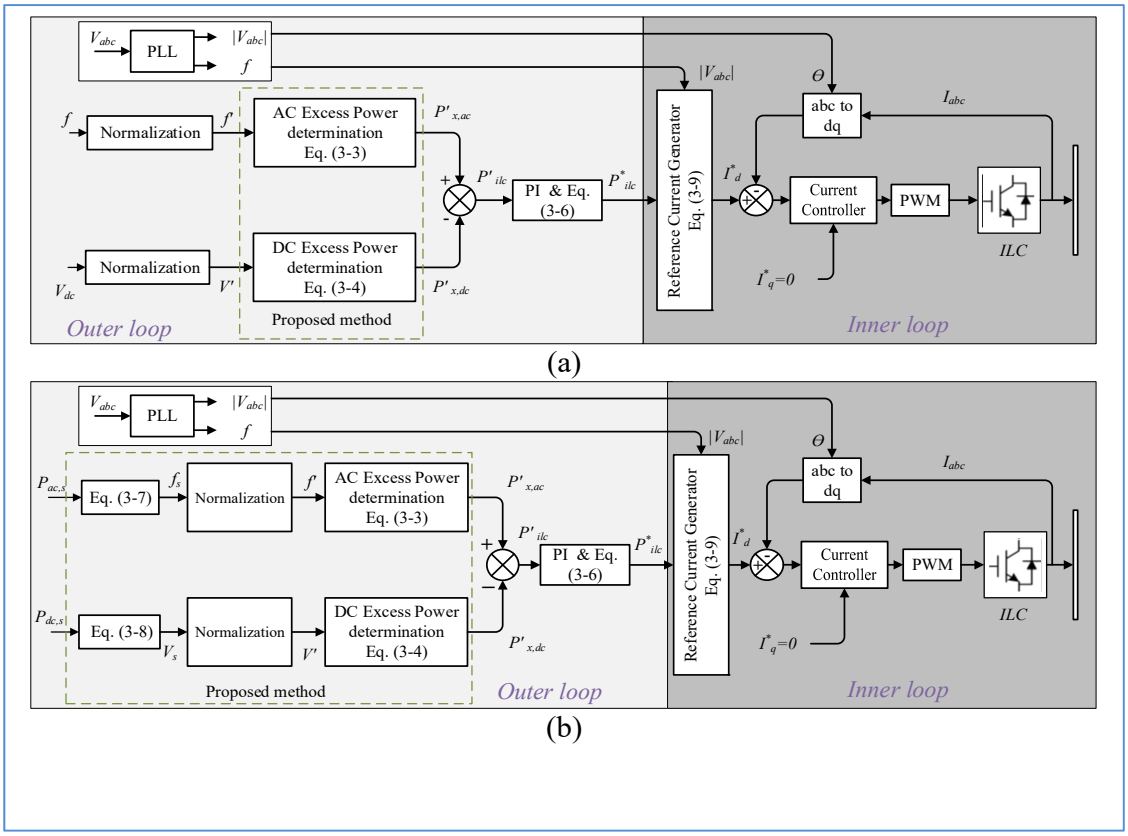

Figure 3.5 (a) Control block diagram for primary control level, (b) Control block diagram for primary and secondary control level

3.3.3 Interlinking Converter Control

Figure 3.5 shows the detailed block diagram of the ILC control for both the primary only and the combined primary and secondary control levels. The following steps illustrate the control process in detail. Within the primary-level proportion of the block diagram, many processes take place. Firstly, a PLL is used to detect the frequency (f), phase angle (θ), and the voltage magnitude of the three-phase voltage ($|V_{ac}|$). Secondly, the voltage of the DC SMGs (V_{dc}) is sensed. Then, the measured parameters are converted to their p.u. values using the normalization formula (3-2). After that, the multi-region band is defined to segment the ILCs

operation as given in (3-3) and (3-4). The differences between the values (f', V'_{dc}) are used to determine the reference power (P'_{ilc}) that is then processed by the PI controller.

The sign of the merging process gestures the direction of power flow. The reference power (P^*_{ilc}) is then found through (3-6) and then converted to the active reference current (I^*_d) as in (3-9).

Table 3-2 Parameters of HMG and Control System.

Unit	Parameters	Simulation
AC SMG	$P_{ac}{}^{max}$	8 kW
	$Q_{ac}{}^{max}$	2 kVAR
	f^{max}	51 Hz
	f^{min}	49 Hz
	$\|V^{max}\|$	240 V
	$\|V^{min}\|$	220 V
	α_i	2.5×10^{-4}
	β_i	1×10^{-3}
DC SMG 1	$DG_1{}^{max}$	4 kW
	λ_1	12.5×10^{-3}
	$DG_2{}^{max}$	6 kW
	λ_2	8.33×10^{-3}
	$P_{dc}{}^{max}$	10 kW
	$V_{dc}{}^{max}$	650 V
	$V_{dc}{}^{min}$	600 V
DC SMG 2	$P_{dc}{}^{max}$	10 kW
	$V_{dc}{}^{max}$	450 V
	$V_{dc}{}^{min}$	400 V
	λ_1	5×10^{-3}

$$I_d^* = \frac{2\times P^*_{ilc}}{3\times|V_{ac}|} \tag{3-9}$$

Here, P^*_{ilc} and $|V_{ac}|$ represent the delivered power and the AC voltage magnitude, respectively. The active current reference (I^*_d) is then supplied to the inner control loop. The current control

loop, which is part of the double control loop, is used in conjunction with the modified vector decoupling control technique [85]. This is implemented by feed-forwarding the line voltage components to achieve better performance. It also facilitates decoupling the active and reactive power control and allows operation at a unity power factor when the reactive reference current (I^*_q) is set to zero. The output of the double control loop, *dq* components of the reference voltage, is then transformed into its corresponding *abc* components.

The main difference between the block diagram of the primary control only (Figure 3.5(a)) and the combined primary and secondary control (Figure 3.5(b)) is the supposed values f_s and V_s discussed earlier and obtained before the normalization process takes place.

3.3.4 Simulation Results

The validity and capability of the proposed structure, power management and control strategy are confirmed through a Matlab/Simulink (Simscape toolbox) simulation. The system specifications are Intel(R) Core ™ i7-7600U @ 2.80 GHz with an installed 16.0 GB RAM, 64-bit operating system and x64- based processor. The HMG configuration is given in Figure 3.1. The DGs are represented by DC/DC converters in the DC SMGs and three-phase DC/AC converter in the AC SMG. The AC SMG is rated at 8 kW, and the DC SMG1 & SMG2 are rated at 10 kW for each. DC SMG1 consists of two DGs that are rated at 4 kW for DG1 and 6 kW for DG2. DC SMG2 and AC SMG are represented by one DG for each. The detailed control and system parameters are listed in Table 3-2.

A). Simulation results under different loading conditions:

The simulation is carried out for testing the performance of the proposed HMG structure, power management, and control strategy through five different scenarios. Through these five

scenarios, different loading conditions are adopted to assess each SMG's performance in delivering and importing the active power. Furthermore, changing the loading condition for each SMG allows the ILCs to confirm their capability to work according to the operational constraints and conditions discussed earlier. The scenarios mentioned above are analysed and discussed in detail as follows.

(i). Scenario 1: All SMGs are under-loaded (t= 0 – 2s)

This is the steady state event at which the three SMGs work in the $f'_b \leq f' < f'_{\max}$ and $V'_b \leq V' < V'_{\max}$ band for the AC and DC SMGs in accordance with (3-3) and (3-4). In this scenario, the resulting P'_{ilc} is zero and each SMG supplies its own load without any power transfer among the SMGs.

(ii). Scenario 2: DC SMG1 is over-loaded (t= 2 – 4s)

This scenario assumes DC SMG1 becomes over-loaded while the other SMGs demand remains unchanged at t = 2s. In this case, the V' starts to decrease gradually as the demand increase. Once V' becomes less than V'_n, the SMG is considered over-loaded. The additional power required to cover the shortage in DC SMG1 should originate from the other SMGs to maintain the stability of the whole system. In this case, the AC bus acts as a common bus and the required power flows through the ILC1 that operates as a rectifier.

(iii). Scenario 3: AC SMG is over-loaded (t= 4 – 6s)

Following the previous scenario, at t = 4s the load in the AC SMG starts to increase and force f' to be below f'_n. This reduces P'_{ilc} as both SMGs are now considered over-loaded. The DC SMG2 remains in the under-loaded situation and accordingly delivers most of the power, P'_{ilc}.

(iv). Scenario 4: All SMGs are over-loaded (t= 6 – 8s)

This scenario is implemented to clarify that when all SMGs operate in the over-loaded condition, the power exchange is reduced to zero as each SMG has to manage its own demand. In this situation, it is strongly recommended that additional power generation should be created or a load shedding operation should take place.

(v). Scenario 5: AC SMG and DC SMG1 are under-loaded (t= 8 – 10s)

This scenario starts at t = 8s, where DC SMG2 remains over-loaded while the load of the AC SMG and DC SMG1 falls significantly. Since both SMGs are now under-loaded, the power shortage at DC SMG2 is met through the power generated from the AC SMG and DC SMG1.

Discussions and analysis: Figure 3.6 illustrates the results for active power sharing in DC SMG1 for the five scenarios. It shows that the output current of each DG in the SMG can share the DC load in proportion to their rating capacity while neglecting the cable voltage drop. The ratio P_{dc1}/P_{dc2} in all states is maintained at $P_{dc1}^{\max} / P_{dc2}^{\max} = 2/3$. It is also noticed that the load current is always equal to the sum of the current of all DGs and that coming from the ILC.

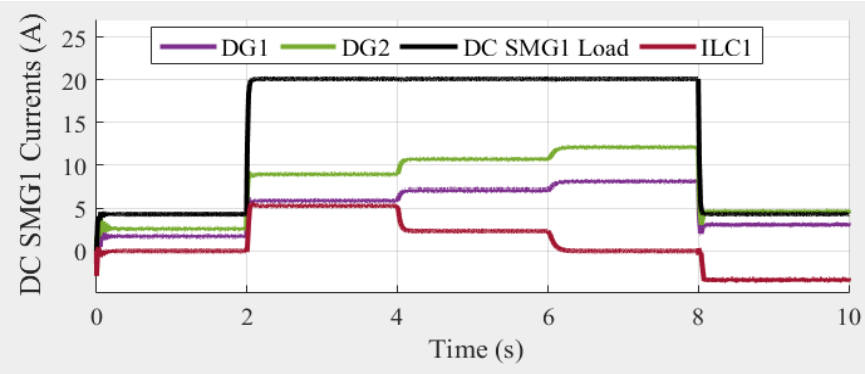

Figure 3.6 Power sharing in DC SMG1.

Figure 3.7 shows the total output active power in DC SMG1 in the different scenarios. As seen, there is a considerable difference between the output power under the primary control (red line) and that of the secondary one (blue line).

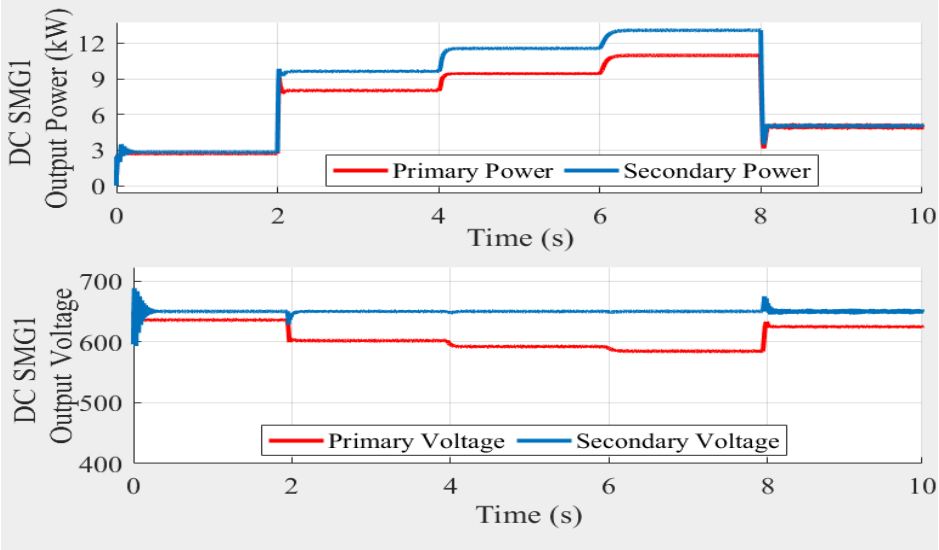

Figure 3.7 DC SMG1 power and voltage using primary and secondary control level.

Unlike the constant output voltage at the secondary control level, the output voltage at the primary level varies with the output power. This explains the minimum voltage in the primary control voltage occurring in Scenario 4 (at t = 6s) since it has the maximum output power. The constant value of the voltage at the secondary level is due to the continuous restoration to the same reference after every transient step.

Figure 3.8 shows the output power and voltage waveforms for DC SMG2 throughout the different scenarios. The same behaviour of output power and voltage at both control levels for DC SMG1 is noticed for DC SMG2. In this SMG, the secondary voltage reference is set to 450 V.

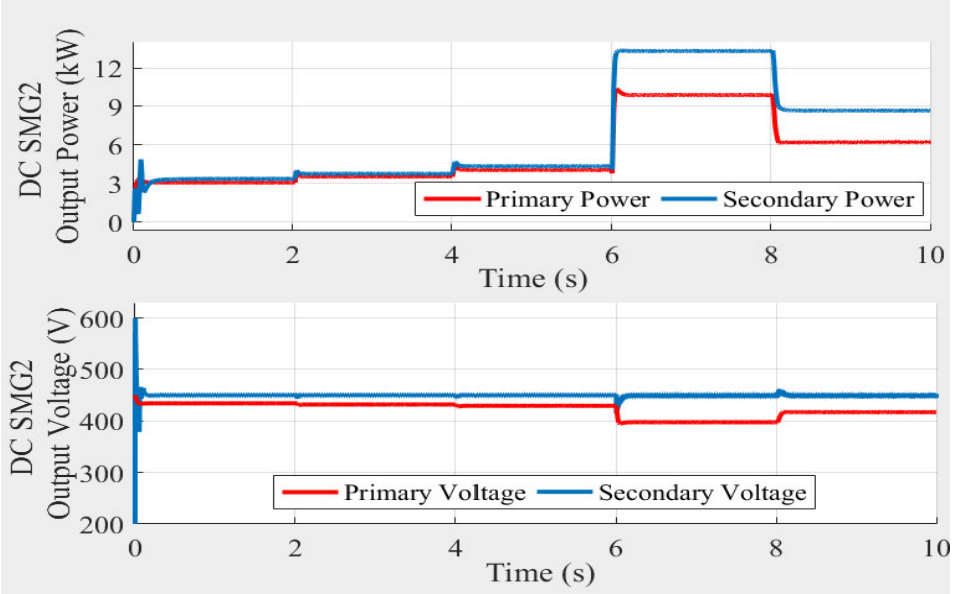

Figure 3.8 DC SMG2 power and voltage using primary and secondary control level.

Figure 3.9 illustrates the behaviour of output active power in the AC SMG at the secondary control level throughout the five scenarios. It can be noted that the frequency at the primary level varies with the active power in all the five scenarios, while with the secondary control, it is restored to the reference after every load step change.

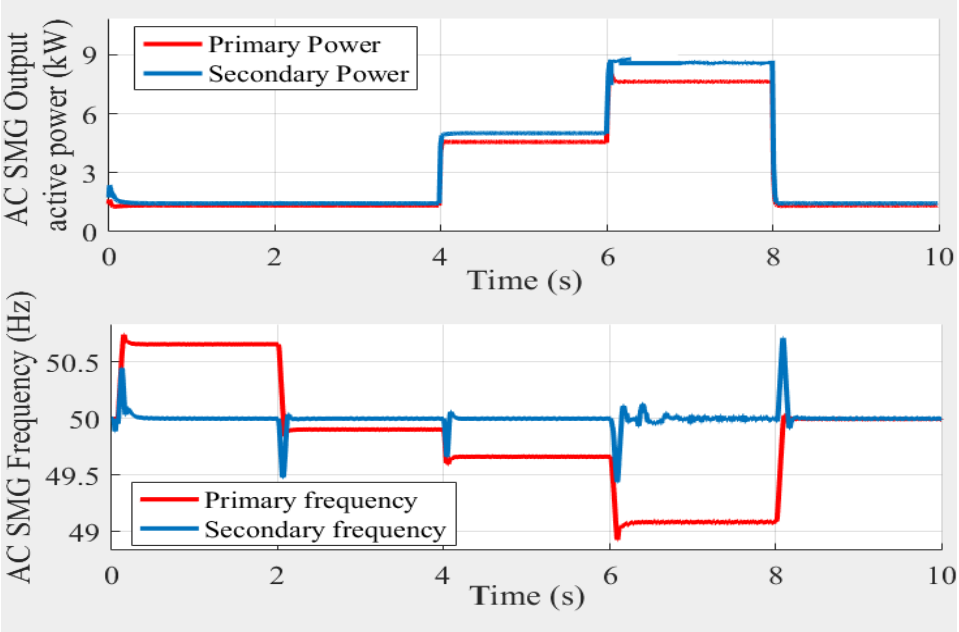

Figure 3.9 AC SMG Active power and frequency waveforms at primary and secondary level.

On the other hand, the relation between the AC voltage amplitude ($|V|$) and the reactive power (Q) is shown in Figure 3.10. In this figure, the reactive power is increased from 0 to 300 VAR at t = 4s and then increased to a maximum of 800 VAR at t = 6s. From both Figure 3.9 and Figure 3.10, it can be seen that the frequency and voltage magnitude in the AC SMG can be regulated separately using the modified vector decoupling technique mentioned earlier. Also, it can be observed that the secondary voltage magnitude is constantly restored to 240 V after every load step changes.

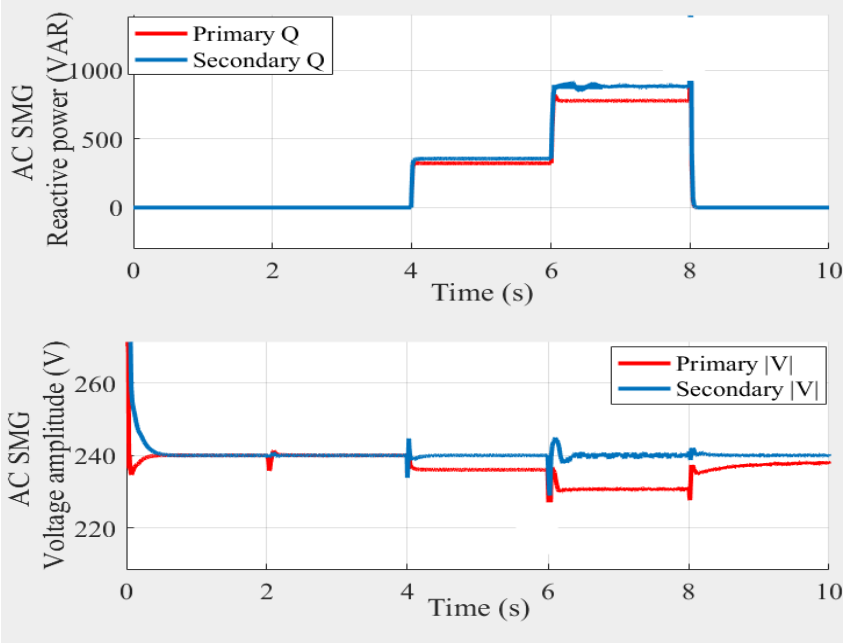

Figure 3.10 AC SMG reactive power and voltage waveforms at primary and secondary control level.

Figure 3.11 shows the simulation results of the voltage, current and current magnitude waveforms for both ILC1 and ILC2. The changing operation mode from rectifier mode to inverter mode can be observed for both ILCs. In Figure 3.11(a), during Scenarios 2 and 3 (t = 2-6s), the transferred current is in phase with the voltage waveform (rectifier mode); while, during Scenario 5, the ILC1 reverses the power flow direction, so that the current and voltage is now out of phase (inverter mode). Moreover, it can be seen that the current magnitude at ILC1 gradually changes from 0 to 6 A at t = 2s and from 0 to -4A at t = 8s. Unlike the sequential change of ILC1 operation from the rectifier to inverter mode, the ILC2 reverses its operational sequence from the inverter mode (Scenario 3) to the rectifier one (Scenario 5) as shown in Figure 3.11(b). It can also be observed that the maximum AC current obtained in Scenario 5 is in phase with the voltage.

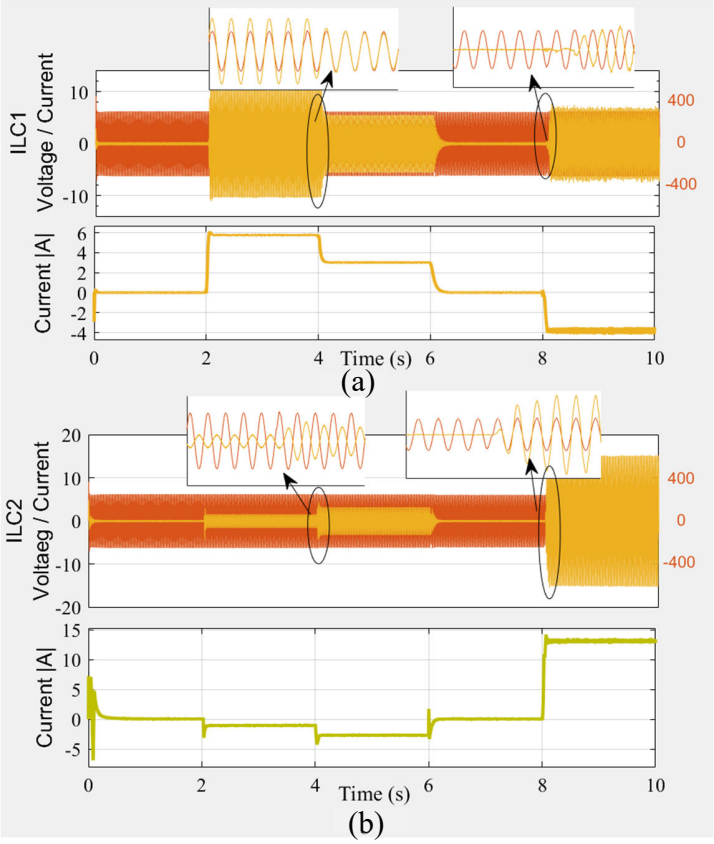

Figure 3.11 ILCs converters current, voltage and current magnitude (a) ILC1 (b) ILC2.

Figure 3.12 illustrates the voltage and frequency waveforms that are used as a reference for the ILCs. In the figure, the blue lines represent the voltage and frequency references (V, f) obtained at the primary control level, while the red lines represent the supposed voltage and frequency (V_s, f_s) obtained at the secondary control level. As mentioned earlier, these values give a clear indication of the amount of output power in each SMG. Moreover, the primary references (V, f) are the output parameters for each SMG as compared to the secondary ones (V_s, f_s) which are utilized for power transfer only.

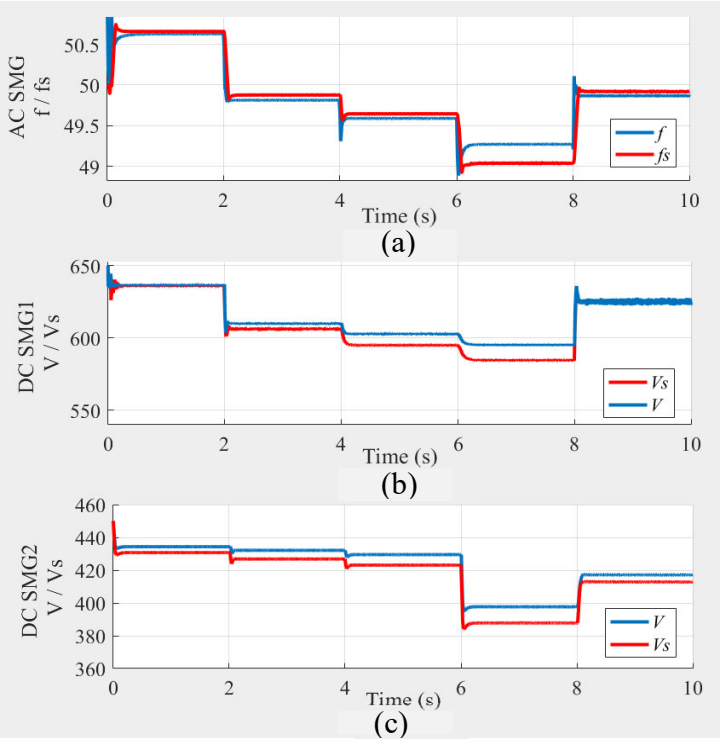

Figure 3.12 Primary and secondary ILC references (a) AC SMG frequency (b) DC SMG1 voltage (c) DC SMG2.

B). Comparison results between the proposed approach and the conventional one:

Figure 3.13 shows the simulation result of the active power flow of sources, loads, and ILCs at both the primary control and secondary control levels. Three simulation tests are conducted for the five loading scenarios to confirm the performance of the proposed approach and make a comparison between the conventional technique [106] and our proposed ones. It is worth mentioning that the execution time for the 9-second simulation of the proposed approach is 0.266531 s; this is comparable to that of the conventional one which is 0.263756 s. Figure 3.13(a) shows the response of the power flow across the HMG when the ILCs operate without any constraints as in the conventional technique. Under this technique, it can be clearly seen

that in Scenario 1 (t=0-2s) and Scenario 4 (t=6-8s), the ILCs exchange the power among the SMGs despite the fact that all SMGs are either underloaded or overloaded.

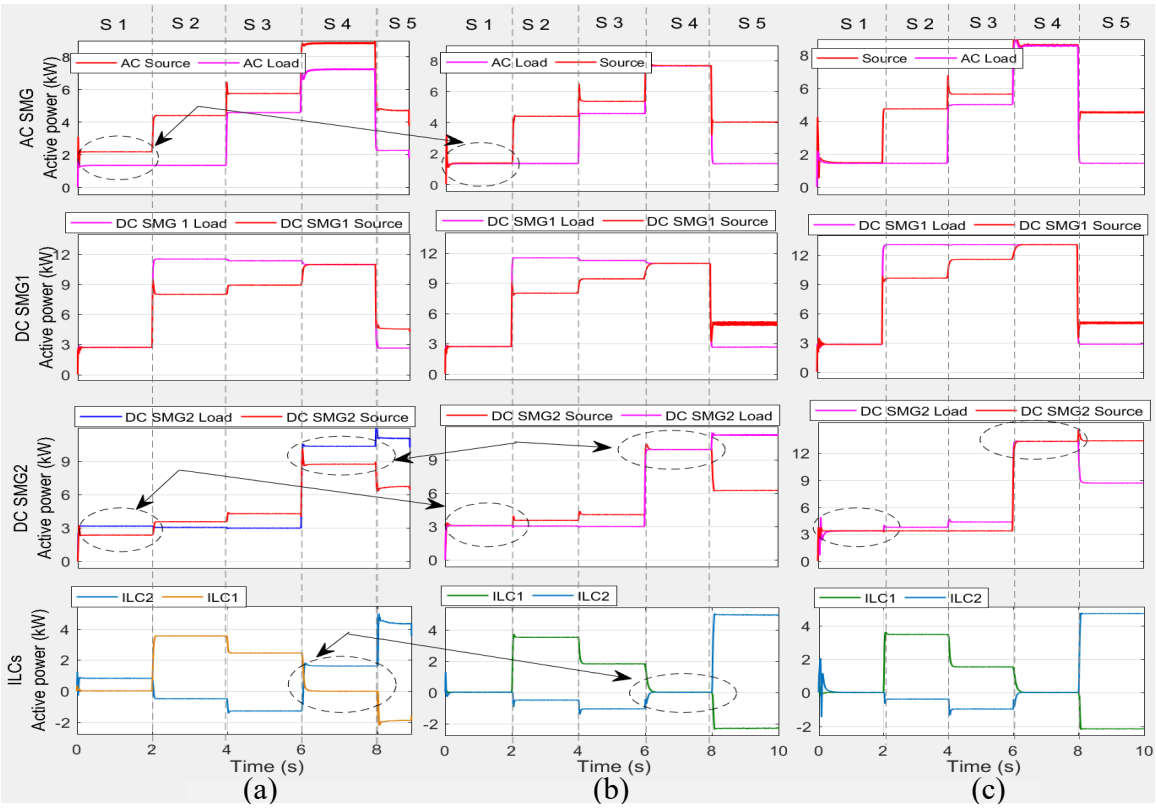

Figure 3.13 Simulated power waveforms within hybrid MG for five load step scenarios with (a) Conventional method (b) Proposed primary control level (c) Proposed primary and secondary control level.

Contrarily, the results of the proposed approach as shown in Figure 3.13(b) clearly illustrate the optimization of ILCs' operation. In detail, Figure 3.13(b) and Figure 3.13(c) show that in Scenario 1, each SMG has to cover its own demand and no power is transferred. At t = 2 s, the previously discussed Scenario 2 takes place since the load at DC SMG1 increases from 2.5 kW to 11.7 kW, and DC SMG 1 is now over-loaded. This situation forces the ILCs to transfer the power from the AC bus to cover the shortage in DC SMG1. With a total capacity of 10 kW, the output power of DC SMG1 is only around 8 kW. Such discrepancy in capacity

and generated power is in line with the proposed management strategy. The 8 kW generated power is the threshold point for DC SMG1 referred to as V_n' (Section 3.3.1-(iii)) and in accordance with (3-3) and (3-4) and Figure 3.2. A total of 3.7 kW active power is transferred through ILC1 to cover the shortage in this scenario. As shown in the figure, the power is supplied from the AC SMG to aid the over-loaded DC SMG1 which is viewed as an additional load for the AC SMG. Due to the relation between active power and frequency, the load increase for the AC SMG triggers its frequency decrease. This decrease in frequency then triggers DC SMG2 to intervene with its share of supplied power to the common bus and implicitly to the over-loaded DC SMG1. In this simulation, the power delivered from DC SMG2 to DC SMG1 is 0.7 kW while that delivered from the AC SMG is 3.7 kW.

In Scenario 3, a load spike from 1.6 kW to 5 kW for the AC SMG causes an over-loaded state for the AC SMG. This turns the AC SMG from a power supplier to an SMG in need. This not only causes the AC SMG frequency to drop but also decreases the total transferable power (P_{ilc}') as both DC SMG1 and AC SMG are now over-loaded. Naturally, more amount of power is drawn from the DC SMG2 that has an unchanged local load with the ability to spare its power to the over-loaded SMGs. In Scenario 4, DC SMG2 enters an over-loaded state. All the SMGs are now over-loaded so the transferrable power (P_{ilc}') drops to zero. Finally, in Scenario 5, the load drops for DC SMG1 and the AC SMG while the DC SMG2 remains over-loaded. The results show the applicability of the proposed strategy to power transfer with high effectiveness.

The power loss values in all 5 scenarios for both ILCs with and without using the proposed power management and control strategy are shown in Table 3-3.

Table 3-3 Summary of the power losses for ILCs with and without using the proposed strategy.

Scenario	ILC	Power losses (kW)	
		Proposed method	Conventional method
Scenario 1	ILC1	0	0.01
	ILC2	0	0.025
Scenario 2	ILC1	0.03	0.03
	ILC2	0.02	0.02
Scenario 3	ILC1	0.025	0.025
	ILC2	0.02	0.02
Scenario 4	ILC1	0	0.01
	ILC2	0	0.02
Scenario 5	ILC1	0.035	0.035
	ILC2	0.025	0.025

3.4 Summary

An improved and fast power management and control strategy for an islanded HMG at the primary and secondary control levels is proposed in this chapter. The presented system consists of multiple SMGs with different voltage levels, where the AC SMG serves as the common bus that mediates the power transfer. The proposed power management and control strategy improves the power exchange among the SMGs by reducing the continuous operation of the ILCs. Within this strategy, a new method is used to identify the standardized frequency and voltage values which characterize the power condition for each SMG at the secondary control level. These values are also used as references that govern the exact amount and direction of power transfer among the SMGs through the ILCs.

The proposed approach has been tested by comparing the proposed structure, power management, and control strategy when operating under the primary control level only and

both the primary and secondary control levels. Moreover, the performance of the proposed control scheme is compared with that of the conventional one under the same operating conditions. The various case studies and obtained results confirm that the proposed scheme can operate autonomously with the required stability margin. The results also verify that the proposed scheme ensures a continuous and seamless power transfer among the SMGs even if the constant frequency and DC voltage are enforced at the secondary level.

The approach proposed in this chapter demonstrates a high level of flexibility and ensures a high degree of control reliability through the proper regulation of the connected ILCs. However, linking multiple SMGs into one system poses a new challenge due to the need for communication among those SMGs or what is referred to as distributed control. The inclusion of the effect of distributed control in the control scheme must be included in the analysis. The next chapter presents the distributed control analysis during normal and emergency conditions.

Chapter 4

Distributed Control and Power Management Strategy for an Autonomous Hybrid Microgrid with Multiple Sub-Microgrids

Distributed coordination control for multiple SMGs within a hybrid AC/DC microgrid is the focus of this chapter. The conventional control approach for managing power flow among AC and DC SMGs is based on the proportional power sharing principle. This is mainly implemented by equalising the normalized voltage at the DC side and the frequency at the AC side for any interfaced SMGs. The proposed novel approach suggests a distributed control system that ensures a total controllability for the ILCs. It overcomes the total dependency on a specific variable for power exchange. The proposed method not only enables control of the power flow between SMGs but also ensures the continuity of power transfer if any single SMG fails.

4.1 Introduction

Conventionally, the droop control technique is widely used as a decentralized control method of the three microgrid structures mentioned before. In the case of the HMG which is our focus in this thesis, many studies use the droop characteristic as indicators (representatives) of the power conditions in AC and DC SMGs [35, 93, 96, 107, 108]. This implies that the frequency and voltage should slightly vary when the active power changes at the AC and DC side.

Depending on this variation, a sequential process is used so that the results of such processes are used as references to the ILCs. Thus, every individual SMG cooperates with other SMGs and shares the active power proportionally to its total capacity.

Implementing HMG with multiple SMGs requires an effective power management and control strategy to coordinate power exchange among participating SMGs. In such a system, each SMG can have voltage and frequency requirements, and act as autonomous and independent entities. The properly designed HMG integrates the advantages of individual SMG as well as enhancing the consistency and economic performance of an individual system. Reference [109] provides a preliminary review of HMGs where each SMG communicates with neighboring areas through controllable ILCs. The structure and features of HMG proposed as a small community network are discussed in [111, 112]. In previous studies, it is assumed that each SMG is connected to the main grid while also connected to the other SMG by a common bus. However, these studies have not proposed a detailed formulation for the implementation of power management and coordinated control of the HMG system.

This chapter proposes a new approach to the control strategy to manage the power flow among SMGs. A global control technique is implemented through the participation of the normalized variables of all SMGs to control the power flow through each ILC without relying on one single variable for each ILC.

4.2 Autonomous Hybrid Microgrid Structure

Schematic diagram of the hybrid AC/DC microgrids with multiple SMGs is the same as used in the previous chapter (Figure 3.1). In the AC SMG, every DG is emulated by a DC/AC converter that is linked to the local AC bus and directly connected to the common AC bus.

The DC SMGs are linked to their local DC buses via voltage source inverters (VSIs), and each DC SMG is linked to the common AC bus by an ILC. The AC common bus links all the SMGs and mediates the power exchange that may occur. Each ILC acts as a bi-directional converter and operates in two modes depending on the direction of the power flow.

4.3 Conventional Control Methodology

Essentially, the conventional control method of the AC/DC HMG is discussed in detail in Chapter 3, however, further analysis is necessary to understand the conventional control strategies from a different point of view to build a sound understanding of the overall control strategy presented for the ILC in this chapter.

In the case of HMG with multiple SMGs, the droop technique is used for every interfaced SMG. Thus, the AC bus works as a common bus and mediates the power flow from one SMG to another according to the SMG power condition. The frequency works as a transferable indicator between the SMGs even when the power flows from DC to DC SMG. Although this method obtains a high level of flexibility and reliability, it has many drawbacks that limit its implementation. For instance, the conventional droop method is not suitable when the HMG consists of multiple SMGs. Moreover, once the AC SMG is disconnected from the HMG, there will no longer be any power transfer in the system as the frequency of the AC SMG is what triggers the ILCs.

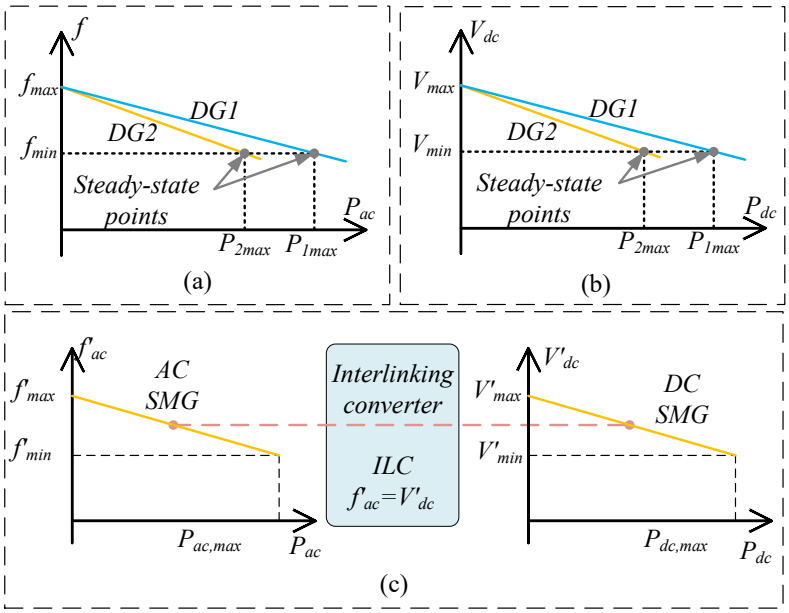

Figure 4.1 Active power droop characteristics of (a) AC (b) DC (c) AC/DC HMG.

Once the voltage and frequency have been regulated in accordance with the power management strategy in each single SMG, the ILCs energise in the system and link each DC SMG with the common AC bus, not only to manage the transferable power among SMGs, but also to increase the whole system stability by reducing the voltage and frequency variations in each SMG. The conventional method for managing the power flow in HMG basically depends on the characteristics of the droop curves (*P/f* in the AC SMG and *P/V* in the DC SMGs) as illustrated in Figure 4.1. That is because these curves reflect the amount of active power in each SMG. This is further shown through the merge of all the individual droop curves of all DGs into one curve for each SMG. The droop equations in (3-1) are also used here, with the output frequency f replaced with f_S at the AC SMG and the voltage V with $V_{S,i}$ at the DC SMG$_i$, which simplifies the understanding of the approach described in this chapter. The modified equation can be given as follows:

$$f_S = f^* - \alpha_S P_{ac,S}, \quad \alpha_S = \frac{1}{\sum_{i=1}^{n} \frac{1}{a_i}}$$
$$V_{S,i} = V^* - \lambda_{S,i} P_{dc,S,i}, \quad \lambda_{S,i} = \frac{1}{\sum_{i=1}^{n} \frac{1}{\lambda_i}} \tag{4-1}$$

where α_S and $\lambda_{S,i}$ are the combined droop gain of the total output active power ($P_{ac,S}$ and $P_{dc,S,i}$) of the AC SMG and the i^{th} DC SMG (DC SMG$_i$) respectively. Then, these droop curves undergo a normalization process so that it could be compared to each other as a standardized indicator of the power condition. Equations (3-2) given in Chapter 3 are rewritten as the following expression that represents the normalized frequency (f'_{SMG}) at the AC SMG and voltage ($V'_{SMG,i}$) at the DC SMG$_i$. Notice that f'_{SMG} is used instead of f' and $V'_{SMG,i}$ is used instead of V'.

$$f'_{SMG} = (f_S - f_{\min}) / (f_{\max} - f_{\min})$$
$$V'_{SMG,i} = (V_{S,i} - V_{\min,i}) / (V_{\max,i} - V_{\min,i}) \tag{4-2}$$

Now the normalized parameters are comparable since they have the same range scale which varies between 0 to 1. According to this range, when the SMGs has the maximum output power, the normalized values (f'_{SMG} & $V'_{SMG,i}$) will be 0 and consequently, the output voltage will be the minimum allowable value.

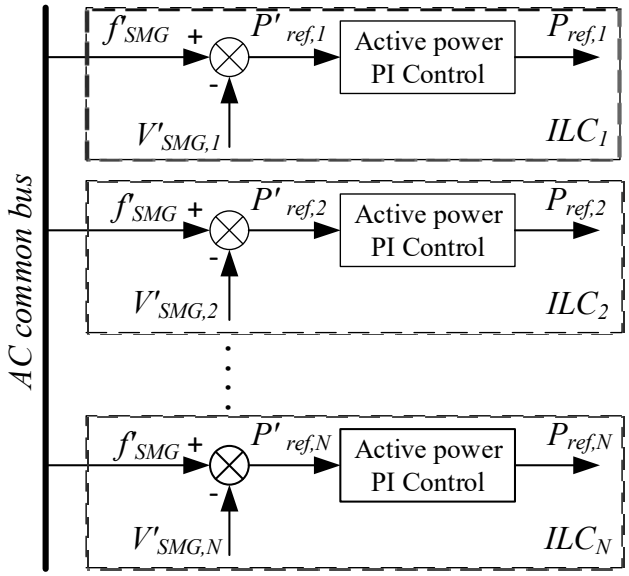

Figure 4.2 Conventional control method for ILCs

Once the normalized parameters (f'_{SMG} , $V'_{SMG,i}$) are equalized, these parameters are simultaneously utilized as an input of the power management strategy, and the interfaced SMGs share the active power proportionally to their ratings. Thus, the ILC manages the power flow between the involved SMGs and at the same time maintains the stability of the AC and DC SMGs. The per unit transferred power can be achieved by merging f'_{SMG} and $V'_{SMG,i}$ obtained from (4-2) and can be given as:

$$P'_{ref,i} = f'_{SMG} - V'_{SMG,i} \tag{4-3}$$

A similar approach can be adopted for the HMG with a multi-SMG structure. The difference here is that the normalized frequency is compared with each normalized voltage as shown in Figure 4.2 and each DC SMG will deliver or absorb power to/from the AC bus based on $P'_{ref,i}$. The conventional control approach presented above can achieve an accurate power sharing

among SMGs without any communication links among DGs or ILCs. On the other hand, the problem in such approach is that it can easily fail if the AC SMG is disconnected for a planned (maintenance process) or unplanned condition (faults). In such case, the power transfer will no longer take place.

4.4 Proposed Control Methodology

In order to avoid the interruption of power transfer among SMGs due to the isolation of the AC SMG from the whole system, a distributed control system approach is proposed in this chapter. The main idea is to implement an outer control loop (primary loop) as a local controller that includes the normalized factors (f'_{SMG} , $V'_{SMG,1}$, $V'_{SMG,2}$, ..., $V'_{SMG,N}$) of all SMGs in each ILC. Figure 4.3 shows the total schematic diagram of the proposed distributed control system of ILCs.

In the proposed control strategy, the controller of each ILC collects all the measured parameters (DC voltages $V_{SMG,i}$ and AC frequency f_{SMG}) at the defined sampling interval through the communication link (Figure 4.3(a)). Once normalised as in (4-2), these parameters are sent to the other ILCs.

The symbol $V'_{SMG,i}$ represents the resulting normalized voltage where i stands for the i^{th} DC SMG, while f'_{SMG} represents the normalised frequency. These variables are averaged and the control signal is sent out to the primary control loop for each ILC. This can mathematically be expressed as follows:

$$\overline{y}_{SMG} = \frac{\sum_{i=1}^{N} V'_{SMG,i} + f'_{SMG}}{N+1} \tag{4-4}$$

where $\bar{y}_{SMG}$ is the averaged variable of the $V'_{SMG,i}$ (normalised voltage) and f'_{SMG} (normalised frequency) and ranges between 0 to 1. The averaged variable $\bar{y}_{SMG}$ is then equalized with each DC SMG's normalised factor $V'_{SMG,i}$ through the continuous feed of the p.u error (γ_i) to a PI controller. The controller accordingly triggers the power transfer and minimises the difference between $\bar{y}_{SMG}$ and $V'_{SMG,i}$ as in (4-5). The output value ($P_{ref,i}$) represents the p.u transferred active power reference. This reference triggers the ILC to share the active power proportionally to its rating where the sign of the subtraction process given in (4-5) gestures the direction of the power flow. The normalized active power reference ($P_{ref,i}$) can be obtained as:

$$P_{ref,i} = k_P(\gamma_i) + k_I \int (\gamma_i); \quad \gamma_i = (\bar{y}_{SMG} - V'_{SMG,i}) \tag{4-5}$$

where k_P and k_I represent the PI control parameters of the outer loop of the ILC. Once the normalized reference power ($P_{ref,i}$) is found through (4-5), it can then be converted to the actual active power ($P^*_{ref,i}$) as in (4-6).

$$P^*_{ref,i} = \gamma_i \cdot P_{ref,i} \tag{4-6}$$

where γ_i is the active power capacity of the i^{th} SMG. Then, the actual active power ($P^*_{ref,i}$) is converted to the active reference current ($I^*_{i,d}$) according to (4-7).

$$I^*_{i,d} = \frac{2 \times P^*_{ref,i}}{3 \times |V_{abc}|} \tag{4-7}$$

Here, $|V_{abc}|$ represents the AC voltage magnitude of AC SMG. The active current reference ($I^*_{i,d}$) is then supplied to the inner control loop which has a current and voltage control loop (Figure 4.3(b)). Similar to Chapter 3, these control loops are used in conjunction with the modified vector decoupling control technique which is implemented by feed-forwarding the line voltage components. The final step in the control process is to transform the *dq* components of the reference voltage into its corresponding *abc* components.

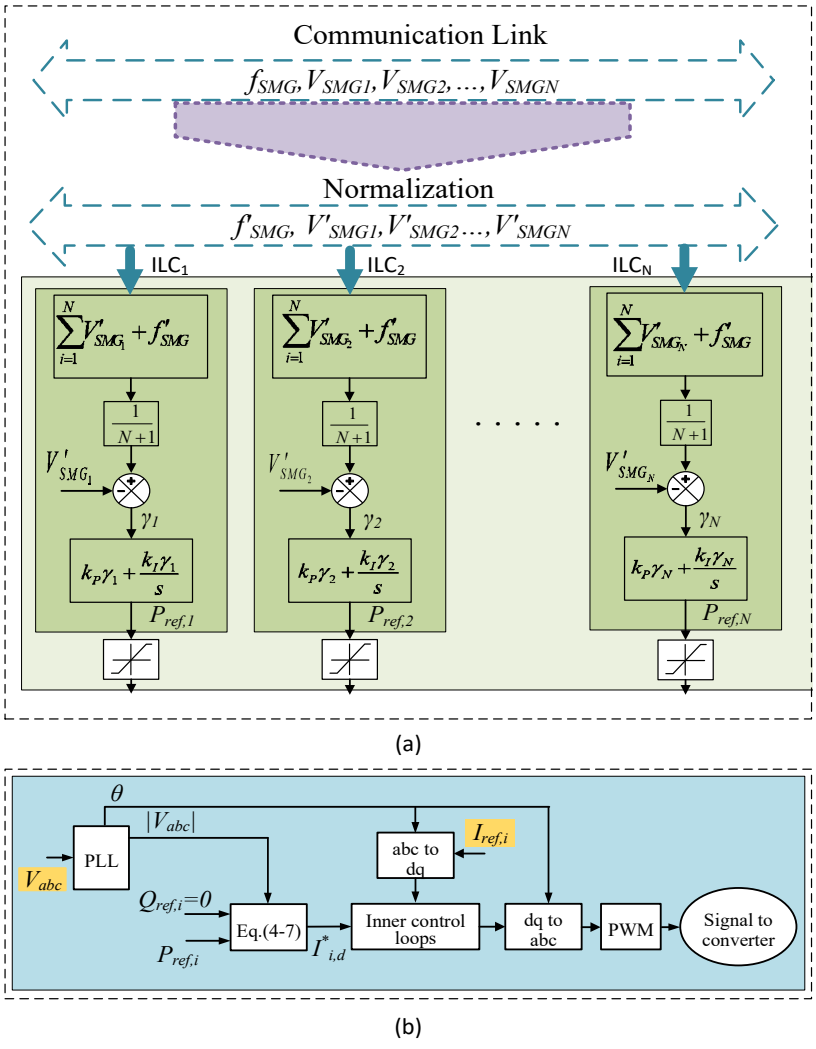

Figure 4.3 The proposed control approach diagram

When all the SMGs are online, and the HMG is considered under normal operating conditions, the proposed approach can lead to a similar output to the conventional one. However, if the AC SMG is disconnected from the system, the transferred power in the conventional method will no longer take place even when the remaining DC SMGs are still connected to the HMG. This is due to the loss of the normalized frequency (f'_{SMG}) that mainly balances the normalized voltages of the DC SMGs ($V'_{SMG,i}$) to trigger the ILCs. On the other hand, through the proposed method, the power transfer will continue among SMGs that are connected to the AC common bus even if the AC SMG is disconnected from the system.

Moreover, under the proposed scheme and in the case of the AC SMG disconnection mentioned earlier, the voltage and frequency at the AC common bus are now regulated by one of the ILCs to fill in the absent role of the disconnected AC SMG. The other ILCs continue to manage the power flow as intended.

4.5 Case Studies and Discussions

For verifying the performance and validity of the proposed control approach and power management strategy, a Matlab/Simulink simulation is executed with the presented multi-SMG structure shown in Figure 3.1. DC SMG1 consists of two DGs where each DG is represented by a DC/DC converter. A three-phase DC/AC converter is used to represent the DG in the AC SMG. Each of the DC SMG2 and AC SMG is supplied through one DG only. The total output power rating of all SMGs is set at the same rating of 6 kW so that their droop factors (α_S, λ_S) given through equation (4-1) are constantly tuned to maintain the generated output powers in a balanced state for different loads. The DC voltage range is 600 V< V <650 V for DC SMG1 and 400 V < V <450 V for DC SMG2 while the frequency range for AC

SMG is 49 Hz < f< 51 Hz. The proposed HMG is tested by carrying out a simulation at different loading conditions in each SMG. Such conditions ensure the validity of the findings in terms of the bidirectional power flow. Three case studies are presented to confirm the performance of the proposed approach and make a comparison to the conventional method.

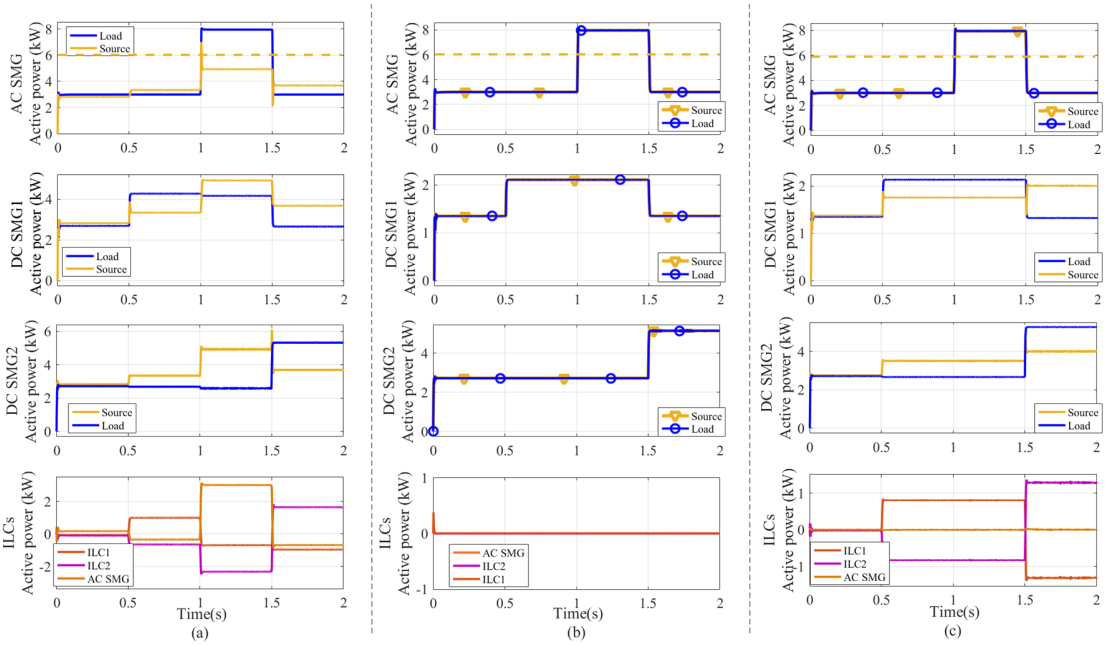

Figure 4.4 Simulated power waveforms within hybrid MG for four load step scenarios during three case studies (a) case A, (b) case B, (c) case C.

4.5.1 Case A: Power Exchange under Normal Conditions Using the Proposed Control Strategy

In this case, the three SMGs are online, and they are linked to the common AC bus through the ILCs. Power exchange takes place according to the loading status of each SMG. The waveforms of the active power flow for loads, sources, and ILCs are shown in Figure 4.4(a). Prior to t=0.5 sec, the SMGs are equally loaded and limited power exchange is noted. The first load transient takes place for the DC SMG1 at t=0.5 sec at which the load demand

increases to 4.3 kW. This triggers the ILCs to transfer active power through the AC common bus to the DC SMG1. In this case, the transferred power is supplied from the AC SMG and DC SMG2 as shown in the ILCs waveform representation in Figure 4.4(a). Moving forward, it can be seen that the active power transfer from DC SMG1 and DC SMG2 to the AC SMG due to the load increase at t=1 sec for the AC SMG. The last load transient takes place at t=1.5 sec at which DC SMG2 has an added load while DC SMG1 and the AC SMG has considerable load reductions.

4.5.2 Case B: Power Exchange when AC SMG is Isolated Using Conventional Control Method

Meanwhile, the AC SMG may need to be detached from the HMG during an emergency or planned maintenance. Figure 4.4(b) shows the power flow waveforms for all the SMGs. It can be noted that for each SMG, the power demand is identical to that of the generated power. Accordingly, there is no power transferred among the SMGs as each SMG is capable of meeting its own demand. Using this method (conventional), load shedding is usually needed to overcome the case in which the load of an SMG exceeds its supply capacity.

4.5.3 Case C: Power Exchange when AC SMG is Isolated Using the Proposed Control Method

This case study demonstrates the flexible performance of the proposed method as compared to the conventional one. Figure 4.4(c) illustrates the continuity of power transfer between DC SMG1 and DC SMG2 when the AC SMG is cut off from the HMG.

The figure depicts three load transients that occur at t=0.5 sec, t=1 sec, and t=1.5 sec. In more details, the first transient takes place when the load at DC SMG1 increases from 3 kW to 4.3 kW, the second transient takes place at AC SMG1 when the load increases from 3 kW to 8 kW, and the third transient takes place at DC SMG2 when the load increases from 3 kW to 5.5 kW. Unlike the previous case, the DC SMGs are still connected and interchange power despite the loss of the AC SMG as part of the HMG. This is further shown through the DC SMG1 and DC SMG2 waveforms that are not affected by the load transient that occurred in the AC SMG at t = 1 sec.

Figure 4.5 shows the difference in voltage and frequency between the AC SMG (Figure 4.5(a)) and the AC common bus (Figure 4.5(b)) throughout the case C. It confirms the continuous operation of the AC common bus while the AC SMG is isolated from the HMG. It also can be noted that the frequency and voltage in the AC SMG are regulated by its local controller in accordance with the droop control. On the other hand, the AC common bus under the proposed method is regulated by one of the DC SMG ILCs with a standard external reference to substitute the AC SMG role. The main aim of such coordination is to maintain the operation of the AC common bus when the AC SMG is no longer connected to the HMG.

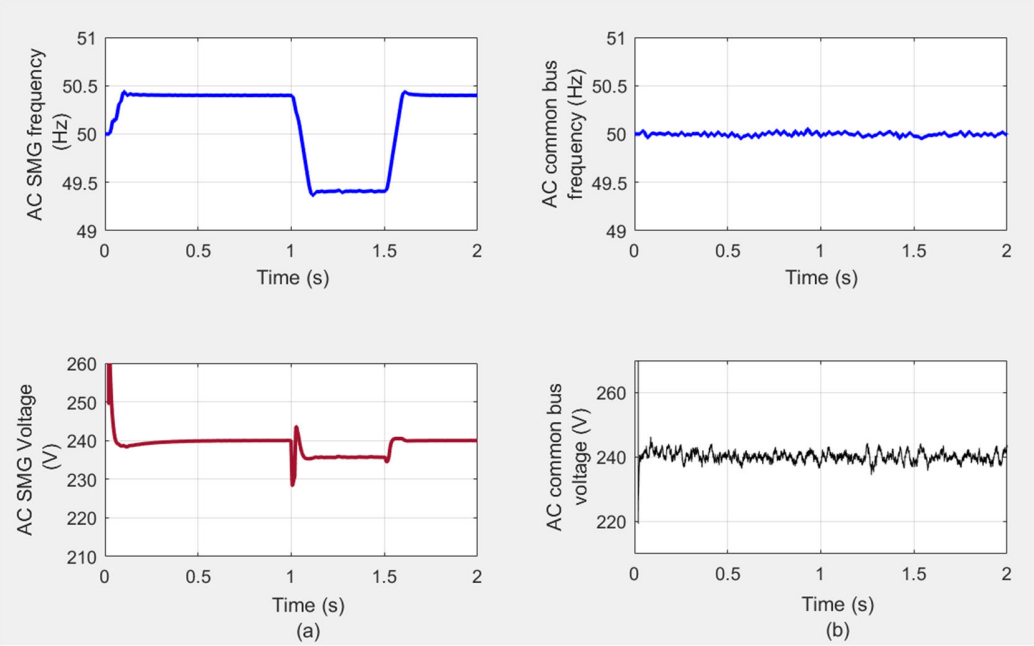

Figure 4.5 Comparison between (a) AC SMG and (b) AC common bus for case C.

Figure 4.6 shows the voltage and frequency waveforms of all SMGs for the case A (Figure 4.6(a)) and case C (Figure 4.6(b)) throughout the three load changes. It also shows the normalized variables of the three SMGs. It clearly shows that in case A, all the variables were equalized since the generated power is balanced for all SMGs. However, in Figure 4.6(b), the normalized variables are only equalized for DC SMG1 and DC SMG2 as these SMGs are the ones connected to the HMG. The output results for the p.u error (γ_i) given in (4-5) are shown in the last section of Figure 4.6 which confirms the equalization process of the normalized variables after each load transient. Figure 4.6(b) also shows the advantage of the proposed method in terms of sharing active power between DC SMGs when the AC SMG is isolated from the HMG. The voltage and frequency variations are relatively small for each SMG since the linking of the DC SMGs increases the total power rating. Accordingly, the whole system is considerably more stable.

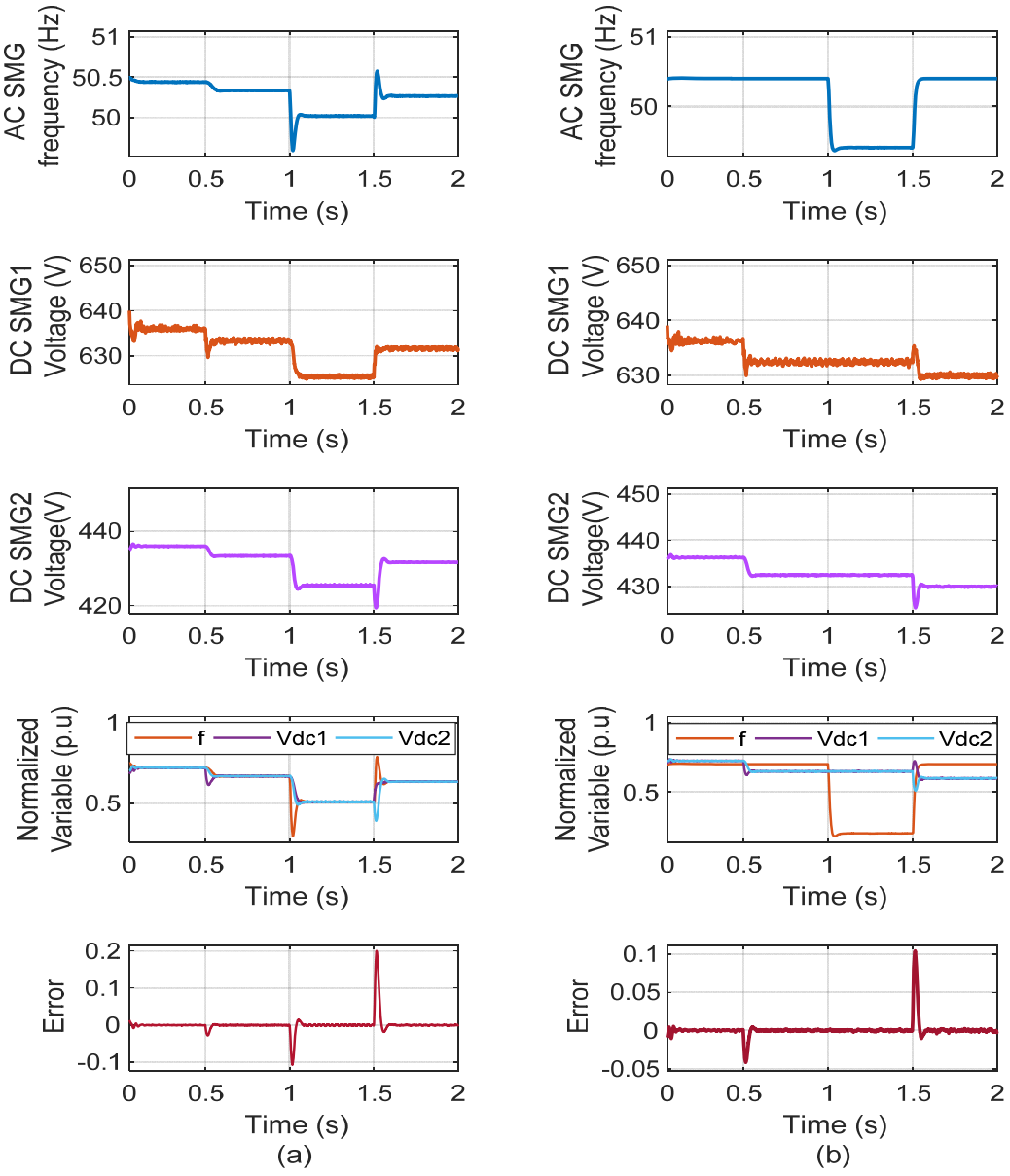

Figure 4.6 Frequency and voltage waveforms for (a) case A, and (b) case C

4.5.4 Case D: Impact of Communication Latency

Communications have a major role in providing the infrastructure that allows data exchange within each SMG and among all the SMGs. In real-life applications, the situation of communication link failure is a common phenomenon. Communication latency is more important when it is used at the primary level of ILC control scheme where the goal is to ensure global regulation of the entire system.

In this case study, the effect of communication latency on the proposed control strategy is presented for three fixed communication delays, 5 ms, 10 ms and 20 ms. Figure 4.7 illustrates the effects of different communication delays on the performance of the control strategy where the delay is activated at t = 1s. As shown in Figure 4.7(a), a delay of 5 ms has a slight impact on ILCs control performance as the HMG system quickly reaches the steady-state condition. In the cases that the connection delay is increased to 10 ms and 20 ms as shown in Figure 4.7(b) and (c), respectively, the HMG system remains stable while experiencing larger transients, due to the proposed reliable control strategy.

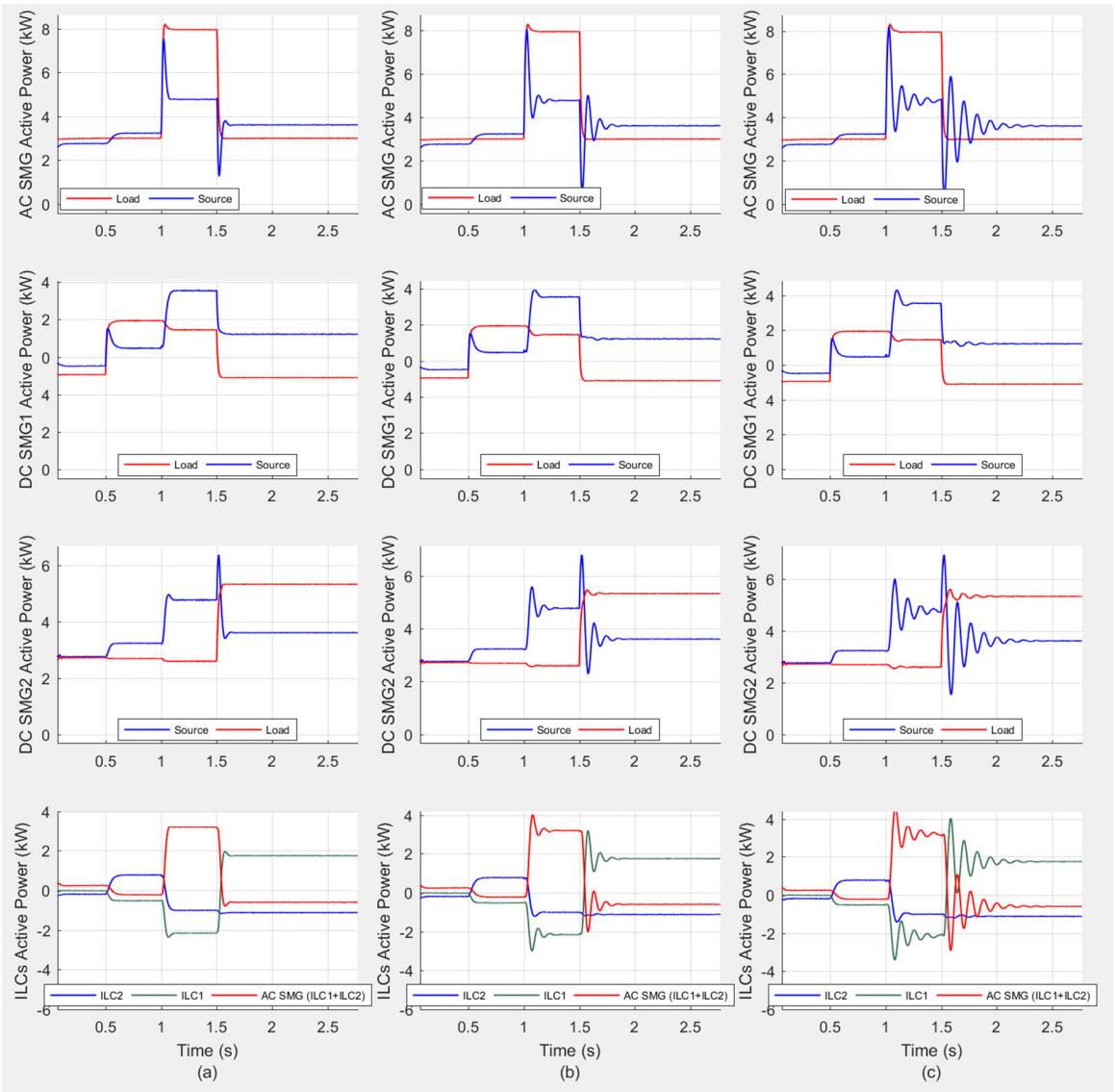

Figure 4.7 Performance of ditributed control and power management strategy considering communication latency, when comparing three amounts of fixed communication delay, (a) 5 ms, (b) 10 ms and (c) 20 ms

4.6 Summary

In this chapter, a new control method for accurate active power sharing for the hybrid AC/DC microgrid with multiple SMGs is presented. The proposed method suggests a distributed control system that ensures global controllability for the ILCs specifically in the case of disconnection of the AC SMG. This overcomes the total dependency on a specific variable for stable power exchange which is the case in the conventional method. The proposed control method has been compared with the conventional one under different conditions. The various simulations and their results verify that the proposed scheme ensures a continuous and seamless power transfer irrespective of the failure of the AC SMG.

While in Chapters 3-4 only one ILC was used between any of the interfaced SMGs, the next chapter will illustrate how the use of multiple parallel ILCs is a better option. This is mainly due to the converters' current limitations and the reactive or proactive maintenances for any of the HMG's components.

Chapter 5

Power Management and Control Strategy for Multiple Bidirectional Power Converters in an Autonomous Hybrid Microgrid

Coordinated control and power management strategy for the multiple parallel ILCs that link the AC and DC SMGs in an autonomous HMG is the focus of this chapter. The new approach outlined in this chapter aims to manage the power flow across the hybrid AC/DC microgrid while regulating the voltage and frequency for the SMGs as part of the process. The main objective of the proposed method is to keep the HMG in autonomous operation with active power proportionally shared among its ILCs and distributed sources. Regulation of the AC voltage and frequency is maintained by the control of active and reactive powers delivered to the AC bus. Similarly, reliable regulation of the DC voltage at the DC SMG is achieved by controlling the flow of active power through the DC bus.

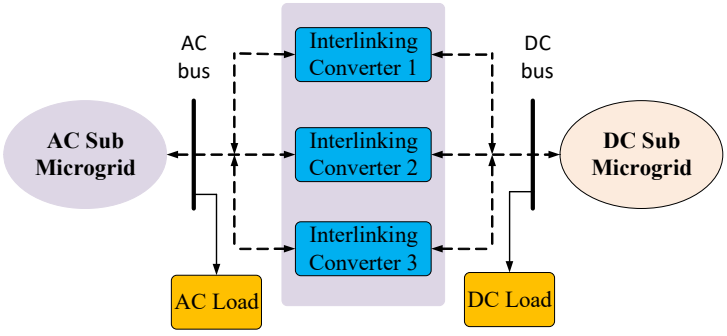

Figure 5.1 Structure of the HMG with multiple parallel ILCs

The schematic diagram of the HMG with multiple parallel ILCs proposed in this chapter is shown in Figure 5.1. In the HMG, the ILCs can work in three different control mode according to the system's need and the presence of the storage element. Firstly, a bidirectional power control mode is to regulate the power flow between the DC and the AC SMGs. Secondly, a DC voltage control mode is to regulate the voltage at the DC bus. Finally, an AC voltage control mode is to regulate the voltage and frequency at the AC bus. In this chapter, for simplicity purpose, it is assumed that the ILCs have an identical power rating.

One of the key gains of this structure is the mitigation of the circulating current that results from the parallel operation of the ILCs. Although the circulating current is more present at the AC side, it can also exist at the DC side. At the AC side, this is achieved through the implementation of the d-q-0 axis control strategy. The presented outer control loop is a modified arrangement that could not only ensure accurate power sharing but also suppress the circulating current at the DC side.

5.1 Background and Literature Review

The ILCs not only manage and control the power exchange among SMGs, but also support the frequency and voltage regulation at the SMGs. The control of the ILC is very critical since its reliability is highly correlated to the microgrid efficiency and stability. The power management and control of HMG have been discussed and investigated in many previous studies and most of these works propose a single ILC linking the AC and DC microgrids [39, 110].

The presence of storage elements plays an essential role in determining the ILC control and operation objective. The control scheme for ILCs varies in accordance with the fact whether

a battery is connected to the AC side, DC side or both. Once the storage element is online, it provides additional support to the bus voltage regulation. However, the ILC controller should carry out the bus voltage regulation role when no storage medium is present. A few studies discuss about linking multiple ILCs between AC and DC SMGs, and the focus of these works is to suppress the circulating current that would result from such an arrangement.

Power management and control coordination of multiple parallel ILCs within the HMG is more complicated than that in the individual ILC as the main difficulties are the power sharing among the connected ILCs. Master-slave and distributed control are the main techniques used to regulate the power flow between ILCs in such cases. As mentioned above, the master-slave is a communication-based method and has a defect in reliability because there is one failure point [111, 112]. Multiple parallel bidirectional converters are used with an improved control strategy to reduce the circulating current and power sharing deviation in [113]. In [95], multiple bidirectional power converters are used to control the amplitude and frequency of the AC bus voltage with the storage elements connected to the DC side. Ref. [112] discusses the distributed coordination control techniques for multiple bidirectional power converters. In that study, the AC SMG is connected to the storage element, and thus the DC voltage is regulated by the bidirectional converter. Furthermore, parallel three-phase ILCs operating under unbalanced voltage in a hybrid AC/DC microgrid is proposed in [114]. In the previous studies, the same control strategy is suggested for all the ILCs, and the ILCs are limited to either controlling the power flow among the SMGs, regulating the voltage at the DC side or controlling the voltage and frequency at the AC side only.

For the ILCs' parallel operation, circulating current is one of the most critical issues that could result in reducing the conversion efficiency and increasing the power losses. These effects are

of utmost importance and should be rectified as it may damage the whole converter. There are two main reasons for the circulating current, superficial reasons such as the difference of inductors and dead time, and the intrinsic reason that results from the voltage drop among the converters due to the different switching states. In [115, 116], different techniques are studied to improve the circulating current reduction. For eliminating the zero-sequence current of the circuit, an isolation transformer is used in [117]. Although this method is effective in eliminating the circulating current, it is very costly and makes the system bulky.

In [116], a circulating-current control strategy is applied in back-to-back parallel three-phase converters with individual DC links for permanent magnet synchronous motor (PMSM) drives. The proposed centralized control strategy consists of two main loops defined as difference control and sum control. In this solution, the circulating current is suppressed through the shared feedback and exchange of parameter information among the ILCs to ensure a coordinated response to the circulating current. Some other simple methods are used to reduce the zero-sequence circulating current by controlling the zero voltage space-vector [117-120]. This can efficiently eliminate the circulating current and is considered physically compatible with the implementation in the HMG. Similar to previous chapters, this chapter only discusses the circulating current reduction and current sharing of power converters for the hybrid AC/DC microgrid operating in the islanded mode as the circulating current and current sharing deviation are relatively small during the grid-connected mode.

Another crucial issue in the HMG is power management. This involves the power sharing among ILCs and the power exchange among SMGs. Usually, only one ILC is used in the HMG and hence, the power management is mostly limited to manage the power interaction between AC and DC SMGs. Several control techniques and normalization methods are

developed to manage and regulate the power flow among AC and DC SMGs [35, 93-96, 121]. The common concept of such methods is based on different modifications of the droop control methods. These techniques are able to balance the output power of DGs in DC SMGs with their counterparts in the AC ones. This can be achieved by comparing the normalized voltage at the DC SMG and the normalised frequency at the AC one. The surplus power will flow from the underloaded SMG to the overloaded one. A similar technique can then be implemented for the HMG with multiple ILCs when all the ILCs operate under the same control scheme. However, when multiple ILCs operate under different control strategies, the above method can easily fail in managing the active power flow accurately. Previous studies have focused on optimising the power flow by using parallel converters under the same control strategy in the HMG, without taking into consideration that each ILC could operate with a different control method.

The focus of this chapter is the development of new control algorithms for power management of HMGs with multiple parallel bidirectional converters. In the HMG studied in this chapter, three interlinking converters are connected in parallel between the AC and DC SMGs operating under different control strategies as shown in Figure 5.1. Unlike previous research studying parallel ILCs in which the ILCs operate using the same control strategy, the proposed technique suggests a different control system for each ILC. These ILCs have to carry out the responsibility to manage the power flow between the AC and DC SMGs and simultaneously support the voltage and frequency regulation at the AC bus and support the voltage at the DC bus. This effort has not been previously pursued by other researchers and the main challenge is the simultaneous coordination of the bidirectional interlinking converters and controllers

of the AC and DC SMGs. The major contributions proposed in this chapter are listed as follows:

1) A new distributed coordination control and power management strategy is proposed for the hybrid AC/DC microgrid with multiple bidirectional converters. This involves all the converters in which each converter is assumed as operating under a different control scheme.
2) The d-q-0 three-axis control strategy is implemented to suppress the circulating current among the three ILCs at the AC side of the converters. This approach is employed for each control system according to the corresponding ILC.
3) A modified outer control loop is proposed to ensure accurate power sharing as well as suppressing the circulating current at the DC side.

5.2 Autonomous Hybrid Microgrid Structure

The proposed structure has three main parts, namely: the AC SMG, the DC SMG, and the parallel ILCs. These three parts cooperate to ensure a seamless transfer of power flow between the SMGs, increase the total power rating of the HMG and improve the system reliability. Such an arrangement would not only increase the power rating for each SMG and the whole HMG, but also increase the ability to respond to the sudden load changes and reduce the need for load shedding of the system. Both of the presented DC and AC SMGs include one DG, where the DG is represented by a DC/DC converter for the DC SMG and a three-phase DC/AC converter for the AC SMG. The three ILCs are represented by three-phase DC/AC converters. These ILCs linking the AC and DC SMGs and working as bidirectional converters

mediate any power exchange taking place. Each SMG has its own load that is connected to its corresponding common bus.

5.3 Description of the Proposed Control Method

The key point of this section is the control and power management strategies of the parallel ILCs that are more difficult to coordinate according to the system structure and control design. The HMG proposed in this chapter consists of three parallel ILCs that are used to share the large power flow and overcome the power limitations present in the single ILC structure. Although all the ILCs have the same objective to share the power flow among the SMGs, it is important to note that it is not necessary for all the parallel ILCs to operate in the same control mode together. For example, in this work, the first ILC is used to balance the power between the AC and DC SMGs, while the second ILC is used to control the DC link voltage, and the third ILC is used to control the AC link voltage. Hence, further coordination among the ILCs, DGs at the DC bus, and DGs at the AC bus is required for such combination of control strategies. This coordination is more needed for the HMG operating in the islanded mode. The three control strategies mentioned earlier will be discussed in the following sections in detail.

5.3.1 ILC in a bidirectional power control mode

Three parallel converters are utilized in the presented structure operating under different control mode. These ILCs are necessary to link the individual AC and DC SMGs together. In this section, the first ILC is supposed to operate as a bidirectional power converter. Balancing the demand power and the total power generation of HMG is the main aim of the control

strategy during this mode. The droop characteristics given in (2-5) and (2-21) illustrate that the voltage at the DC bus and the frequency at the AC bus indicate the amount of the active power in each SMG. Therefore, the frequency (f) and voltage (V_{dc}) are the critical variables used to determine the direction and amount of the power flow among SMGs. While operating in the first mode (bidirectional power control mode), the control system is structured as shown in Figure 5.2 to identify the reference power signal of the ILC. The control block scheme mainly consists of two loops, that is, the inner and outer control loops.

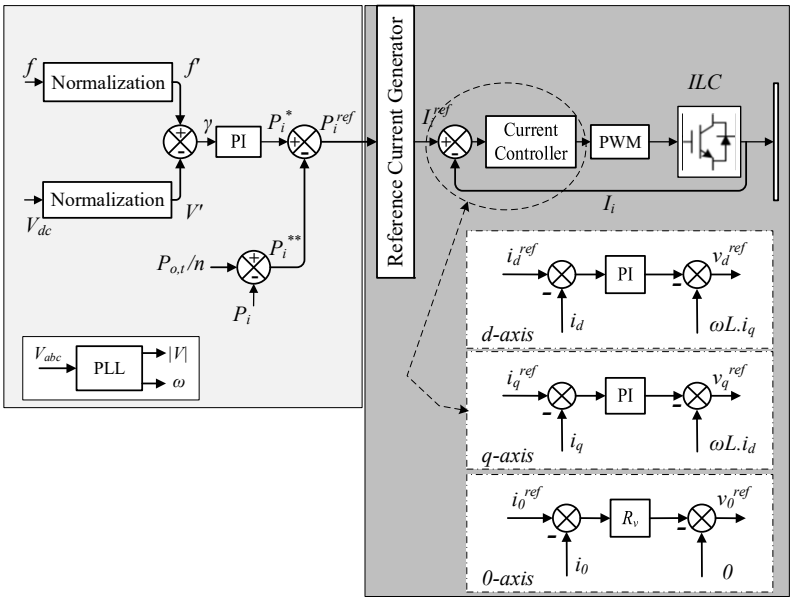

Figure 5.2 Control scheme of ILC in a bidirectional power control mode.

The main aim of the outer control loop is to manage the power flow between SMGs that also includes the power sharing among the ILCs. The block diagram of the outer loop is shown on the left-hand side of Figure 5.2. During this control mode, the ILC power reference, P_i^* is generated by utilizing the regulated AC frequency at the AC SMG and the DC voltage at the DC SMG. As discussed earlier (Chapter 3 and 4), the measured values (V_{dc} and f) undergo a

normalization mechanism that enables the use of the normalised values, V' and f', as the standardized indicators of power condition. Figure 4.1(c) illustrate the mathematical expression of the normalized DC voltage, V', and AC frequency, f', given in (3-2) [35, 93]: The resulting values of the normalization technique from both the SMGs now have the same scale range and thus are comparable. Instantaneously, these parameters are used as an input to the control and power management strategy by balancing f' and V', as shown in Figure 5.2. This means that $\gamma = f' - V'$ is then used as an input to the PI controller. The power reference signal, P^*_i resulting from the balancing process represents the amount and direction of the power flow. In other words, when P^*_i has a negative sign, the power will flow from the DC SMG to the AC SMG, and thus the ILC will work as an inverter. On the other hand, the positive sign of P^*_i indicates that the ILC would be operated as a rectifier, and the power will flow from the AC SMG to the DC SMG. The amount of the transferred power basically depends on the total power rating of each individual SMG. Thus, both SMGs have an active power share that is proportional to their power ratings. The power command can eventually be written as:

$$P_i^* = k_P(\gamma) + k_I \int \gamma \, dt \; ; \quad \gamma = (f' - V') \tag{5-1}$$

where k_P and k_I are the proportional and integral control parameters.

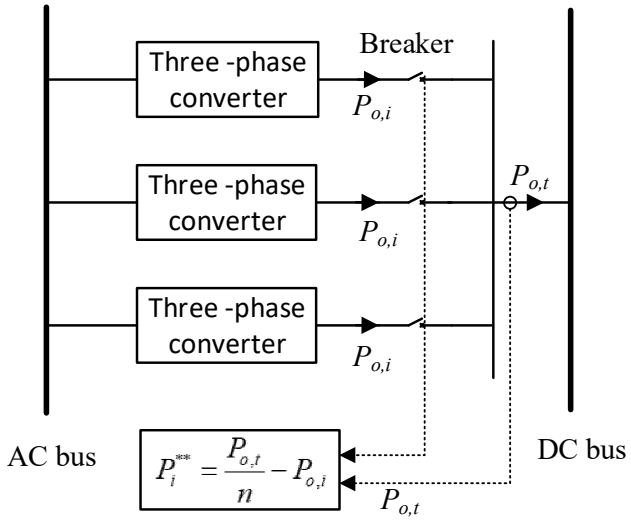

Figure 5.3 The proposed modified outer control loop for the three ILCs.

For the HMG with multiple parallel ILCs, a similar technique can be assumed only when all the ILCs are working in the same control mode. However, when all ILCs are operated in different control modes at the same time, the control function and scheme of each ILC will vary in accordance with the corresponding control mode. This means that some ILCs running in a certain mode will have a faster response time than other ILCs operated at different control modes. This, in turn, will affect the power-sharing accuracy as the droop control mechanism is very sensitive to the response time of converters and output line parameters. Therefore, in this chapter, an improved control method is proposed to address this issue. The solution involves the real-time recording of the power-sharing deviation for each ILC, P_i^{**}, and using it as a feedback to the corresponding controller as shown in Figure 5.3. The proposed loop is implemented within the boundary of the outer control loop. The power-sharing deviation for each ILC, P_i^{**}, can be given by:

$$P_i^{**} = \frac{P_{o,t}}{n} - P_{o,i} \tag{5-2}$$

Here $P_{o,t}$ is the total output power of the multiple bidirectional power converters and can be given as :

$$P_{o,t} = \sum_{i=1}^{n} P_{o,i} \tag{5-3}$$

where $P_{o,i}$ is the output power of the i^{th} converter and n the number of parallel converters connected in the HMG. As mentioned above, the power ratings for the ILCs are identical, so the transferred output active power of the i^{th} ILC is equal to $P_{o,t}/n$. The total output reference power, P_i^{ref}, is the output of the proposed outer control loop and the optimum amount of power transferred for the i^{th} ILC when the ILCs are operated in different control modes. Using (5-1) and (5-2), one can calculate P_i^{ref} by:

$$P_i^{ref} = \overbrace{\left[k_P(f'-V') + k_I \int (f'-V')\,dt\right]}^{P_i^{*}} - \overbrace{\left[\frac{P_{o,t}}{n} - P_{o,i}\right]}^{P_i^{**}} \tag{5-4}$$

According to (5-4), the main purpose of the controller is to suppress the circulating current at the DC side and optimise the power sharing among ILCs through controlling the regulated variables, P_i^{*} and P_i^{**}. Whereas the power exchange is taking place, P_i^{ref} will be the optimum output power transferred with no circulating current at the DC side. However, once the power transfer is settled or no power exchange is needed, the controller will eventually balance the

controlled variables, P_i^{*} and P_i^{**}, ensuring that $P_i^{ref} = 0$. This means that the power sharing among the bidirectional converters can be ensured by using the improved outer control loop while eliminating the circulating current at the DC side. The last step in the control scheme for this mode is to convert the resultant total output reference power, P_i^{ref}, to an active current reference, I_i^{ref}, using current reference generator which in turn is considered as an input to the inner current control loop. The active current reference, I_i^{ref}, can be given as:

$$I_i^{ref} = \frac{2 \times P_i^{ref}}{3 \times |V_{abc}|} \tag{5-5}$$

where $|V_{abc}|$ is the three-phase AC voltage amplitude. Unlike the outer control loop that is utilized to manage the power flow and suppress the circulating current at the DC side, the inner control loop is mainly used to regulate the active and reactive output current components in addition to suppressing the circulation current at the AC bus. The output line impedances and the asymmetry of the output voltage across the converter terminals are considered to be the main reasons for the circulating current at the AC side. The adverse impacts of such current can be concluded in increasing the power losses of the converters and reducing the conversion efficiency. The circulating current is mostly found on the AC side of the converter. Therefore, to suppress the circulation current at the AC side, a virtual resistance controller is adopted on the 0-axis of the *d-q-0* components. This virtual resistance, R_v, is designed as a proportional controller as shown in Figure 5.2.

5.3.2 ILC in a bidirectional DC voltage control mode

Usually, the DGs of the DC SMG that is emulated by a DC/DC converters entirely control and regulate the voltage at the DC bus in the HMG. Despite the fact that the ILC should be able to support the voltage regulation at the DC bus in this mode, it also should be able to substitute the absent DGs and fully control the voltage at the DC bus in cases of breakdowns or disconnections of the DGs. The schematic diagram of the presented control strategy is shown in Figure 5.4. In this mode, the proposed design is mainly composed of an outer and inner control loop. The main aim of the outer control loop is to manage the power exchange among SMGs. The power management includes the power sharing among the ILCs that would result in eliminating the circulating current at the DC side. On the other hand, the inner control loop is mainly designed to regulate the DC voltage and suppress the circulating current at the AC side.

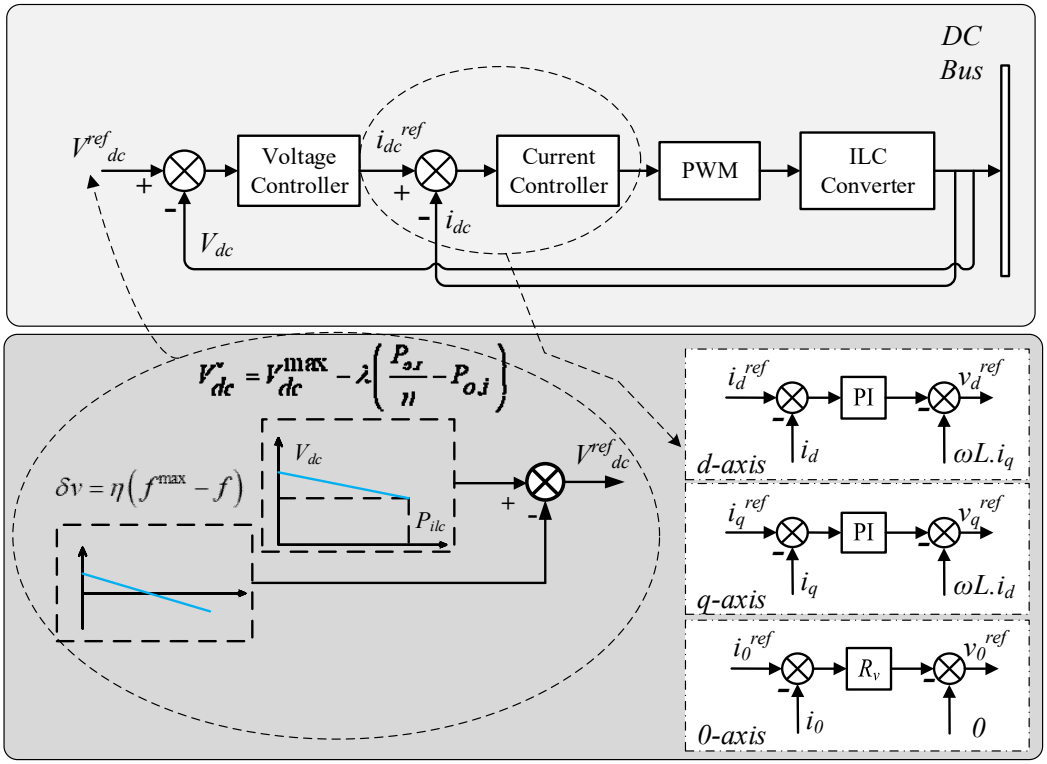

Figure 5.4 Control scheme of the ILC in a bidirectional DC voltage control mode.

As shown in Figure 5.4, an improved control technique is implemented to achieve the DC voltage reference, V_{dc}^{ref}, that would reflect the amount of transferred power. The mathematical expression of the voltage reference, V_{dc}^{ref} can be given as:

$$V_{dc}^{ref} = \left(V_{dc}^{\max} - \delta v\right) - \lambda\left(\frac{P_{o,t}}{n} - P_{o,i}\right) \tag{5-6}$$

where $V_{dc}^{\max}$, λ, and V_{dc}^{ref} are the maximum allowable DC voltage, the droop control coefficient factor, and output DC voltage reference respectively. Notice that δv is the power transfer variable that represents the power flow between AC and DC SMGs. Within this control mode, if there is a transient power in either the DC SMG or AC SMG, both SMGs

will interact and support each other to reach the steady state. Furthermore, the voltage at the DC SMG and the frequency at the AC SMG would change simultaneously. Such reliability is achievable through this control strategy by taking into account the active power capacity of each SMG and the total capacity of the whole HMG. In other words, V_{dc}^{ref} which regulates the DC voltage accounts for the frequency of the AC SMG, and this ensures a reliable and accurate power transfer. The control law of the power exchange variable, δv, can be given as:

$$\delta v = \eta\left(f^{\max} - f\right) \tag{5-7}$$

where f and $f^{\max}$ are the actual output frequency and the maximum frequency, respectively, and η is the power exchange droop coefficient that can be calculated by:

$$\eta = \left(\left(\frac{1}{P_{ac,t}}\right)\cdot\left(V_{dc}^{\max} - V_{dc}^{\min}\right)\right) \Big/ \left(\left(\frac{1}{P_{dc,t}}\right)\cdot\left(f_{ac}^{\max} - f_{ac}^{\min}\right)\right) \tag{5-8}$$

where P_t is the total active power capacity of the whole HMG, and $P_{ac,t}$ and $P_{dc,t}$ are the total active power capacities of the DC and AC SMGs, respectively.

The inner control loop involves two main loops. Firstly, the voltage loop is to ensure accurate control of the DC voltage reference with zero steady-state error. Secondly, the current loop is mainly designed to improve the dynamic response of the power management strategy by regulating the current reference, i_{dc}^{ref} .

The voltage reference found earlier in (5-6) is used to regulate the voltage at the DC bus and simultaneously manage the power flow. Figure 5.4 shows the schematic diagram of the whole control strategy. Any sudden increase in the load demand at the DC SMG or AC SMG results

in a voltage error, $V_{dc}^{ref} - V_{dc}$, with a positive sign that is caused by the voltage drop (decrease in V_{dc}). As illustrated in Figure 5.4, the voltage error with a positive sign causes an increase in the magnitude of $i_{dc}{}^{ref}$ which in turn increases i_{dc} and triggers the ILC converter to transfer the power from the AC SMG to the DC SMG. On the contrary, any drop in the load demand will increase V_{dc} and cause a negative voltage error, $V_{dc}^{ref} - V_{dc}$. This triggers a decrease in the active current, i_{dc}^{ref}, and signals the ILC converter to transfer the power from the DC SMG to the AC SMG. To suppress the circulating current resulting from the parallel ILC connection at the AC bus, the *d-q-0* control strategy is adopted. As shown in Figure 5.4, the detailed *d-q-0* control diagram illustrates the current suppressing control loop that implements a vector decoupling control technique. The decoupling technique enhances the system performance and allows efficient and segregated control of active and reactive power. It is important to note that if the reference value of i_q^{ref} is set to zero, the ILC converter will operate with a unity power factor.

5.3.3 ILC in a Bidirectional AC Frequency and AC Voltage Control Mode

Normally, the amplitude and frequency of the AC bus voltage are regulated by the DGs of the AC SMG through droop control techniques, as discussed earlier. However, the bidirectional converters also have the ability to control the AC voltage bus and simultaneously to manage the power flow between the AC and DC SMGs. Figure 5.5 shows the detailed control block diagram for the third ILC that operates in the AC frequency and AC voltage control mode. The dynamic design for the outer and inner control loops are presented and derived as in the following sections.

1) The outer loop

The main aim of the outer loop in this strategy is to manage the power interaction among SMGs and accordingly control the voltage and frequency at the AC bus. The ILC controller should take into consideration the regulated parameters that are obtained from the DGs in the AC SMG. Accordingly, some coordination between the control schemes of DGs in the AC SMG and the ILC controller should be adopted to achieve higher control reliability.

Figure 5.5 illustrates the detailed block diagram of the control scheme. Firstly, the instantaneous output voltage V_{oabc} and current I_{oabc} are sensed and transformed to their corresponding *d-q-0* axis components. Secondly, the measured parameters are used to calculate the output active and reactive power for the ILC. The calculated values are then filtered through the low pass filter. The resulting values are utilised to compute the reference voltage amplitudes and frequency (E, f_{ac}^{ref}) through the *P/f* and *Q/V* droop control mechanism. From the AC SMG point of view, the ILC is considered as a parallel converter connected to the AC SMG during the power flow from the DC bus to AC one. On the other hand, it is treated as a load when the power flows from the AC bus to the DC bus. The frequency reference (f_{ac}^{ref}) in terms of the power interaction variable (δf) can be given as:

$$f_{ac}^{ref} = \left(f_{ac}^{\max} - \delta f\right) - \alpha\left(\frac{P_{o,t}}{n} - P_{o,i}\right) \tag{5-9}$$

where α, f_{ac}^{ref} and $f_{ac}^{\max}$ are the AC droop control coefficient, output frequency reference and the maximum allowable AC frequency, respectively. δf is the power interaction variable that represents the amount of power that flows from the AC to the DC side. It can be given as:

$$\delta f = \frac{1}{\eta}\left(V_{dc}^{\max} - V_{dc}\right) \tag{5-10}$$

where $V_{dc}^{\max}$ is the maximum allowable DC voltage, V_{dc} is the actual output DC voltage, and η is the droop coefficient of power interaction as given in (5-8). In this mode, the parameter δf has a similar function as that of δv in the DC voltage control mode discussed earlier. While it also represents the amount of power that flows among the SMGs, and another significance of this variable is to gesture the frequency reference f_{ac}^{ref} in terms of the DC voltage. For the reactive power sharing, droop control is also implemented to allow the ILC to share the reactive load of AC SMG and simultaneously regulate the AC voltage magnitude E. The mathematical equation of the AC reactive power is given in (2-5).

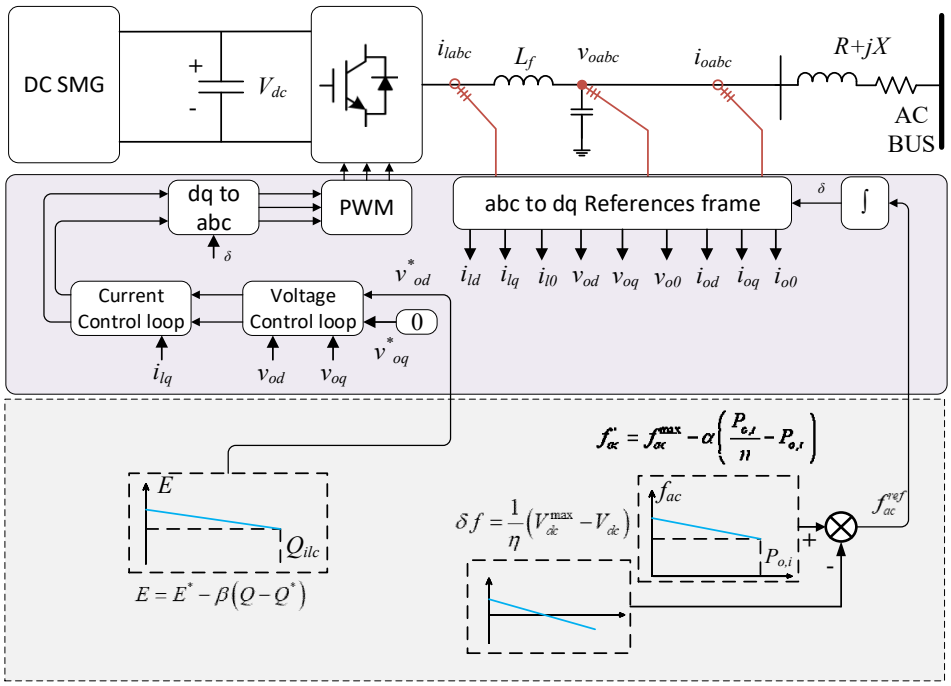

Figure 5.5 Control scheme of the ILC in a bidirectional AC frequency and AC voltage control mode.

2) The inner loop

The defined voltage and frequency references (f_{ac}^{ref} , E) are then fed to the inner voltage and current control loop as shown in Figure 5.5. The frequency references (f_{ac}^{ref}) is used to generate the angle (δ) for the computation of the d-q-0 components.

Figure 5.5 shows the control scheme and system components that consist of three-phase pulse width modulation inverter, LC filter, and line impedance ($R+jX$). The voltage and current controllers are based on the PI controller. The vector decoupling control technique is also employed here by feed-forwarding the line voltage components.

Table 5-1 Parameters of HMG and Control System.

Unit	Parameter	Value
AC SMG	$P_{ac}^{\max}$	10 kW
	f^{max}	51 Hz
	f^{min}	49 Hz
	$\lvert V^{max} \rvert$	240 V
	$\lvert V^{min} \rvert$	220 V
	α_i	2.5×10^{-4}
	β_i	1×10^{-3}
DC SMG	λ_1	8.33×10^{-3}
	$DG_1^{\max}$	10 kW
	λ_2	12.5×10^{-3}
	$P_{dc}^{\max}$	10 kW
	$V_{dc}^{\max}$	450 V
	$V_{dc}^{\min}$	400 V

5.4 Interaction between Different Control Strategies

In the above design of the control system, coordination between control strategies is necessary to ensure a reliable and stable system. The DC bus voltage regulation in the DC SMG has been taken into account when designing the bidirectional DC voltage control system. The DC voltage reference generated from the conventional droop in the DC SMG should match that resulting from the bidirectional DC voltage control system. On the other hand, the frequency reference that results from the P/f droop at the AC SMG should also match the reference that is found in the proposed bidirectional AC voltage and frequency. The proposed plug-and-play system enables the HMG to keep running even when the power source is totally disconnected at one of the SMGs.

5.5 Case Studies and Discussions

The performance of the proposed power management and control strategy is tested and validated using the Matlab/Simulink software. The total output power rating of both SMGs is set at the same rating of 10 kW. The continuous tuning of the droop factors (α, λ), given through (2-5) and (2-21), maintains the generated output power for both SMGs at a balanced state even at different load levels. For the DC SMG, the voltage range is set at 400 V < V <450 V while the frequency range for the AC SMG is set at 49 Hz < f < 51 Hz. The AC voltage is set at 240 V rms. To test the HMG performance under the proposed control and management strategy, different loading conditions for each SMG are assumed. The detailed control and system parameters that are used for this simulation are listed in Table 2-1. Three scenarios are presented to ensure the validity of the findings in terms of the multiple bidirectional power flow and the suggested control strategy.

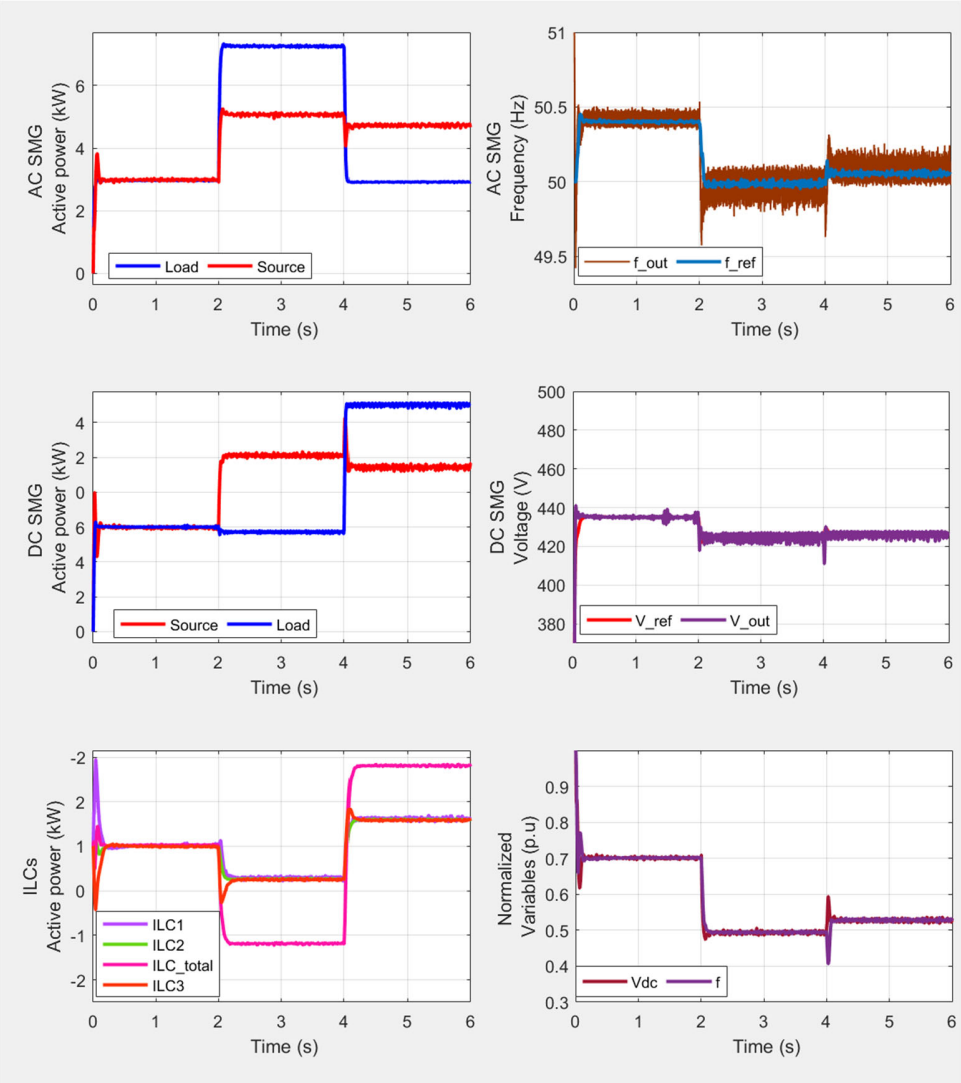

Figure 5.6. Scenario 1 simulation results, waveforms of power, voltage, and frequency for all the HMG.

5.5.1 Scenario 1: Different Loading Conditions

This scenario discusses and analyses the power flow among the three parallel ILCs through different loading conditions as shown in Figure 5.6. The first loading condition is the steady-state event at which both SMGs are equally loaded, and no power exchange exists. Within the second loading condition (at t = 2s), AC SMG becomes overloaded while the load of DC

SMG remains unchanged. In this case, each of the ILCs' controllers senses the change in the system conditions and triggers the ILC converter to transfer the required power from the DC to the AC SMG. Since all the ILCs have the same power rating, the transferred power through each of the ILCs will be identical and the total transferred power is the sum of all of the ILCs output power. During this event (t = 2-4 s), the current and voltage waveforms are out of phase as the ILCs are operating in the inverters mode. Following the previous events, at t = 4s, the load of the AC SMG falls significantly while the DC SMG becomes overloaded. During this event (t = 4-6 s), all the ILCs reverse the power flow direction to respond to the changed condition. Since the ILCs are operating as rectifiers under this condition, the current and voltage waveforms are now in phase.

Figure 5.6 also shows the actual output frequency at the AC SMG and the reference frequency that is produced from the controller of the ILC1. It can be noted that both waveforms have the same value that is slightly decreased with the increase of the output power demand; and when the load decreases, the frequency slightly increases. Similarly, the output voltage at the DC SMG is identical to the reference voltage that is obtained from the ILC2 controller. It also illustrates the normalized DC voltage and AC frequency variables that are used in the control scheme of the ILC3.

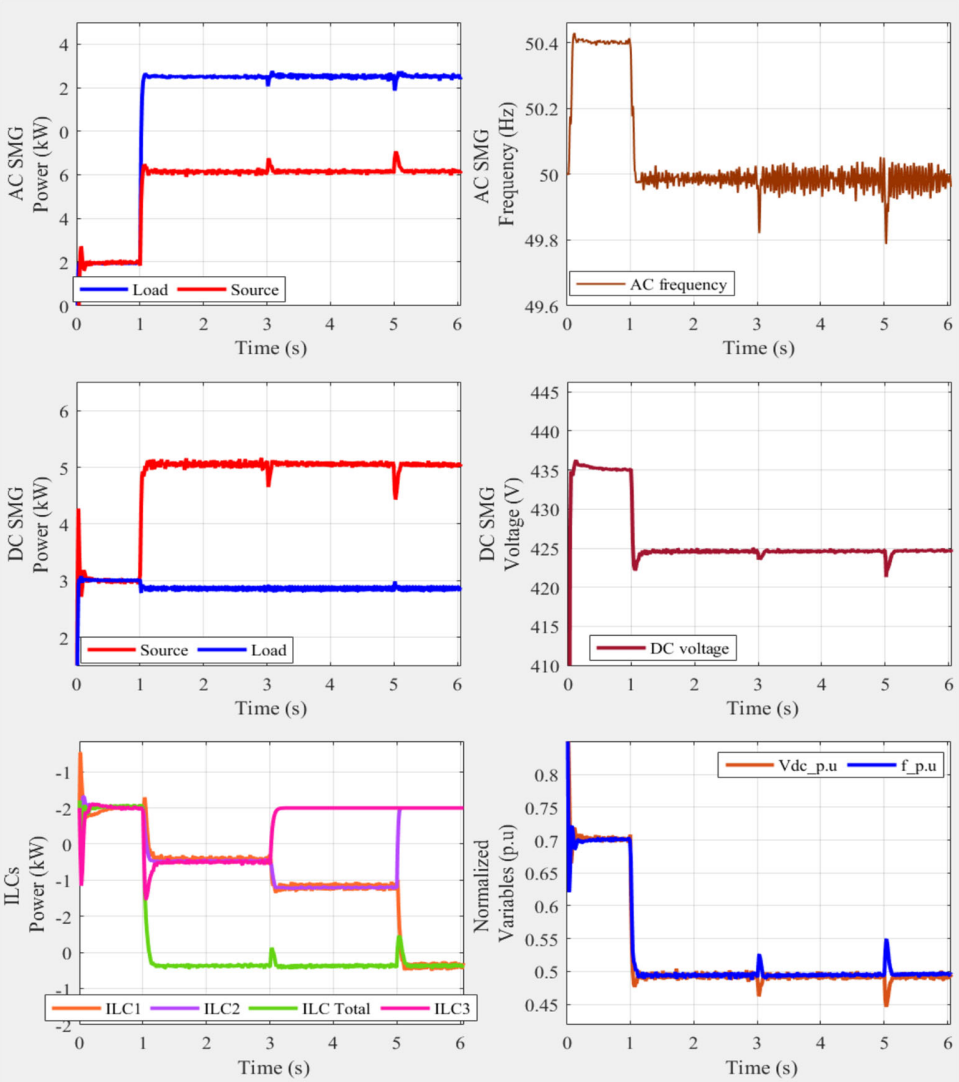

Figure 5.7 Scenario 2 simulation results, waveforms of power, voltage, and frequency for all the HMG.

5.5.2 Scenario 2: A Plug-and-Play Comparison Study:

Figure 5.7 studies the plug-and-play capability of the proposed controller and power management strategy. During t= 1-3s, all the ILCs are online and transfer the required power from the DC to the AC SMG due to the overload condition in the AC SMG. ILC1 is unplugged at t= 3s; thus, the output power from ILC3 decays to zero. Notice that this amount of power

is distributed to the other ILCs and the AC frequency is controlled by the AC SMG only. The total power exchange between AC and DC SMGs remain the same as long as the output power of each SMG has no change. ILC1 is disconnected from the microgrid at t=5s. Consequently, the remaining ILC2 has the role of carrying out the total power exchange.

Figure 5.7 also shows the frequency, DC voltage and the normalized voltage and frequency waveforms. As seen, there is a continuity of power transfer between AC and DC SMGs with the same power rating.

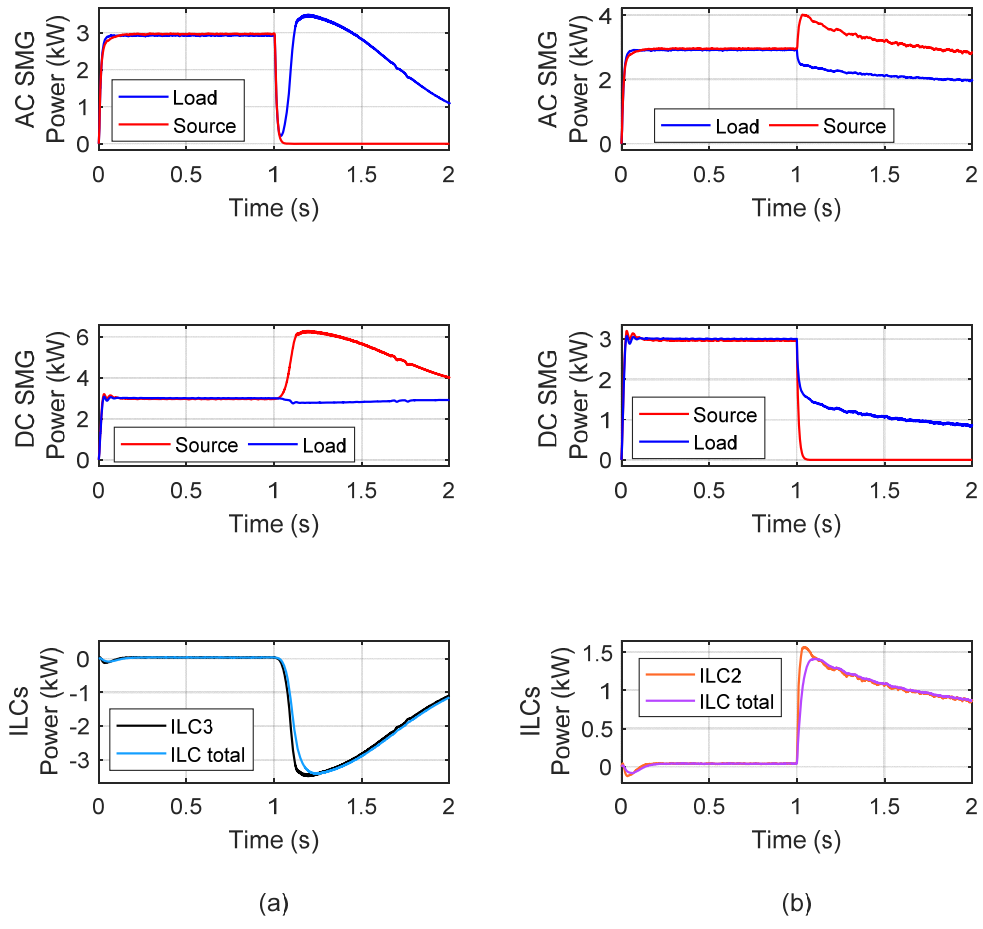

Figure 5.8 Scenario 3 simulation results, waveforms of power using the conventional method. (a) test 1. (b) test 2.

5.5.3 Scenario 3: Power Exchange when the DG in the AC or DC SMG is Isolated:

This scenario confirms and demonstrates the flexible performance of the proposed control method as compared to the conventional one. The advanced control and power management strategy are tested through the resiliency to a single SMG failure by conducting two tests. In the first test, the AC and DC SMGs are linked by the ILC3 only (ILC in the bidirectional AC frequency and voltage control mode), and the DG in the AC SMG is isolated at t= 1s. Similarly, in the second test, the DG in the DC SMG is disconnected at t= 1s.

The conventional method is first applied. For test 1, Figure 5.8(a) shows the output power flow of the AC SMG, the DC SMG, and the ILCs when isolating the DG from the AC SMG. It can be clearly seen how the whole HMG collapses with the conventional control method while the load is not changed in all SMGs. This breakdown occurs as the traditional method can only manage the power flow but fails to regulate the AC voltage at the same time. For test 2, Figure 5.8(b) shows the power waveforms of AC SMG, the DC SMG, and the ILCs when the DG in the DC SMG is disconnected.

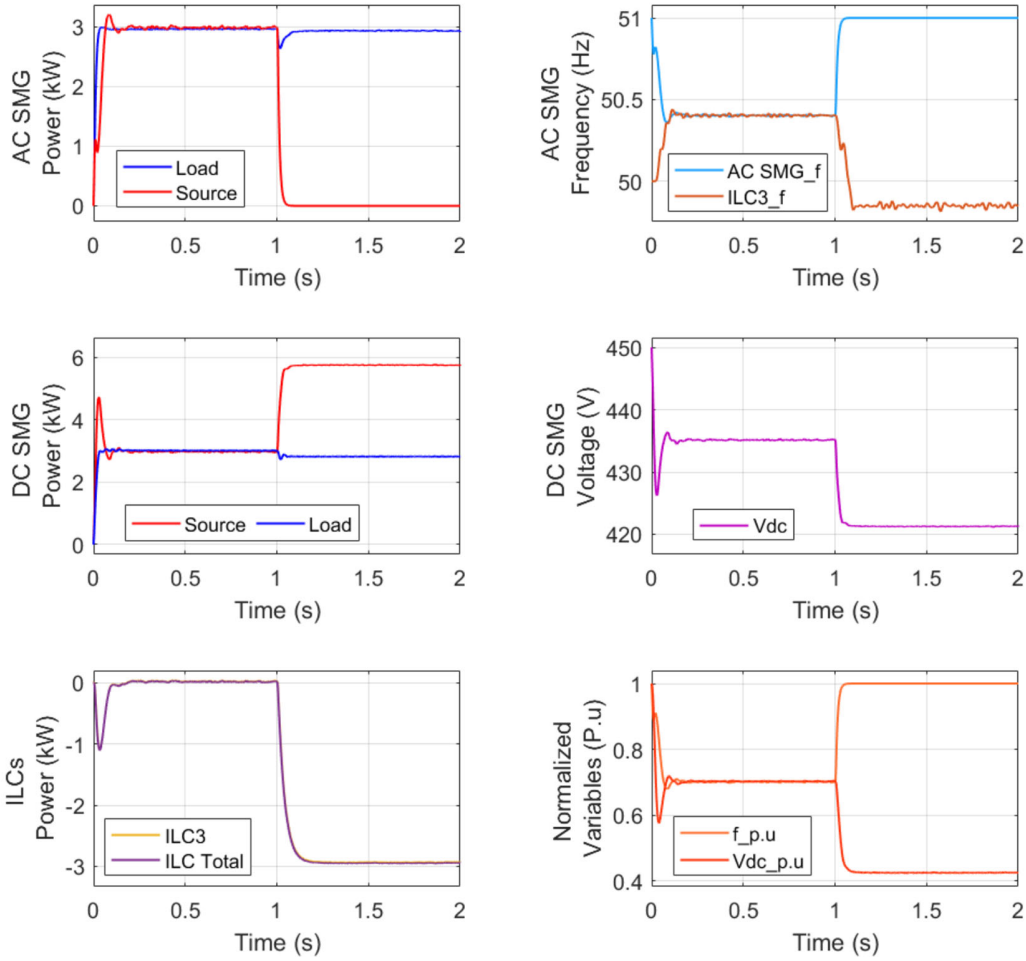

Figure 5.9. Scenario 3 simulation results test 1 waveforms of power, voltage, frequency using the proposed method.

The proposed method is then implemented. For test 1, Figure 5.9 shows the reverse of power direction from the DC to AC SMG, and the DC SMG sources cover the total HMG demand. Furthermore, the difference between the frequency at the output source (51Hz) and the frequency at the ILC3 terminal (49.8 Hz) can be noted. This difference is because the AC SMG now becomes unloaded, and accordingly, the frequency will be at the maximum value (51 Hz). On the other hand, during this test, the ILC3 transfers the total AC SMG's demand

and the frequency reflects the amount of ILC3 output power (49.8 Hz). The normalized variable of the frequency and the voltage (V', f') is no longer balanced as previous due to the disconnection of the AC power sources.

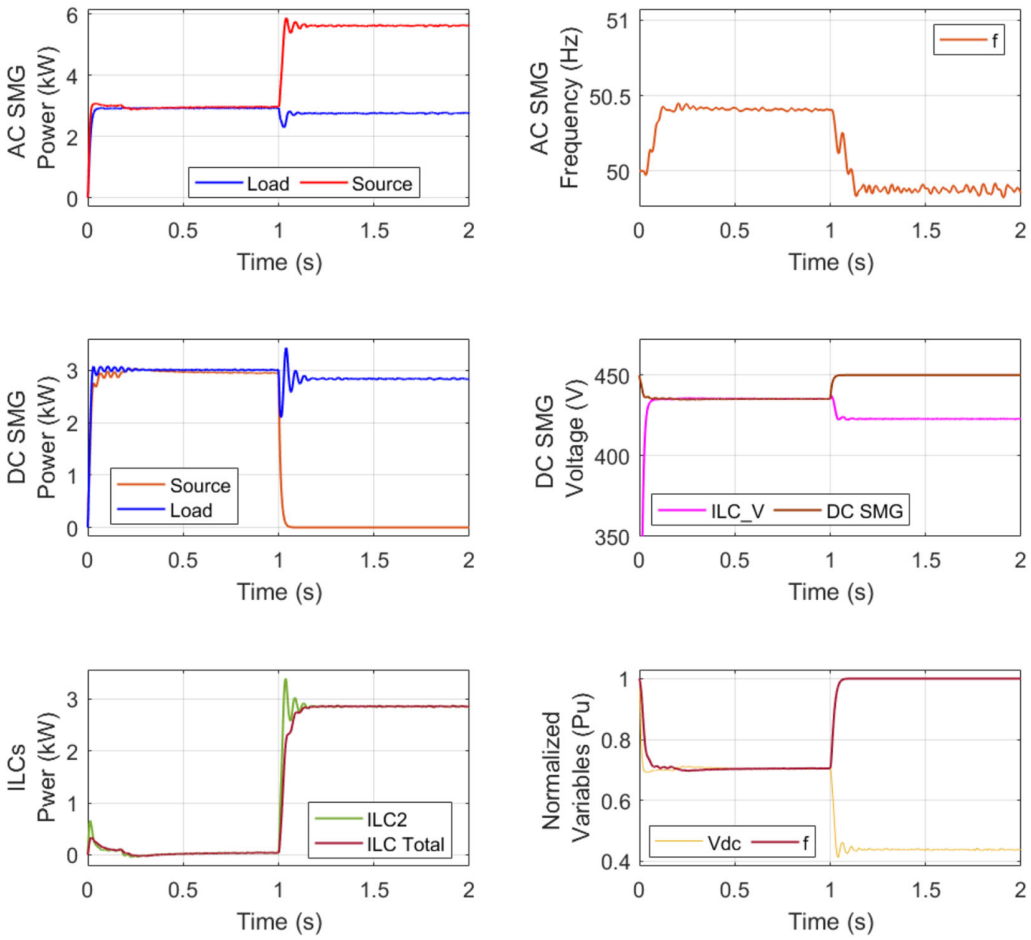

Figure 5.10 Scenario 3 simulation results test 2 waveforms of power, voltage, frequency using the proposed method.

For test 2, unlike the conventional control, Figure 5.10 illustrates the continuity of power transfer from the AC SMG to DC SMG when the DG in the DC SMG is cut off from the HMG using the proposed control system. It can be noted that the demand of DC SMG is

covered from the power transferred through the ILC3, which comes from the AC SMG. Furthermore, the voltage at the DC side is now controlled by the proposed control strategy of the ILC2. On the other hand, it can be seen that the conventional method fails to supply the DC power demand of the DC SMG under the same condition. Notice that the voltage of the output source is now different from the voltage at the DC load terminal since they are separate systems. The AC frequency is dropped from 50.4 Hz to 49.8 Hz due to the new loading conditions that result from isolating the AC SMG's sources.

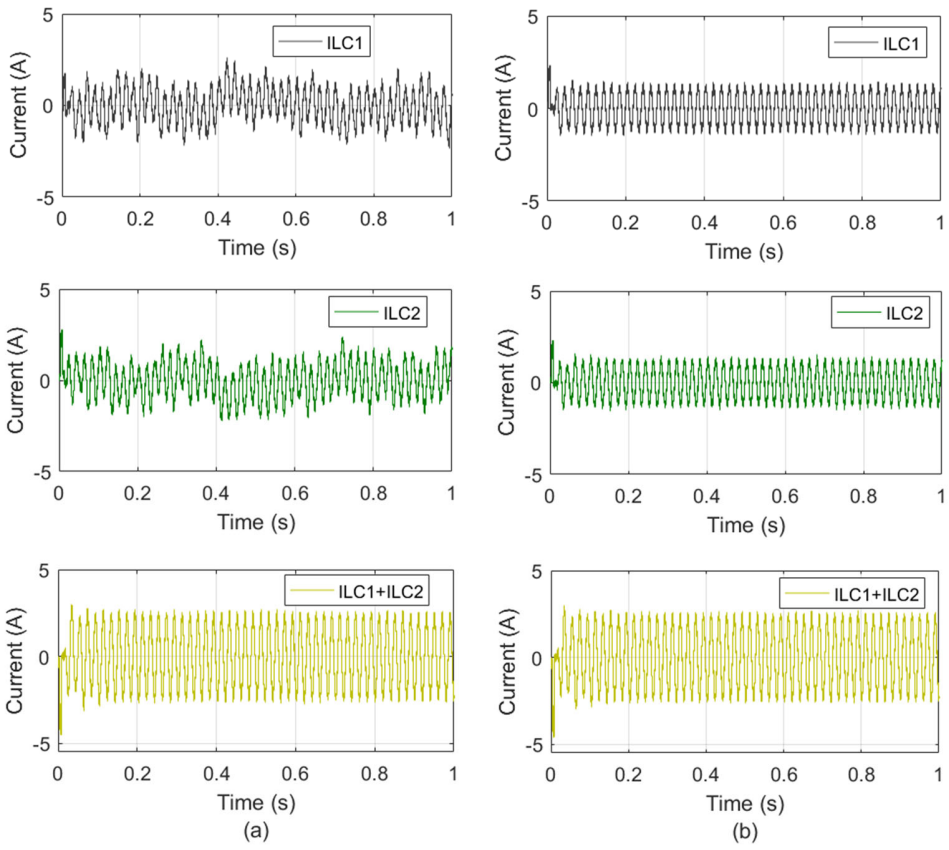

Figure 5.11 AC currents in a-phase of the ILCs when Rv changes. (a) R_v =0. (b) R_v =4.

5.5.4 Effect of Virtual Resistance on Suppressing the Circulating Current

The effect of the virtual resistance controller that is adopted on the 0-axis of the d-q-0 components is shown in Figure 5.11. The AC current of the a-phase for two ILCs with different values of virtual impedance (R_v) is shown. Figure 5.11(a) shows the damping of the AC current in the ILC1 and ILC2 when R_v of the 0-axis is set to zero, which is the case of conventional control methods. It can be noted that the a-phase current has large asymmetrical components and highly fluctuates despite that the sum of these two currents is symmetrical. Figure 5.11(b) shows the changes in the AC current waveforms when adopting the 0-axis (proposed method) with R_v =4. Significant changes can be noted when using R_v compared to Figure 5.11(a). As seen, the AC current is almost symmetry, and the circulating current is totally suppressed.

5.6 Summary

This chapter proposed a new coordinated control and power management scheme for multiple parallel ILCs to control the power flow between the AC and DC SMGs. The presented system includes three parallel ILCs linking the DC and AC SMGs with an individual load connected to each SMG. Unlike the conventional method that controls the multiple parallel ILCs with the same control strategy, the proposed approach suggestes operating the ILCs under different control scheme, thus ensuring full controllability for the whole HMG. The first ILC (ILC1) is designed to operate in a bidirectional power control mode to manage the power flow between the AC and DC buses. The control strategy for ILC2 is to operate in a bidirectional DC voltage control mode to regulate the voltage at the DC bus. Finally, the ILC3 operates in an AC

voltage control mode to regulate the voltage and frequency at the AC bus. MATLAB/Simulink software is used to test the proposed power management and control strategies that are employed in this chapter. The simulation results confirm that the suggested scheme can operate autonomously with significantly improved reliability and stability. The proposed control scheme is compared with the conventional one under different conditions. A seamless power exchange between SMGs is also confirmed, irrespective of the failure of the DG in one SMG, by using the proposed mechanism.

Chapter 6

Conclusions and Suggestions for Future Work

Power management and control strategies for the hybrid AC/DC microgrid are the focus of this thesis. This chapter provides a review and summary of the main contribution of the previous chapters, discussion of significant and novel results as well as identifying the important areas for further research.

6.1 Conclusions

HMGs is the future trend of the electrical power system due to the environmental, economic, and physical advantages. Such arrangement features higher integration adaptability, more control efficiency, and better operating flexibility to meet the overall system reliability and power quality that are difficult to achieve with any single microgrid system. Although many research in the literature studied HMG, only a few of these studies focus on the power management and control coordination for multiple SMG and there are still many challenges and drawbacks in these innovations.

While the previous studies have focused on optimising the power flow in the HMG without considering the detailed hierarchical control, this work has proposed an approach that considers the hierarchical coordination of power management and control strategy and includes both the primary and secondary control levels.

After an introduction of the proposed hybrid architecture and control schemes, in the aspect of power management and control strategy, an improved technique has been proposed that aims to reduce the continuous operation of the ILCs and thus eliminate the unnecessary power exchange among the SMGs. The operational viability for the ILCs in the islanded microgrid under different loading condition is stressed in Chapter 3.

This thesis also studied the HMG that consist of multiple SMGs from a different point of view. A novel approach has been proposed in Chapter 4 to ensure a global controllability for the ILCs. Such approach has been developed to overcome the total dependency on a specific variable for stable power exchange which is the case in the conventional method. This contribution was verified by analyzing the results of the comparison between the traditional and the proposed approach.

Concerning the converters' current limitations and their planned maintenances or unplanned faults during the converter operation, the use of multiple parallel ILCs has been addressed in Chapter 5, where three parallel ILCs linking the DC and AC SMGs with an individual load connected to the corresponding SMG. The strategy presented suggests that the parallel ILCs operate under different control strategy, unlike the conventional ones that usually have a similar control scheme for all ILCs. These ILCs have to carry out the responsibility to manage the power flow between the AC and DC SMGs and simultaneously support the voltage and frequency regulation at the AC bus as well as supporting the voltage at the DC bus. Moreover, to ensure an accurate power sharing among the parallel ILCs and to suppress the circulating current at the DC side, the outer control loop has been modified by implementing an additional control loop. This adaptation involves real-time recording of the power-sharing deviation for each ILC and using it as a feedback to the corresponding controller.

MATLAB/Simulink software is used to test the proposed strategy and schemes that are employed in this work. The proposed approach and strategies have been verified by comparing the suggested structure, power management, and control strategy with the corresponding conventional one. The HMG has been tested when operating under the primary control level only and both the primary and secondary control levels. The novel arrangement provides the suggested HMG structure with elevated flexibility and represents a scalable concept. The analysis confirms the applicability of the proposed scheme to larger systems that can integrate more SMGs while preserving the local hierarchical control system of each SMG. Based on the analysis carried out in this thesis, it can be concluded that with the proposed power and control management strategies, the reliability of the comprehensive HMG system can be significantly improved. The proposed strategies also reduce the amount of power exchange by mitigating the unnecessary power exchange. Various scenarios, case studies, and tests performed on the proposed HMG structure confirm the validity of all the proposed approaches. These results support the hypothesis that the introduction of novel control strategies, such as the ones presented in this work, is an effective tool to enhance the total power management of the HMG. This also confirms that the presented schemes facilitate independent operation with improved reliability and stability in all operating conditions.

In summary, the applicability and implementation of power management and control strategy presented in this thesis have been validated both in theory and simulation. Certainly, this work will improve the utilization of the HMG structure in various applications of distribution systems.

6.2 Future Work

While several techniques and strategies of power management and control scheme of HMG have been carried out in this work, there are many topics that need further in-depth investigation related to HMGs and can be considered worthy of attention in future work.

The future aim of this work is to develop and implement a coordinated power management and control strategy for an HMG with parallel inverter integrating renewable energy sources and electric vehicles. This can be accomplished by using a different renewable and nonrenewable power source that acts as DGs. For instance, PV and ESS can be connected to the AC bus, while wind turbines and fuel cells are connected to a DC bus.

Another aim is to design robust distributed control schemes for multiple microgrids considering practical communication channels that improve the overall system efficiency and stability. Using the appropriate technology that differentiates between wireless and wired communication based on the applications has not been investigated yet.

This research clearly illustrates how to employ the droop control method for power management in the HMG, however, to achieve more accurate load sharing, it is highly recommended to use the improved droop control techniques discussed in Chapter 2 (Section 2.7.2) which are essentially suggested for the individual microgrid.

One of the interesting extensions of the project would be to implement and verify the proposed approach experimentally. Currently, the authors are working on improving the results of the proposed approach using a Real-Time Simulator (OPAL-RT). The system has already been installed recently at the Tech Lab of the University of Technology Sydney. The results will be reported in the subsequent work.

Finally, economic concerns should be taken into account when designing the HMG. Unlike an individual microgrid that may not be economical in some regions with high electricity

tariff and demand charges compared to the traditional grid, HMG can be more cost-effective due to the reduction in the required conversion devices. Consequently, the economic study should consider the optimum number of parallel ILCs between AC and DC SMGs and the level of optimization that regulates the power flow between HMG and the main grid.

References

[1] R. W. Lobenstein and C. Sulzberger, "Eyewitness to dc history," *IEEE Power and Energy Magazine,* vol. 6, no. 3, pp. 84-90, 2008.

[2] P. Wang, L. Goel, X. Liu, and F. H. Choo, "Harmonizing AC and DC: A Hybrid AC/DC Future Grid Solution," *IEEE Power and Energy Magazine,* vol. 11, no. 3, pp. 76-83, 2013.

[3] M. E. El-Hawary, *Electrical energy systems*. Crc Press, 2018.

[4] R. W. Erickson and D. Maksimovic, *Fundamentals of power electronics*. Springer Science & Business Media, 2007.

[5] H. Jiayi, J. Chuanwen, and X. Rong, "A review on distributed energy resources and MicroGrid," *RENEW. SUST. ENERG. REV.,* vol. 12, no. 9, pp. 2472-2483, 2008.

[6] J. Cardell and R. Tabors, "Operation and control in a competitive market: distributed generation in a restructured industry," *The Energy Journal,* pp. 111-136, 1997.

[7] J. M. Guerrero, J. C. Vasquez, J. Matas, D. Vicuna, L. García, and M. Castilla, "Hierarchical control of droop-controlled AC and DC microgrids—A general approach toward standardization," *IEEE Trans. Ind. Electron.,* vol. 58, no. 1, pp. 158-172, 2011.

[8] X. Liu, P. Wang, and P. C. Loh, "A Hybrid AC/DC Microgrid and Its Coordination Control," *IEEE Trans. Smart Grid,* vol. 2, pp. 278-286, 2011.

[9] J. C. Vasquez, J. M. Guerrero, M. Savaghebi, J. Eloy-Garcia, and R. Teodorescu, "Modeling, analysis, and design of stationary-reference-frame droop-controlled

parallel three-phase voltage source inverters," *IEEE Trans. Ind. Electron.,* vol. 60, no. 4, pp. 1271-1280, 2013.

[10] A. N. Celik, "A statistical analysis of wind power density based on the Weibull and Rayleigh models at the southern region of Turkey," *Renewable energy,* vol. 29, no. 4, pp. 593-604, 2004.

[11] T. Ackermann, G. Andersson, and L. Söder, "Distributed generation: a definition," *Electric power systems research,* vol. 57, no. 3, pp. 195-204, 2001.

[12] M. Grubb, *Renewable Energy Strategies for Europe: Foundations and Context*. Earthscan, 1995.

[13] M. Grubb and R. Vigotti, *Renewable Energy Strategies for Europe: Electricity systems and primary electricity sources*. Earthscan, 1995.

[14] M. Nehrir *et al.*, "A review of hybrid renewable/alternative energy systems for electric power generation: Configurations, control, and applications," *IEEE Transactions on Sustainable Energy,* vol. 2, no. 4, pp. 392-403, 2011.

[15] B. Horner, R. D. Jeffery, and C. M. E. Krogh, "Literature Reviews on Wind Turbines and Health Are They Enough?," *Bulletin of Science, Technology & Society,* vol. 31, no. 5, pp. 399-413, 2011.

[16] C. D. Feinstein, R. Orans, and S. W. Chapel, "The distributed utility: A new electric utility planning and pricing paradigm," *Annual Review of Energy and the Environment,* vol. 22, no. 1, pp. 155-185, 1997.

[17] M. Ilic, R. Tabors, and J. Chapman, "Conceptual design of distributed utility system architecture: Final report," Technical report, Massachusetts Institute of Technology1994.

[18] S. Anand, B. G. Fernandes, and J. Guerrero, "Distributed Control to Ensure Proportional Load Sharing and Improve Voltage Regulation in Low-Voltage DC Microgrids," *IEEE Transactions on Power Electronics,* vol. 28, no. 4, pp. 1900-1913, 2013.

[19] N. Author, "Review of electrical energy storage technologies and systems and of their potential for the UK," *EA Technology,* vol. 1, p. 34, 2004.

[20] H. Chen, T. N. Cong, W. Yang, C. Tan, Y. Li, and Y. Ding, "Progress in electrical energy storage system: A critical review," *Progress in natural science,* vol. 19, no. 3, pp. 291-312, 2009.

[21] H. Chen, Y. Ding, T. Peters, and F. Berger, "Method of Storing Energy and a Cryogenic Energy Storage System," ed: Google Patents, 2016.

[22] J. Makansi and J. Abboud, "Energy storage: the missing link in the electricity value chain," *Energy Storage Council White Paper,* 2002.

[23] H. Zhao, Q. Wu, S. Hu, H. Xu, and C. N. Rasmussen, "Review of energy storage system for wind power integration support," *Applied Energy,* vol. 137, pp. 545-553, 2015.

[24] F. Díaz-González, A. Sumper, O. Gomis-Bellmunt, and R. Villafáfila-Robles, "A review of energy storage technologies for wind power applications," *Renewable and Sustainable Energy Reviews,* vol. 16, no. 4, pp. 2154-2171, 2012.

[25] P. Alotto, M. Guarnieri, and F. Moro, "Redox flow batteries for the storage of renewable energy: A review," *Renewable and Sustainable Energy Reviews,* vol. 29, pp. 325-335, 2014.

[26] N. Hirano, T. Watanabe, and S. Nagaya, "Development of cooling technologies for SMES," *Cryogenics,* vol. 80, pp. 210-214, 2016.

[27] L. Van der Sluis, J. Verboomen, A. Van Voorden, L. Ramirez Elizondo, and G. Paap, "The application of super capacitors to relieve battery-storage systems in autonomous renewable energy systems," *Power Tech 2007,* 2017.

[28] M. M. Pérez-Madrigal, M. G. Edo, and C. Alemán, "Powering the future: application of cellulose-based materials for supercapacitors," *Green Chem.,* vol. 18, no. 22, pp. 5930-5956, 2016.

[29] S. M. Mousavi G, F. Faraji, A. Majazi, and K. Al-Haddad, "A comprehensive review of Flywheel Energy Storage System technology," *Renewable and Sustainable Energy Reviews,* vol. 67, pp. 477-490, 2017.

[30] R. Sebastián and R. Peña Alzola, "Flywheel energy storage systems: Review and simulation for an isolated wind power system," *Renewable and Sustainable Energy Reviews,* vol. 16, no. 9, pp. 6803-6813, 2012.

[31] E. Barbour, I. A. G. Wilson, J. Radcliffe, Y. Ding, and Y. Li, "A review of pumped hydro energy storage development in significant international electricity markets," *Renewable and Sustainable Energy Reviews,* vol. 61, pp. 421-432, 2016.

[32] L. Chen, T. Zheng, S. Mei, X. Xue, B. Liu, and Q. Lu, "Review and prospect of compressed air energy storage system," *Journal of Modern Power Systems and Clean Energy,* vol. 4, no. 4, pp. 529-541, 2016.

[33] J. Hua, Q. Ai, and Y. Yao, "Dynamic equivalent of microgrid considering flexible components," *IET Generation, Transmission & Distribution,* vol. 9, no. 13, pp. 1688-1696, 2015.

[34] S. K. Sahoo, A. K. Sinha, and N. Kishore, "Control techniques in AC, DC, and hybrid AC–DC microgrid: A review," *IEEE Trans. Emerg. Sel. Topics Power Electron,* vol. 6, no. 2, pp. 738-759, 2018.

[35] P. C. Loh, D. Li, Y. K. Chai, and F. Blaabjerg, "Autonomous operation of hybrid microgrid with AC and DC subgrids," *IEEE Trans. Power Electron.,* vol. 28, no. 5, pp. 2214-2223, 2013.

[36] C. Dou, N. Li, D. Yue, and T. Liu, "Hierarchical hybrid control strategy for micro-grid switching stabilisation during operating mode conversion," *IET Generation, Transmission & Distribution,* vol. 10, no. 12, pp. 2880-2890, 2016.

[37] F. Nejabatkhah and Y. W. Li, "Overview of power management strategies of hybrid AC/DC microgrid," *IEEE Trans. Power Electron.,* vol. 30, no. 12, pp. 7072-7089, 2015.

[38] M. Abuhilaleh, L. Li, M. Begum, and J. Zhu, "Power management and control strategy for hybrid AC/DC microgrids in autonomous operation mode," in *Electrical Machines and Systems (ICEMS), 2017 20th International Conference on*, 2017, pp. 1-6: IEEE.

[39] E. Unamuno and J. A. Barrena, "Hybrid ac/dc microgrids—Part II: Review and classification of control strategies," *RENEW SUST ENERG REV,* vol. 52, pp. 1123-1134, 2015.

[40] T. D. C. Huayllas, D. Ramos, and R. Vasquez-Arnez, "Microgrid systems: Current status and challenges," in *2010 IEEE/PES Transmission and Distribution Conference and Exposition: Latin America (T&D-LA)*, 2010, pp. 7-12: IEEE.

[41] N. Lidula and A. Rajapakse, "Microgrids research: A review of experimental microgrids and test systems," *Renewable and Sustainable Energy Reviews,* vol. 15, no. 1, pp. 186-202, 2011.

[42] S. Morozumi, H. Nakama, and N. Inoue, "Demonstration projects for grid-connection issues in Japan," *e & i Elektrotechnik und Informationstechnik,* vol. 125, no. 12, pp. 426-431, 2008.

[43] X. Zhou *et al.*, "A microgrid cluster structure and its autonomous coordination control strategy," *INT J ELEC POWER,* vol. 100, pp. 69-80, 2018.

[44] H. A. Alsiraji, A. A. A. Radwan, and R. El-Shatshat, "Modelling and analysis of a synchronous machine-emulated active intertying converter in hybrid AC/DC microgrids," *IET Generation, Transmission & Distribution,* vol. 12, no. 11, pp. 2539-2548, 2018.

[45] B. John, A. Ghosh, F. Zare, and S. Rajakaruna, "Improved control strategy for accurate load power sharing in an autonomous microgrid," *IET Generation, Transmission & Distribution,* vol. 11, no. 17, pp. 4384-4390, 2017.

[46] M. Nehrir *et al.*, "A review of hybrid renewable/alternative energy systems for electric power generation: Configurations, control, and applications," *IEEE Trans. Sustain. Energy,* vol. 2, no. 4, pp. 392-403, 2011.

[47] X. Zhou *et al.*, "Power coordinated control method with frequency support capability for hybrid single/three-phase microgrid," *IET Gener. Transm. Distrib.,* vol. 12, no. 10, pp. 2397-2405, 2018.

[48] J. P. Lopes, C. Moreira, and A. G. Madureira, "Defining control strategies for microgrids islanded operation," *IEEE Trans. Power Syst.,* vol. 21, no. 2, pp. 916-924, 2006.

[49] Y. Li *et al.*, "Optimal scheduling of isolated microgrid with an electric vehicle battery swapping station in multi-stakeholder scenarios: A bi-level programming approach via real-time pricing," *Applied Energy,* vol. 232, pp. 54-68, 2018.

[50] P. Jin, Y. Li, G. Li, Z. Chen, and X. Zhai, "Optimized hierarchical power oscillations control for distributed generation under unbalanced conditions," *Applied energy,* vol. 194, pp. 343-352, 2017.

[51] J. M. Guerrero, J. C. Vasquez, J. Matas, M. Castilla, and L. G. de Vicuna, "Control strategy for flexible microgrid based on parallel line-interactive UPS systems," *IEEE Trans. Ind. Electron.,* vol. 56, no. 3, pp. 726-736, 2009.

[52] J.-Y. Kim *et al.*, "Cooperative control strategy of energy storage system and microsources for stabilizing the microgrid during islanded operation," *IEEE Transactions on Power Electronics,* vol. 25, no. 12, pp. 3037-3048, 2010.

[53] K. Tan, P. So, Y. Chu, and M. Chen, "Coordinated control and energy management of distributed generation inverters in a microgrid," *IEEE transactions on power delivery,* vol. 28, no. 2, pp. 704-713, 2013.

[54] J. M. Guerrero, M. Chandorkar, T.-L. Lee, and P. C. Loh, "Advanced control architectures for intelligent microgrids—Part I: Decentralized and hierarchical control," *IEEE Trans. Ind. Electron.,* vol. 60, no. 4, pp. 1254-1262, 2013.

[55] T. John and S. P. Lam, "Voltage and frequency control during microgrid islanding in a multi-area multi-microgrid system," *IET Generation, Transmission & Distribution,* vol. 11, no. 6, pp. 1502-1512, 2017.

[56] J. M. Guerrero, J. Matas, L. G. D. V. D. Vicuna, M. Castilla, and J. Miret, "Wireless-Control Strategy for Parallel Operation of Distributed-Generation Inverters," *IEEE Transactions on Industrial Electronics,* vol. 53, no. 5, pp. 1461-1470, 2006.

[57] X.-P. Zhang, "Multiterminal voltage-sourced converter-based HVDC models for power flow analysis," *Power Systems, IEEE Transactions on,* vol. 19, no. 4, pp. 1877-1884, 2004.

[58] J. M. Guerrero, L. Hang, and J. Uceda, "Control of Distributed Uninterruptible Power Supply Systems," *IEEE Transactions on Industrial Electronics,* vol. 55, no. 8, pp. 2845-2859, 2008.

[59] M. C. Chandorkar, D. M. Divan, and R. Adapa, "Control of parallel connected inverters in standalone AC supply systems," *IEEE Transactions on Industry Applications,* vol. 29, no. 1, pp. 136-143, 1993.

[60] P. Wang, C. Jin, D. Zhu, Y. Tang, P. C. Loh, and F. H. Choo, "Distributed Control for Autonomous Operation of a Three-Port AC/DC/DS Hybrid Microgrid," *IEEE Transactions on Industrial Electronics,* vol. 62, no. 2, pp. 1279-1290, 2015.

[61] M. Abuhilaleh, L. Li, and J. Hossain, "Power management and control coordination strategy for autonomous hybrid microgrids," *IET Generation, Transmission & Distribution,* 2019.

[62] F. Blaabjerg, R. Teodorescu, M. Liserre, and A. V. Timbus, "Overview of control and grid synchronization for distributed power generation systems," *IEEE Transactions on industrial electronics,* vol. 53, no. 5, pp. 1398-1409, 2006.

[63] M. P. Kazmierkowski, R. Krishnan, F. Blaabjerg, and J. Irwin, *Control in power electronics: selected problems*. Academic press, 2002.

[64] S. Fukuda and T. Yoda, "A novel current-tracking method for active filters based on a sinusoidal internal model [for PWM invertors]," *IEEE transactions on industry applications,* vol. 37, no. 3, pp. 888-895, 2001.

[65] D. N. Zmood and D. G. Holmes, "Stationary frame current regulation of PWM inverters with zero steady-state error," *IEEE Transactions on power electronics,* vol. 18, no. 3, pp. 814-822, 2003.

[66] M. Ciobotaru, R. Teodorescu, and F. Blaabjerg, "Control of single-stage single-phase PV inverter," *EPE Journal,* vol. 16, no. 3, pp. 20-26, 2006.

[67] L. Malesani, P. Mattavelli, and P. Tomasin, "Improved constant-frequency hysteresis current control of VSI inverters with simple feedforward bandwidth prediction," *IEEE Transactions on industry applications,* vol. 33, no. 5, pp. 1194-1202, 1997.

[68] J. M. Guerrero, L. G. De Vicuna, J. Matas, M. Castilla, and J. Miret, "Output impedance design of parallel-connected UPS inverters with wireless load-sharing control," *IEEE Transactions on industrial electronics,* vol. 52, no. 4, pp. 1126-1135, 2005.

[69] J. M. Guerrero, V. Luis Garcia de, J. Matas, M. Castilla, and J. Miret, "Output impedance design of parallel-connected UPS inverters with wireless load-sharing

control," *IEEE Transactions on Industrial Electronics,* vol. 52, no. 4, pp. 1126-1135, 2005.

[70] A. Tuladhar, H. Jin, T. Unger, and K. Mauch, "Parallel operation of single phase inverter modules with no control interconnections," in *Proceedings of APEC 97-Applied Power Electronics Conference*, 1997, vol. 1, pp. 94-100: IEEE.

[71] M. N. Marwali, J.-W. Jung, and A. Keyhani, "Control of distributed generation systems-Part II: Load sharing control," *IEEE Transactions on power electronics,* vol. 19, no. 6, pp. 1551-1561, 2004.

[72] J. P. Lopes, C. Moreira, and A. Madureira, "Defining control strategies for microgrids islanded operation," *IEEE Transactions on power systems,* vol. 21, no. 2, pp. 916-924, 2006.

[73] C. Yuen, A. Oudalov, and A. Timbus, "The Provision of Frequency Control Reserves From Multiple Microgrids," *IEEE Transactions on Industrial Electronics,* vol. 58, no. 1, pp. 173-183, 2011.

[74] E. Unamuno and J. A. Barrena, "Hybrid ac/dc microgrids—Part II: Review and classification of control strategies," *Renewable and Sustainable Energy Reviews,* vol. 52, pp. 1123-1134, 2015.

[75] Q. Shafiee, J. M. Guerrero, and J. C. Vasquez, "Distributed Secondary Control for Islanded Microgrids—A Novel Approach," *IEEE Transactions on Power Electronics,* vol. 29, no. 2, pp. 1018-1031, 2014.

[76] M. Yazdanian and A. Mehrizi-Sani, "Distributed Control Techniques in Microgrids," *IEEE Transactions on Smart Grid,* vol. 5, no. 6, pp. 2901-2909, 2014.

[77] F. Katiraei and M. R. Iravani, "Power Management Strategies for a Microgrid With Multiple Distributed Generation Units," *IEEE Transactions on Power Systems,* vol. 21, no. 4, pp. 1821-1831, 2006.

[78] N. L. Diaz, T. Dragičević, J. C. Vasquez, and J. M. Guerrero, "Intelligent Distributed Generation and Storage Units for DC Microgrids—A New Concept on Cooperative Control Without Communications Beyond Droop Control," *IEEE Transactions on Smart Grid,* vol. 5, no. 5, pp. 2476-2485, 2014.

[79] J. P. Lopes, C. Moreira, and A. Madureira, "Defining control strategies for microgrids islanded operation," *IEEE Trans. Power Electron,* vol. 21, no. 2, pp. 916-924, 2006.

[80] Q. Shafiee, J. M. Guerrero, and J. C. Vasquez, "Distributed secondary control for islanded microgrids—A novel approach," *IEEE Trans. Power Electron,* vol. 29, no. 2, pp. 1018-1031, 2014.

[81] P. T. Baboli, M. Shahparasti, M. P. Moghaddam, M. R. Haghifam, and M. Mohamadian, "Energy management and operation modelling of hybrid AC-DC microgrid," *IET Generation, Transmission and Distribution,* Article vol. 8, no. 10, pp. 1700-1711, 2014.

[82] M. Lexuan, T. Dragicevic, J. Guerrero, J. Vasquez, M. Savaghebi, and T. Fen, "Agent-based distributed unbalance compensation for optimal power quality in islanded microgrids," in *2014 IEEE 23rd International Symposium on Industrial Electronics (ISIE)*, 2014, pp. 2535-2540.

[83] C. Jin, "Distributed control and power quality improvement in hybrid AC/DC microgrids," 2013.

[84] A. R. Panel, "Application of Frequency Operating Standards During Periods of Supply Scarcity," ed: Draft Determination, September, 2008.

[85] M. S. Rahman, M. Hossain, and J. Lu, "Coordinated control of three-phase AC and DC type EV–ESSs for efficient hybrid microgrid operations," *Energy Convers. Manag.,* vol. 122, pp. 488-503, 2016.

[86] H. Kakigano, Y. Miura, T. Ise, and R. Uchida, "DC Voltage Control of the DC Microgrid for Super High Quality Distribution," in *2007 Power Conversion Conference - Nagoya*, 2007, pp. 518-525.

[87] J. A. P. Lopes, C. L. Moreira, and A. G. Madureira, "Defining control strategies for MicroGrids islanded operation," *IEEE Transactions on Power Systems,* vol. 21, no. 2, pp. 916-924, 2006.

[88] T. Caldognetto and P. Tenti, "Microgrids operation based on master–slave cooperative control," *IEEE J Emerg Sel Top Power Electron,* vol. 2, no. 4, pp. 1081-1088, 2014.

[89] M. M. A. Abdelaziz, M. F. Shaaban, H. E. Farag, and E. F. El-Saadany, "A multistage centralized control scheme for islanded microgrids with PEVs," *IEEE Trans. Sustain. Energy,* vol. 5, no. 3, pp. 927-937, 2014.

[90] N. Eghtedarpour and E. Farjah, "Power control and management in a hybrid AC/DC microgrid," *IEEE Trans. Smart Grid,* vol. 5, no. 3, pp. 1494-1505, 2014.

[91] B. K. Johnson, R. H. Lasseter, F. L. Alvarado, and R. Adapa, "Expandable multiterminal DC systems based on voltage droop," *IEEE Transactions on Power Delivery,* vol. 8, no. 4, pp. 1926-1932, 1993.

[92] I. Batarseh, K. Siri, and H. Lee, "Investigation of the output droop characteristics of parallel-connnected DC-DC converters," in *Proceedings of 1994 Power Electronics Specialist Conference-PESC'94*, 1994, vol. 2, pp. 1342-1351: IEEE.

[93] P. C. Loh, D. Li, Y. K. Chai, and F. Blaabjerg, "Autonomous control of interlinking converter with energy storage in hybrid AC–DC microgrid," *IEEE Trans. Ind. Appl.,* vol. 49, no. 3, pp. 1374-1382, 2013.

[94] X. Zheng, F. Gao, H. Ali, and H. Liu, "A Droop Control Based Three Phase Bidirectional AC-DC Converter for More Electric Aircraft Applications," *Energies,* vol. 10, no. 3, p. 400, 2017.

[95] T. Ma, M. H. Cintuglu, and O. A. Mohammed, "Control of a hybrid AC/DC microgrid involving energy storage and pulsed loads," *IEEE Trans. Ind. Appl.,* vol. 53, no. 1, pp. 567-575, 2017.

[96] P. Wang, C. Jin, D. Zhu, Y. Tang, P. C. Loh, and F. H. Choo, "Distributed control for autonomous operation of a three-port AC/DC/DS hybrid microgrid," *IEEE Trans. Ind. Electron.,* vol. 62, no. 2, pp. 1279-1290, 2015.

[97] T. L. Vandoorn, J. C. Vasquez, J. D. Kooning, J. M. Guerrero, and L. Vandevelde, "Microgrids: Hierarchical Control and an Overview of the Control and Reserve Management Strategies," *IEEE Industrial Electronics Magazine,* vol. 7, no. 4, pp. 42-55, 2013.

[98] O. Palizban and K. Kauhaniemi, "Hierarchical control structure in microgrids with distributed generation: Island and grid-connected mode," *Renewable and Sustainable Energy Reviews,* vol. 44, pp. 797-813, 2015/04/01/ 2015.

[99] J. Rocabert, A. Luna, F. Blaabjerg, and P. Rodríguez, "Control of Power Converters in AC Microgrids," *IEEE Transactions on Power Electronics,* vol. 27, no. 11, pp. 4734-4749, 2012.

[100] S. K. Khadem, M. Basu, and M. F. Conlon, "Parallel operation of inverters and active power filters in distributed generation system—A review," *Renewable and Sustainable Energy Reviews,* vol. 15, no. 9, pp. 5155-5168, 2011/12/01/ 2011.

[101] A. Bidram and A. Davoudi, "Hierarchical Structure of Microgrids Control System," *IEEE Transactions on Smart Grid,* vol. 3, no. 4, pp. 1963-1976, 2012.

[102] T. L. Vandoorn, J. D. M. De Kooning, B. Meersman, and L. Vandevelde, "Review of primary control strategies for islanded microgrids with power-electronic interfaces," *Renewable and Sustainable Energy Reviews,* vol. 19, pp. 613-628, 2013/03/01/ 2013.

[103] N. Eghtedarpour and E. Farjah, "Power Control and Management in a Hybrid AC/DC Microgrid," *IEEE Transactions on Smart Grid,* vol. 5, no. 3, pp. 1494-1505, 2014.

[104] X. Sun, Y.-S. Lee, and D. Xu, "Modeling, analysis, and implementation of parallel multi-inverter systems with instantaneous average-current-sharing scheme," *IEEE Transactions on Power Electronics,* vol. 18, no. 3, pp. 844-856, 2003.

[105] H. Kanchev, D. Lu, F. Colas, V. Lazarov, and B. Francois, "Energy management and operational planning of a microgrid with a PV-based active generator for smart grid applications," *IEEE transactions on industrial electronics,* vol. 58, no. 10, pp. 4583-4592, 2011.

[106] Y. Xia, W. Wei, M. Yu, X. Wang, and Y. Peng, "Power management for a hybrid AC/DC microgrid with multiple subgrids," *IEEE Trans. Power Electron.,* vol. 33, no. 4, pp. 3520-3533, 2018.

[107] M. Nehrir *et al.*, "A review of hybrid renewable/alternative energy systems for electric power generation: Configurations, control, and applications," *IEEE Trans. Sustain. Energy,* vol. 2, pp. 392-403, 2011.

[108] Q. Xu, J. Xiao, P. Wang, and C. Wen, "A Decentralized Control Strategy for Economic Operation of Autonomous AC, DC, and Hybrid AC/DC Microgrids," *IEEE Trans. Energy Convers,* vol. 32, no. 4, pp. 1345-1355, 2017.

[109] E. J. Ng and R. A. El-Shatshat, "Multi-microgrid control systems (MMCS)," in *IEEE PES General Meeting*, 2010, pp. 1-6: IEEE.

[110] J. C. Vasquez, J. M. Guerrero, M. Savaghebi, J. Eloy-Garcia, and R. Teodorescu, "Modeling, analysis, and design of stationary-reference-frame droop-controlled parallel three-phase voltage source inverters," *IEEE Transactions on Industrial Electronics,* vol. 60, no. 4, pp. 1271-1280, 2013.

[111] S. K. Mazumder, M. Tahir, and K. Acharya, "Master–slave current-sharing control of a parallel DC–DC converter system over an RF communication interface," *IEEE Transactions on Industrial Electronics,* vol. 55, no. 1, pp. 59-66, 2008.

[112] Y. Xia, Y. Peng, P. Yang, M. Yu, and W. Wei, "Distributed coordination control for multiple bidirectional power converters in a hybrid AC/DC microgrid," *IEEE Transactions on Power Electronics,* vol. 32, no. 6, pp. 4949-4959, 2017.

[113] H. Xiao, A. Luo, Z. Shuai, G. Jin, and Y. Huang, "An improved control method for multiple bidirectional power converters in hybrid AC/DC microgrid," *IEEE Transactions on Smart Grid,* vol. 7, no. 1, pp. 340-347, 2016.

[114] F. Nejabatkhah, Y. W. Li, and K. Sun, "Parallel three-phase interfacing converters operation under unbalanced voltage in hybrid AC/DC microgrid," *IEEE Transactions on Smart Grid,* vol. 9, no. 2, pp. 1310-1322, 2018.

[115] C.-T. Pan and Y.-H. Liao, "Modeling and coordinate control of circulating currents in parallel three-phase boost rectifiers," *IEEE Transactions on Industrial Electronics,* vol. 54, no. 2, pp. 825-838, 2007.

[116] F. Wang, Y. Wang, Q. Gao, C. Wang, and Y. Liu, "A control strategy for suppressing circulating currents in parallel-connected PMSM drives with individual DC links," *IEEE Transactions on Power Electronics,* vol. 31, no. 2, pp. 1680-1691, 2016.

[117] S. Xu, J. Wang, and J. Xu, "A current decoupling parallel control strategy of single-phase inverter with voltage and current dual closed-loop feedback," *IEEE Transactions on Industrial Electronics,* vol. 60, no. 4, pp. 1306-1313, 2013.

[118] D. Zhang, F. F. Wang, R. Burgos, and D. Boroyevich, "Common-mode circulating current control of paralleled interleaved three-phase two-level voltage-source converters with discontinuous space-vector modulation," *IEEE Transactions on Power Electronics,* vol. 26, no. 12, pp. 3925-3935, 2011.

[119] Z. Ye, D. Boroyevich, J.-Y. Choi, and F. C. Lee, "Control of circulating current in two parallel three-phase boost rectifiers," *IEEE Transactions on Power Electronics,* vol. 17, no. 5, pp. 609-615, 2002.

[120] T.-P. Chen, "Zero-sequence circulating current reduction method for parallel HEPWM inverters between AC bus and DC bus," *IEEE Transactions on industrial electronics,* vol. 59, no. 1, pp. 290-300, 2012.

[121] M. Khederzadeh, H. Maleki, and V. Asgharian, "Frequency control improvement of two adjacent microgrids in autonomous mode using back to back Voltage-Sourced Converters," *Int J Electr Power Energy Syst,* vol. 74, pp. 126-133, 2016/01/01/ 2016.